An analysis of basement membrane repair *in vivo*

By

William David Ramos-Lewis

Dissertation

Submitted to the Faculty of the

Graduate School of Vanderbilt University

in partial fulfillment of the requirements

for the degree of

DOCTOR OF PHILOSOPHY

in

Cell and Developmental Biology

January 31st, 2020

Nashville, Tennessee

Approved:

Christopher Wright, D.Phil.

Jeffrey Davidson, Ph.D.

Heinrich Matthies, Ph.D.

Gautam Bhave, M.D., Ph.D.

Andrea Page-McCaw, Ph.D.

To my wife, Andrea, for her love and support

and

To my daughter, Emma, for showing me what true courage looks like

Acknowledgements

Thank you to my advisor, Andrea Page-McCaw, for her support and guidance both in this body of work and in my personal development as a scientist. I would also like to thank my committee members: Christopher Wright, Jeffrey Davidson, Heinrich Matthies, and Gautam (Jay) Bhave. Their advice and support have proven invaluable to my research and professional growth.

This work would not have been possible without advice and help from all members of the Page-McCaw lab. Special thank you to Kimi LaFever Hodge for her assistance in creating fly stocks and carrying out experiments. I am also grateful to the many other members of the Department of Cell and Developmental Biology, whom have never hesitated to offer their time and expertise. Notably, I would like to say thank you to Anthony Tharp for laboratory equipment training, Marc Wozniak for IT support, and to both Kristi Hargrove and Elaine Caine for all the administrative work they did in the background.

I wish to thank the Bloomington *Drosophila* Stock Center, the Vienna *Drosophila* RNAi Center and Sally Horne-Badovinac for supplying fly stocks. I am also grateful to Guy Tanentzapf for locating GFP-fusion fly lines and to the Developmental Studies Hybridoma Bank for supplying antibodies.

Research reported in this publication was supported by the National Institutes of Health, grant numbers 501GM073883 and R21AR072510. The content is solely the responsibility of the authors and does not necessarily represent the official views of the National Institutes of Health.

Finally, I would like to thank my friends and family for always giving me much needed support. I am especially thankful to my wife, Andrea Ramos-Lewis, for joining me in this endeavor and supporting me to the very end. Special thank you to my parents, Bill and Gail Lewis, Andrea's mother, Lynn Ramos, and to Jorge Wellman for getting us to the finish line.

Table of Contents

List of Tables

List of Figures

Chapter 1

Introduction

One of the earliest innovations of nature that allowed for the development of multicellular organisms was the extracellular matrix (ECM) [1]. Composed of hundreds of secreted glycoproteins and proteoglycans, the ECM provides mechanical support to tissues and organs throughout the body and creates a microenvironment that influences cellular behaviors such as differentiation, proliferation, and migration [2]. The basement membrane is a specialized sheet-like form of ECM that underlies all epithelial tissue, and surrounds muscles, nerves and other organs [3]. It is present in almost all metazoans, including some of the most ancient animal phyla, suggesting its evolution was an early requirement for animal life [4,5].

From embryogenesis until death, basement membranes serve a multitude of vital functions. They provide structural support for adherent cells, compartmentalize tissues and organs, and influence cellular behavior [3,6,7]. The early appearance of basement membranes in development requires them to be dynamic; as an animal grows and develops, basement membranes must grow, break down, and/or change composition [8]. Many of these dynamics have been studied in the context of development and disease. However, the process of basement membrane repair following injury remains under-explored. Damaged or defective basement membranes are a driver of human diseases [9], and devising a strategy to correct such defects will require a better understanding of how basement membranes are repaired *in vivo*. Therefore, to address this topic, my

study sought to understand some of the basic processes of basement membrane repair in *Drosophila melanogaster*. Specifically, I sought to describe the morphology of repaired basement membrane, determine the source of each component, and test for the dependency of each component on the other for incorporation during repair.

To put this study into context, the rest of this chapter will describe what is known about the structure of basement membrane, its functions, and the mechanisms of its *de novo* assembly during development. Furthermore, this chapter will summarize what little is known about basement membrane repair outside of this study. The list of components that can be found in basement membranes is vast and variable between tissues and species. For the sake of simplicity, this review will focus primarily on the core components, defined as proteins that affect gross basement membrane structure via their physical presence, that are conserved between *Drosophila* and mammals: laminin, collagen IV, perlecan, and nidogen. Where relevant, similarities and differences between *Drosophila* and mammals will be highlighted in order to clarify the strengths and limitations of this study.

Basement membrane structure and function

The basement membrane is an electron dense, highly organized, sheet-like ECM, ranging from less than 100 nm to 10 μm in thickness [10]. Basement membranes can be found on the basal surface of epithelial cells, in association with neurons and adipocytes, surrounding muscle fibers, and compartmentalizing organs throughout the body [6,7]. As an integral part of so many tissues and organ systems, the functions of basement membrane are extensive.

Structurally, basement membranes act as anchoring points for cells by binding with integrins [11-13], dystroglycans [14-16], and sulfated glycolipids [17]. Rather than being a passive scaffolding upon which cells are layered, both the composition and physical properties of a basement membrane can dramatically influence the shape and function of associated tissues, not only by physically constricting tissue shape, but by altering cellular behavior (Reviewed in Appendix). Much of the basement membrane's influence over cellular behavior is mediated by integrins and dystroglycans. Downstream signals from these attachment points inform cells of their position within a given tissue, directing cellular polarization and promoting differentiation [16,18-20].

Basement membranes also influence associated cells by sequestering secreted signaling molecules or presenting them to cell surface receptors. For example, collagen IV has been shown to influence diffusion of the bone morphogenic protein (BMP) signaling molecule, Dpp, in developing *Drosophila* embryos and in adult *Drosophila* ovaries. In embryos, collagen IV appears to promote Dpp gradient formation, while restricting its diffusion in the adult germarium [21]. Furthermore, hemocyte-secreted collagen IV has been shown to sensitize developing renal tubules to BMP signaling, possibly by presenting Dpp to the associated cells [22]. Basement membrane-associated heparan sulfate proteoglycans (HSPG) have also been shown to influence BMP signaling in the developing zebrafish myotome [23], the embryonic compartment from which skeletal muscles are derived [24].

Defects in basement membranes have been linked with a wide range of diseases. Alport syndrome and Pierson syndrome, genetic disorders that disrupt kidney function, are linked to mutations in collagen IV and laminin respectively. In both cases,

the structure of the glomerular basement membrane becomes defective and the ability of the glomerulus to properly filter circulating blood is disrupted [9]. Laminin defects have also been linked to certain muscular dystrophies, presumably due to an inability of muscles cells to properly adhere to the surrounding basement membrane [25,26]. These examples and many other basement membrane-related disorders underscore the importance of basement membranes to human health.

Building a basement membrane: core components

As stated above, the composition of basement membranes can vary dramatically between tissues and organs, and many basement membrane proteins are specific to vertebrates. For example, agrin is a HSPG that is highly enriched in the glomerular basement membrane of the kidney and is present in other mammalian tissues [27,28], but it does not have a defined homologue in *Drosophila* [29]. However, the core structural components of basement membrane (laminin, collagen IV, perlecan and nidogen) are highly conserved between *Drosophila* and mammals. These core proteins were the focus of my study and therefore will be the focus of this literature review. Prior to discussing how these components come together to form a basement membrane, this section will first describe each component individually. There are many different versions of these core components, especially in mammals. For the sake of simplicity, only the classical structure of each protein is illustrated below (Fig. 1A). As each component is discussed below, the reader is encouraged to refer to Figure 1 for a visual aid.

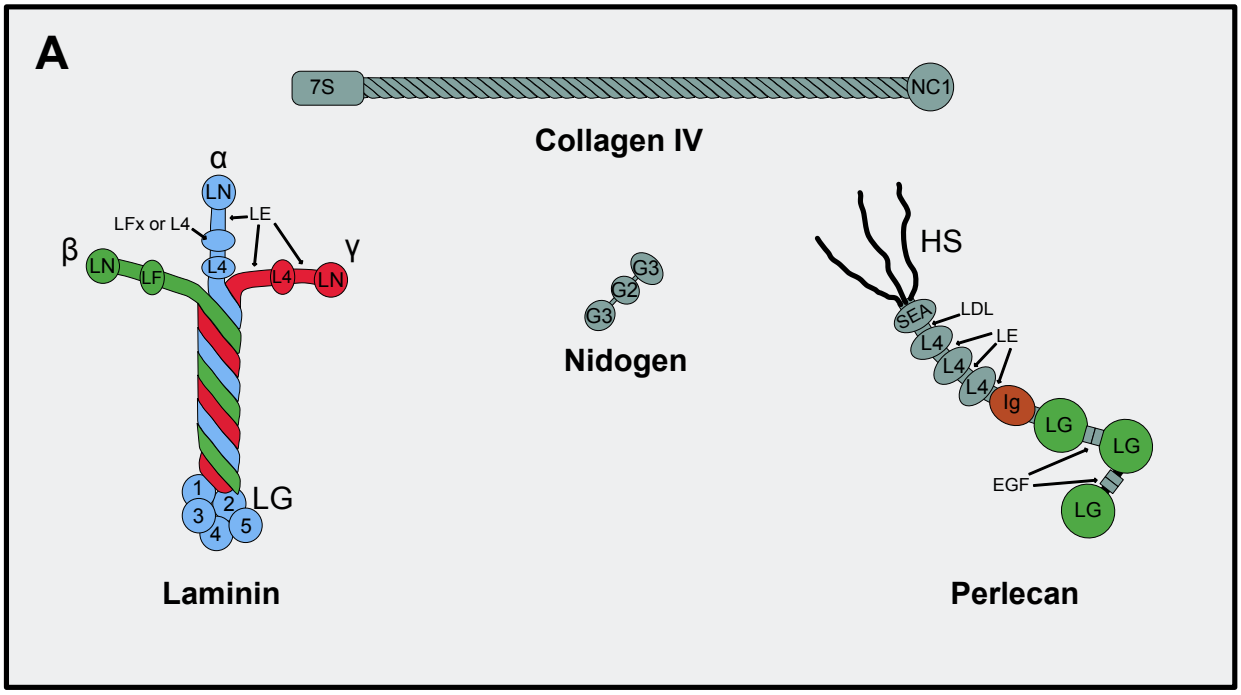
A
7S
NC1
Collagen IV
α
LN
LFx or L4
LE
β
LN
LF
L4
L4
γ
LN
1
2
3
4
5
LG
Laminin
G3
G2
G3
Nidogen
HS
SEA
LDL
L4
LE
L4
L4
Ig
LG
LG
EGF
LG
Perlecan

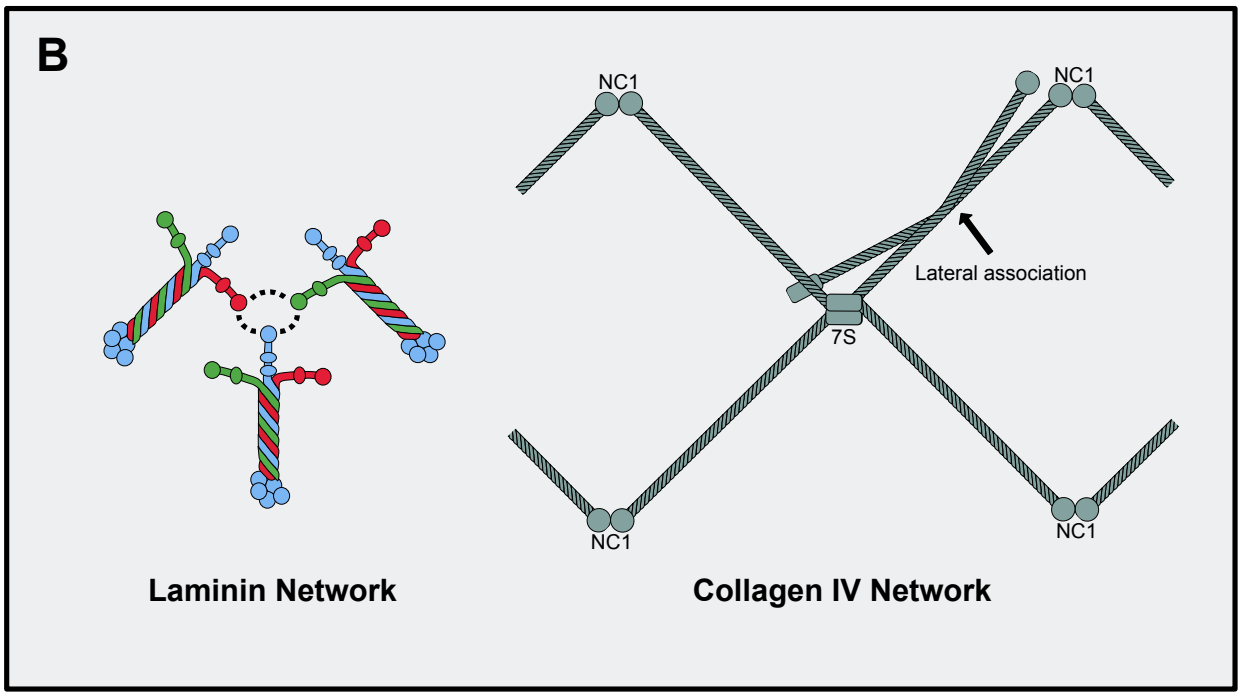
B
Laminin Network
NC1
NC1
Lateral association
7S
NC1
NC1
Collagen IV Network

Figure 1: Core basement membrane components. A) Laminin, collagen IV, perlecan, and nidogen make up the core components of basement membrane that are conserved from *Drosophila* to mammals. Laminin is a glycoprotein that is composed of three subunits (α, β, and γ). The exact combination of domains present in laminin varies depending on which subunits are incorporated into the heterotrimer. However, these components can contain carboxy-terminal globular domains (LG domains), amino-terminal globular domains (LN domains), epidermal growth factor-like repeats (LE domains), and globular domains that interrupt LE domains (L4, LF and LFx domains). Collagen IV is a heterotrimer that is composed of three α subunits. These subunits wrap around one another in a triple-helix, forming a protomer with a carboxy-terminal NC1 head and an amino-terminal 7S domain, connected by a collagenous domain. Perlecan is a heparan sulfate proteoglycan (HSPG) with laminin-like LG domains and EGF-like domains near its carboxy-terminal end, followed by Ig-like repeats, then laminin-like L4 and LE domains, followed by LDL-receptor repeats and a sea urchin enterokinase and agrin domain (SEA domain). Heparan sulfates are attached at the amino terminus.
Nidogen consist of three globular domains separate by two rod-like domains.
B) Laminin networks form by non-covalent bonds between LN domains on the short arms of each heterotrimer. Collagen IV networks form by covalent bonds between the NC1 heads of two protomers and the 7S domains of four protomers. Lateral associations between the collagenous domains of collagen IV have also been reported. The illustrations in this figure are not drawn to scale. This figure was informed by illustrations in Yurchenco, 2011 [3].

Laminin

Laminin was first identified as a non-collagenous glycoprotein in the basement membrane of the Engelbreth-Holm-Swarm (EHS) tumor [30]. It is a large heterotrimer [31,32], 400-800 kDa in mass [3] and approximately 100 nm in length [33,34], that self-associates to form networks *in vitro* [35]. Each trimer is composed of an α, β, and γ subunit [36] wrapped around one another through their coiled-coil domains [37] and held together by disulfide bonds [30]. The resulting protomer contains four arms: three short arms and one long arm [38]. The three short arms of laminin are formed by the amino-terminal sides of each polypeptide, which contain multiple globular domains. There are LN globular domains at the amino-terminus of each arm, excluding the α3A and α4

subunits in mammals [3], and additional globular domains, more proximal to the center of the heterotrimer, that vary between subunits [36]. The LN globular domains on each short arm, have been shown to be necessary for the polymerization of laminin networks *in vitro* [34,39] (Fig. 1B). The long arm of laminin begins where the three subunits wrap around one another and ends at the carboxy-terminal globular domains (LG domains) of the α subunit [36]. The LG domains appear to be the primary binding sites for cell surface receptors [14,40-42], though the LN domain of the α subunit appears to bind integrins as well [12,43,44].

In mammals there are five α, four β and three γ subunits [3]. Despite the many possible combinations of each subunit, only 16 distinct trimers have been found in nature [6] and it appears that the number of possible trimers is restricted by the presence of charged residues within the coiled coil domains [45]. Which protomers are present in a given tissue can vary. *Drosophila* laminins, on the other hand, only have two α subunits [46-48], one β subunit, and one γ subunit [49], allowing for only two types of laminin protomers.

Collagen IV

Collagen IV appeared early in the evolution of metazoans [5]. By weight, collagen IV is the most abundant component in the basement membrane [50]. It is a large heterotrimer, with each subunit being 180 kDa and the entire protomer being 400 nm in length [50,51]. Each subunit, referred to as an α chain, contains an amino-terminal 7S domain, a triple helical domain through which the subunits wrap around one another, and a carboxy-terminal NC1 domain [3]. In mammals, there are six α chains that come

together to form three distinct protomers: α112, α345, and α556 [52]. The α112 protomer is the first to appear during mouse embryogenesis [53] and exists in the basement membranes of all tissues [52]. The genes coding for the α1 and α2 chains are located adjacent to one another and share a bidirectional cis-regulatory sequence [54,55]. In *Drosophila*, only two α chains exist to create one protomer that is analogous to the α112 protomer observed in mammals [49]. The genetic loci of the α1 and α2 chains are also adjacent to one another and share a bidirectional cis-regulatory sequence [56,57].

Once secreted into the basement membrane, collagen IV protomers form a covalently cross-linked network (Fig. 1B) that stabilizes the basement membrane [53] and provides its mechanical stiffness [58]. At the amino end of each protomer, the 7S domains are cross-linked by lysyl oxidase-like 2 (LOXL2) [59] to form a tetramer of collagen IV protomers [51,60]. At the carboxy-terminal end, two protomers are cross-linked together by their NC1 heads [51]. This covalent bond, the sulfilimine bond [61], is a unique feature of collagen IV that appears to have evolved in conjunction with it [62]. The sulfilimine bond is catalyzed by peroxidasin [63], using bromine as a cofactor [64]. Finally, collagen IV protomers also associate with one another via lateral interactions between their triple helical domains [65,66].

Nidogen

Nidogen is a 150 kDa glycoprotein, composed of a single polypeptide [67], that is approximately 20 nm in length [68]. Its primary function is thought to be linking other basement membrane components together [67-69]. It is composed of three globular domains separated by two rod-like domains [68]. While invertebrates only possess one nidogen gene [49], vertebrates have two distinct nidogens that code for similar, but not

identical polypeptides [70]. Both nidogen-1 and nidogen-2 are expressed in most tissues in mice, but the levels of expression vary. For example, the basement membranes of heart and skeletal muscles in adult mice contain significantly less nidogen-2 than the basement membranes of blood vessels. Overall, the amount of nidogen-2 present throughout mice is only 3-18% that of nidogen-1 [71]. Despite these differences, nidogen-2 appears to be able to compensate for nidogen-1 deficiencies in mice [72].

Perlecan

Perlecan is the most abundant of basement membrane HSPGs [50]. Its single polypeptide protein core is almost 470 kDa in mass [73] and approximately 100 nm in length [74]. The three heparan sulfate side chains attached at its N-terminus are approximately 65 kDa each [75]. The heparan sulfate side chains are located within the first of five domains, and they provide perlecan with the potential to interact with and mediate the diffusion of secreted growth factors, such as VEGF [76], FGF [77] and TGFβ [78]. Domain II contains a low-density lipoprotein receptor (LDL receptor) motif that may play a role in LDL retention during the development of atherosclerosis [79]. The third domain is composed of laminin-like L4 and LE domains, shown to interact with FGF [80,81], and PDGF [82]. Domain IV is made up of multiple immunoglobin (Ig) domains, and has been shown to interact with PDGF [82], nidogen, and moderately with collagen IV [83,84]. Finally, the fifth domain, containing the C-terminus, is made of laminin G and EGF-like domains that can be cleaved to produce a fragment known as endorepellin, which is thought to inhibit angiogenesis [85].

Building a basement membrane: *de novo* assembly

Laminin polymers are widely believed to be the scaffolding upon which basement membranes are assembled. In both mouse and *Drosophila* embryos, the loss of laminin expression results in a failure to recruit other basement membrane proteins, leading to embryonic death [86,87]. The formation of laminin polymers appears to require cell surface receptors that recruit laminin protomers and increase its local concentration [88-90]. In contrast, the loss of collagen IV, the other polymer-forming basement membrane component, does not appear to be required for laminin or nidogen recruitment to the basement membrane. It does, however, still lead to embryonic death later in development, presumably due to a disruption in the basement membrane's overall structure [53]. It appears that, while the non-covalently bound laminin network initiates basement membrane construction, the heavily cross-linked collagen IV network reinforces basement membrane structure.

Early biochemical studies suggested that laminin and collagen IV networks were linked to one another via nidogen. *In vitro*, it was possible to isolate complexes of laminin, nidogen, and collagen IV, or nidogen and collagen IV, but not laminin and collagen IV in the absence of nidogen [68]. The G3 globular domain of vertebrate nidogen 1 has been shown to associate with the epidermal growth factor-like domain (LE domain) of laminin γ1 chain [91-93], while the G2 domain binds to the triple helix of collagen IV [68,69].

In vivo, however, the story appears to be more complicated. In *C. elegans*, nidogen is not required for collagen IV incorporation into the basement membrane of body wall muscles during development. Furthermore, *C. elegans* lacking nidogen show

no obvious defects in morphology or motility, though they do seem to produce less offspring [94]. Similarly, in *Drosophila*, the loss of nidogen does not noticeably affect viability, but does decrease fertility. While nidogen mutant flies do show basement membrane defects in the fat body and muscles, the physiological consequences of these defects appear to be mild [95]. In contrast, the loss of nidogen 1 and 2 in developing mice leads to basement membrane defects in various organs, resulting in death shortly after birth. However, not all basement membranes are affected by the loss of nidogen in mice. The glomerular basement membrane of the kidneys, for example, is seemingly unperturbed in the absence of nidogen, even while the tubular basement membrane of the kidneys is disrupted [96]. Altogether, the data suggests that nidogen plays a critical role in bridging basement membrane components in some circumstances, while being unnecessary in others.

Perlecan provides additional linkages between basement membrane components. Domain IV of perlecan binds directly to the G2 domain of nidogen, while domain V binds directly to the cell surface via dystroglycans, integrins, and sulfatides [83,84,97,98]. In *Drosophila* larvae perlecan has been shown to require collagen IV for its incorporation into the basement membrane of wing discs [99]. Additionally, perlecan appears to help connect the laminin and collagen IV networks in the basement membrane of human skin, with the core protein associated to laminin and heparan sulfate side chains associated to collagen IV [100].

Basement membrane repair

One of the most dramatic examples of basement membrane dynamics occurs during wound healing. When a tissue is damaged, the basement membrane will often be damaged as well, and repairing the basement membrane appears to be an important step in reestablishing tissue homeostasis. For example, the basement membrane of the cornea appears to be responsible for preventing TGFβ penetration into the underlying stroma. When the basement membrane is damaged, TGFβ is found in the underlying stroma and triggers a fibrotic response. The restoration of basement membrane appears to determine whether or not such a fibrotic response leads to the development of stromal haze post injury [101-103]. Despite the importance of basement membrane repair, surprisingly little is known about the mechanisms driving it, especially when compared to what is known about *de novo* basement membrane assembly. What little information is known about basement membrane repair comes mostly from observations in mammals.

In repairing human skin, for example, basement membrane proteins appear to originate from multiple locations. Laminin is mostly expressed in the epidermis while collagen IV is primarily expressed in the underlying dermis [104]. Furthermore, studies using cultured human skin cells have shown that both keratinocytes and fibroblasts can produce basement membrane proteins [105]. In human corneas, stromal keratocytes express both perlecan and nidogen following injury [106].

The timing of basement membrane repair, relative to reepithelialization, has also been studied in mammals. In the skin of Yorkshire pigs, the appearance of laminin and collagen IV appears to lag behind the leading edge of migrating epidermal cells during

wound repair [107], suggesting that epidermal-dermal contacts must be re-established before laminin and collagen IV are deposited. Similarly, in the skin of guinea pigs, epidermal cells migrate over a provisional matrix that lacks laminin and collagen IV, which later reappear after the wound has closed [108]. However, whether or not basement membrane repair occurs via a specified hierarchy between components, as has been established during *de novo* assembly, remains an open question.

One of the primary hurdles to interrogating this aspect of basement membrane repair in mammals is the fact that all of the core basement membrane proteins are necessary for life [53,96,109,110]. To overcome this obstacle, I turned to an already established wounding model in *Drosophila* larvae [111]. *Drosophila melanogaster* possess many similarities to mammals in both the composition of their basement membranes and in the mechanisms by which they heal wounds. Additionally, *Drosophila* are exceptionally amenable to genetic manipulation, allowing for the spatial and temporal control of dsRNA expression. This allowed for the depletion of *Drosophila* larvae basement membrane proteins post embryogenesis and prior to wounding, making it possible to interrogate aspects of basement membrane repair and its overall role in the wound healing process. Using this model, I sought to examine the morphology of repaired basement membrane, to determine the source of each component during wound repair, and to determine which components, if any, are dependent on one another for their proper incorporation during repair.

Chapter 2 of this thesis will discuss the details of these experiments and their results. Chapter 3 will address the significance of these results, what questions they raise, and propose future experiments to answer those questions. Finally, to further put

in perspective the importance of basement membrane composition and morphology, the appendix at the end of this thesis will review how the biomechanical properties of basement membrane affect development in *Drosophila melanogaster*.

Chapter 2

A scar-like lesion is apparent in basement membrane after wound repair *in vivo*

This chapter has been adapted from Ramos-Lewis, W., LaFever, K., Page-McCaw, A. A scar-like lesion is apparent in basement membrane after wound repair *in vivo*. *Matrix Biology* 74, 101-120 (2018). doi: 10.1016/j.matbio.2018.07.004

Introduction

Basement membrane is the most ancient and conserved type of extracellular matrix in the animal kingdom [5], and it lies under the basal surface of epithelia and wraps around muscles, nerves, and other organs [6]. Basement membrane is also important for signaling, as it can interact with signaling ligands both to promote their activity [21] and conversely to constrain their diffusion [112]. Experimentally, it has been shown that basement membrane confers mechanical stiffness to tissues, important for shaping organs and determining cellular behaviors [58,113-116]. Because of such mechanical functions, the dynamic nature of basement membranes has often been overlooked, but these matrix structures expand and shrink along with tissue growth and destruction, and they must be repaired after injury. These dynamic activities occur in the context of continuing basement membrane mechanical functions.

Basement membranes are composed of four main types of glycoproteins and proteoglycans: laminin, collagen IV, nidogen, and perlecan, and these have been analyzed *in vitro* and *in vivo*. The first is laminin, a heterotrimeric protein that

polymerizes into a two-dimensional scaffold. Laminin binds directly to cell-surface molecules such as integrins and dystroglycans, and these cell surface interactions increase the local concentration of laminin to promote polymerization at cell membranes [16], which appears to be the first step of making a new basement membrane. The second glycoprotein is collagen IV, a non-fibrillar collagen that assembles into a covalently reinforced sheet that gives basement membrane its mechanical stiffness. Although collagen IV can self-assemble *in vitro* [66], *in vivo* the *de novo* assembly of collagen IV into an embryonic basement membrane requires the presence of laminin in both mice and flies [53,87]. The glycoprotein nidogen binds to laminin and collagen IV *in vitro* [68,117,118]. Finally, perlecan is a large heparan sulfate proteoglycan [75], which binds with high affinity to nidogen *in vitro* [84]; yet *in vivo*, perlecan requires collagen IV for its deposition into basement membranes of the fly wing disc [99]. Thus, the binding interactions of these matrix proteins *in vitro* and the genetic data from animal studies suggest a partial hierarchy of assembly *in vivo*: laminin, then collagen IV, then perlecan.

In contrast with basement membrane assembly, there is a paucity of information about how the basement membrane is repaired after damage. Repairing basement membrane is important, as epidermal basement membranes become damaged after sun (UV) exposure, possibly contributing to skin aging [119]; damage of the glomerular basement membrane leads to renal disease [120]; and basement membrane repair after corneal injury appears to reverse injury-induced visual haze [103]. The repair of injury-induced basement membrane damage has been studied primarily in the cornea. When the corneal epithelium and adjacent basement membrane were removed in

experimentally-induced wounds, epithelial cells closed the wounds within 4-6 days. Around this time, patches of repaired basement membrane were evident, and after 4 weeks increased levels of laminin and collagen IV were detected [121]. However, the repaired basement membrane became functional in terms of cell adhesion only after months [122]. These studies establish that the basement membrane can be repaired after wounding and suggest it may be altered after repair. To date, no studies have manipulated the various basement membrane components to examine the effect on its repair.

We have chosen to analyze basement membrane repair in the fruit fly, *Drosophila melanogaster*. Like vertebrates, *Drosophila* has the same core conserved basement membrane components of laminin, collagen IV, nidogen, and perlecan. An advantage of *Drosophila* over vertebrates, however, is that there are far fewer genes encoding each component, making it easier to eliminate components of basement membranes. For example, targeting *LanB1* knocks down all laminin heterotrimers; targeting either *vkg* or *Col4a1* knocks down all collagen IV heterotrimers; targeting *Ndg* knocks down the single nidogen gene, and targeting *trol* knocks down the single perlecan gene [116]. The sophisticated genetic tools of *Drosophila* further allow for spatial and temporal knockdown of each gene. Finally, each of these core basement membrane proteins has been tagged with GFP to permit easy visualization.

In this study, we analyze the repair of the epidermal basement membrane in larvae after a mechanical wound about 100-200 μm across. In similar *Drosophila* larval wounds, it has been observed that basement membrane is present on epidermal cells as they migrate to close the wound [111]. Although this observation seems to suggest that

the epidermal cells secrete the repairing basement membrane components, we report here that both unwounded and repaired epidermal basement membrane is assembled from proteins secreted from adipose and muscle tissue. Further, we show that basement membrane is repaired within 24h after damage, although each component repairs with a visible scar. We investigate the requirements for assembly and find that collagen IV is incorporated into these wound sites independently of the synthesis of new laminin, unlike newly assembled embryonic basement membranes. Not every protein incorporates independently, however, because we find that nidogen requires laminin, and perlecan requires collagen IV for proper assembly into the repairing basement membrane.

Materials and methods

Fly husbandry

Flies were maintained on cornmeal-molasses media supplemented with dry yeast. Flies are listed in Table 1. For all experiments with GFP-labeled BM proteins, flies contained a single copy of the GFP-labeled protein. For basement membrane source experiments, crosses were carried out at 25^{o}C (Fig. 2A). For functional experiments requiring conditional knockdown with *Gal4/Gal80^{ts}*, including basement membrane order of assembly experiments, the following conditions were used: for *LanB1, vkg*, and *trol* knockdown experiments, parents were allowed to pre-mate for 2-3 days at 18^{o}C (permissive temperature) and then moved to fresh bottles to lay for 24 h at 18^{o}C. Parents were removed and embryos developed an additional 24 h at 18^{o}C for *LanB1* and *trol* knockdown experiments, or for an additional 48 h for *vkg* knockdown

experiments. Bottles were then shifted to 29°C (knockdown conditions) and larvae developed to the foraging 3rd instar stage, approximately 4 days for *LanB1* and *trol* knockdown experiments and 3.5 days for *vkg* knockdown experiments (Fig. 2B). 3rd instar larvae were identified by branching of the anterior spiracles. For *Ndg* knockdown experiments, crosses and progeny were maintained at 29°C.

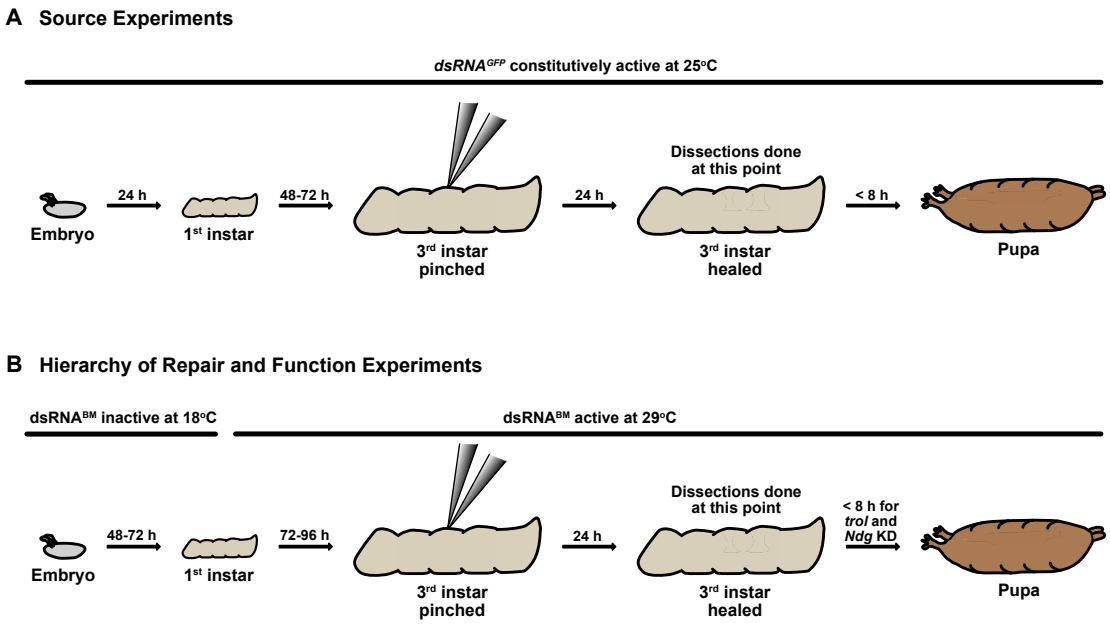

Figure 2: Timeline of experimental protocols for gene knockdown, showing larval development, dsRNA expression, and wounding. A) For all basement membrane source experiments, animals were maintained at 25°C. Larvae developed to early 3rd instars, were pinched, and usually recovered 24 h before dissecting. For experiments where no wound was inflicted, larvae developed to late 3rd instar prior to dissecting. **B)** For basement membrane hierarchy of repair and function experiments in which *LanB1, vkg*, or *trol* was knocked down, embryos were laid and allowed to develop to 1st instar larvae at 18°C, with dsRNA not expressed. During 1st instar, bottles were shifted to 29°C to promote dsRNA expression, and larvae developed to early 3rd instar prior to wounding. After wounding, larvae recovered for 24 h at 29°C prior to dissecting. For *Ndg* KD experiments, bottles were maintained at 29°C for the entire experiment (not shown). Only control, *trol* KD and *Ndg* KD larvae were capable of pupariating. $dsRNA^{BM}$ denotes dsRNA against *vkg, trol,* or *LanB1*.

Table 1: Fly Stocks

Genotype	Source
LanB1GFP	VDRC 318180
vkgGFP^{791}	Sally Horne-Badovinac, U. Chicago [123]
vkgGFP^{205}	[124]
trolGFP^{1973}	[124]
NdgGFP	VDRC 318629
w^{1118}	Todd Laverty, Janelia Farm
UAS-GFP^{S65T}	BDSC 1522
Tub-Gal4/TM6B	[125]
e22c-Gal4	BDSC 5083
A58-Gal4/TM6B	Michael Galko, MD Anderson Cancer Center
Pnr-Gal4/TM6B	Beth Stronach, University of Pittsburgh
Hml-Gal4	BDSC 30139
Mhc-Gal4	BDSC 55133
C564-Gal4	Kathryn V. Anderson, Sloan Kettering
UAS-dsRNA^{GFP}	BDSC 9330
UAS-dsRNA^{vkg}	VDRC 106812
UAS-dsRNA^{Col4A1}	BDSC 44520
w; UAS-dsRNA^{LanB1}	VDRC 23121 (main line used)
y sc v; UAS-dsRNA^{LanB1}	BDSC 42616 (alternate line)
UAS-dsRNA^{trol}	VDRC 1110494
UAS-dsRNA^{Ndg}	VDRC 109625
w; VkgGFP^{205}; TubGal4, TubGal80^{ts}/ SM6-TM6B	This study
w; VkgGFP^{791}; UAS-dsRNA^{GFP}	This study
w; UAS-dsRNA^{GFP}; LanB1GFP	This study
w; LanB1GFP TubGal4 TubGal80^{ts} / TM6B	This study
w TrolGFP^{1973}; UAS-dsRNA^{GFP}	This study
w TrolGFP^{1973}; TubGal4, TubGal80^{ts} / TM6B	This study
NdgGFP, UAS-dsRNA^{GFP}	This study
NdgGFP TubGal4 TubGal80^{ts} / TM6B	This study
w; vkgGFP^{205} / CyO, sChFP; TubGal4, TubGal80^{ts} / TM3, sChFP	This study
w; LanB1GFP TubGal4 TubGal80^{ts} / TM3, sChFP	This study
CyO, sChFP	BDSC 35523
TM3, sChFP	BDSC 35524

Epidermal pinch-wounding

Third-instar larvae were pinched on the dorsal side between the hair stripes segments A3 and A4 for approximately 10 sec with blunted #5 dissecting forceps (Dumont), as adapted from Galko and Krasnow (2004). Care was taken to not puncture the cuticle. However, in *Tub>dsRNA*^{LanB1} larvae the cuticle was more easily damaged than in other larvae, leading to small areas of melanization that autofluoresce in the green channel. Melanization was most visible when Ndg-GFP was imaged (see Fig. 7Q) because the GFP signal is particularly faint in the *LanB1* knockdown. After wounding, larvae recovered on grape juice plates, with access to wet yeast, for 24 h. If larvae were raised at 29^{o}C, then recovery from wounding was also at 29^{o}C; otherwise recovery was at 25^{o}C.

Larval dissection, fixation, and immunohistochemistry

Larvae were decapitated at the cerebral tracheal branch in chilled PBS and filleted along the ventral side. Dissections were performed in PBS + 4% paraformaldehyde, and immediately larval pelts were pinned flat and fixed for 20 min. Samples were washed at room temperature (RT) in PBS + 0.2% Triton X-100 (PBT-X), 2X 5 min. each and 1x 30 min. The pelts were blocked in PBT-X + 5% normal goat serum + 0.02% NaN_3 for 3 h at RT and then incubated in 1° antibodies overnight at 4^{o}C. The following day, pelts were washed twice in PBT-X (1 h per wash) at RT followed by incubation in 2° antibodies for 2 h at RT. Lastly, they were washed in PBT-X for 2 h at RT and quickly washed in PBS prior to mounting on glass slides in Vectashield mounting media with DAPI (Vector Laboratories, Burlingame, CA). For antibodies, rabbit

Anti-GFP (Torrey Pines Biolabs, Secaucus, NJ, catalog number TP401) was used at a 1:200 dilution for imaging Vkg-GFP, Trol-GFP and LanB1-GFP. For imaging Ndg-GFP, Rabbit Anti-GFP (Abcam, catalog number ab6556) was used at a 1:1000 dilution. For imaging FasIII, Mouse 7G10 Anti-FasIII (Developmental Studies Hybridoma Bank, Iowa City, IA) was used at a 1:10 dilution. Secondary antibodies (Jackson Immunoresearch Laboratories, West Grove, PA) were FITC Donkey Anti-Rabbit (code number 711-095-152) and Cy3 Goat Anti-Mouse (code number 115-165-206), each used at 1:500.

Gal4 driver characterization

Gal4 drivers were used to constitutively express GFP in each of the candidate tissues tested. Upon reaching the 3rd instar stage, larvae were dissected and fixed as described above. The entire animal carcass was inspected for GFP expression, with special attention paid to the epidermis, muscles, and fat body. Exposure levels were kept the same between tissues of the same animal in Fig. 7A-D. For *Hml-Gal4* expression, intact larvae were imaged to prevent loss of hemocytes upon dissection.

Microscopy

To image larval pelts and fixed embryos, optical sections were taken using a Zeiss Apotome mounted to an Axio Imager M2 using the following objectives: 10x/0.3 EC Plan-NeoFluar, 20x/0.8 Plan-Apochromat, or 40x/1.3 EC Plan-NeoFluar. Images were acquired with an AxioCam MRm (Zeiss, Thornwood, NY) camera, X-Cite 120Q light source (Excelitas Technologies, Waltham, MA) and AxioVision 4.8 (Zeiss) software. All stacks were exported to ImageJ, version 1.48v (National Institutes of Health, Bethesda, MD), as 16-bit, grayscale, ZVI files for analysis. For basement

membrane source experiments in unwounded larvae, exposure levels were matched to control samples imaged on the same day. For all other experiments, exposure levels were optimized independently. For live embryos, images were acquired with a Zeiss Axiocam MRc camera mounted to a Zeiss Lumar V12 stereomicroscope, using a Neolumar S 1.5x objective, X-Cite 120Q light source and Axiovision 4.8 software. Images were exported to ImageJ version 1.48v, as 8-bit TIFF files, for analysis.

Mean fluorescence intensity measurements and analysis

For basement membrane source experiments (Fig. 6), knock-down animals were always stained for GFP simultaneously with control animals (no knockdown). After staining, a representative region of basement membrane was imaged for each larva by compiling optical sections into a maximum projection, saved as a TIFF file in ImageJ 1.48v software. The ImageJ Measure tool was used to record mean fluorescence intensity for each animal from representative X-Y regions of basement membrane, selected by the absence of obscuring tissue or tears. The mean intensity for each animal was imported into Microsoft Excel and normalized to the mean of the control (no knockdown) samples that were stained simultaneously. Normalizing the mean fluorescence for each larva allowed fluorescence to be compared between experiments without concern for fluctuations in illumination intensity or antibody batches. Normalized data was imported into GraphPad Prism 7.0d and an ANOVA test was used to determine statistical significance among all datasets. An unpaired t-test coupled with a Bonferroni correction was then used to determine significance between two data sets of interest. For these experiments Trol-GFP was analyzed only in female larvae because of dosage compensation on the X chromosome.

For wounded samples (Fig. 8), mean fluorescence was measured from max projections in the repaired region (defined by the indentation of the cuticle following pinch-wounding) and in a representative unwounded region within the same image. The ratio between the two measurements for each sample was then calculated in Excel, and the ratio data was plotted and analyzed in GraphPad. Unpaired t-tests were used to determine significance between control and experimental datasets.

For embryo samples (Fig. 13), images were imported into ImageJ version 1.48v and the Measure tool was used to measure average fluorescence intensity of whole embryos. An ANOVA test was used to determine statistical significance among all data sets, followed by unpaired t-tests coupled with a Bonferroni correction to determine significance between specific data sets.

Fluorescence anisotropy measurements and analysis

Using ImageJ, optical sections were compiled into maximum projections and saved as TIFF files for analysis. Because the least fluorescence within a repaired wound area was found underneath the nuclei, we calculated the mean fluorescence under the nuclei by tracing the nuclei within the cuticle-indentation borders (marking the wound) and calculating the mean fluorescence within these sub-nuclear regions. To reproducibly identify the maximal intensity of basement membrane deposition within the wound, we used the Threshold and Measure tools to record the mean of the top 5% of pixel values. Fluorescence anisotropy within the repaired wound was calculated as the ratio of the top 5% pixel values over the subnuclear fluorescence. This ratio was imported into GraphPad Prism 7.0d and an ANOVA test was used determine statistical

difference among all datasets. Unpaired t-tests coupled with a Bonferroni correction were used to determine significance between specific datasets.

Embryo collection, fixation, and immunohistochemistry

Fattened females were allowed to lay eggs on grape juice-agar plates with wet yeast at 29°C for 4 h, and embryos were aged at 29°C for 9-10 h. To collect embryos for live measurement of LanB1-GFP fluorescence, embryos were rinsed into a beaker with 50% bleach and swirled for 2 min. to remove the chorion and then washed with water and gently blotted dry, then transferred to grape plates and immediately imaged on a fluorescence stereomicroscope (see above). *LanB1-GFP, tub-Gal4/+; UAS-dsRNA^{LanB1}* were compared to siblings lacking *UAS-dsRNA^{LanB1}*, identified by the presence or absence of the red balancer *TM3, sChFP.*

To analyze Vkg-GFP assembly along the ventral nerve cord when *LanB1* was constitutively knocked down in embryos, embryos of genotype *vkgGFP^{205}/+; TubGal4/UAS-dsRNA^{LanB1}* were compared to *vkgGFP^{205}/+; TubGal4/+*. Embryos were laid and aged as above. For fixation, embryos were transferred into 2 ml of 100% heptane in a glass vial. Next, 2 ml of 16% formaldehyde was added to the vial, bringing the embryos to the interface between heptane and formaldehyde, and the vial was shaken for 10 min. The formaldehyde and heptane were removed and replaced with 5 ml of fresh 100% heptane. To remove the vitelline membrane, 5 ml of 100% methanol was added and the vial was immediately shaken vigorously by hand for 30 s. The heptane and methanol were removed and replaced with 2 ml fresh methanol and transferred to an Eppendorf tube. Embryos were rehydrated and washed twice in PBS + 0.2% Triton X-100 (PBT-X) and blocked in 1% bovine serum albumin (BSA) in PBT-X

for 1 h on a rocker at RT. For imaging Vkg-GFP, mouse anti-GFP antibodies (UC Davis catalog # 73-131 and # 73-132) were used at a 1:5 dilution, rocking overnight at 4°C. The following day, embryos were washed in PBT-X three times for 30 min each, rocking at RT. Next, embryos were incubated in FITC Goat anti-Mouse (Jackson Immunoresearch Laboratories, West Grove, PA, code number 115-095-206) diluted 1:500 for 3 h rocking at RT. Finally, embryos were washed three times in PBT-X for 30 min each and once in PBS. All PBS was removed and embryos were resuspended in Vectashield mounting media with DAPI (Vector Laboratories, Burlingame, CA) prior to being mounted on a glass slide. To assess collagen IV assembly into basement membranes around the ventral nerve cord, stage 16-17 embryos were identified by gut morphology. *LanB1* knockdown embryos were identified by the absence of an mCherry balancer. The knockdown embryos were extremely fragile, and 3 intact embryos were identified. Collagen IV was not assembled along the ventral nerve cord grooves in any of them.

Western blots

From 10-100 3rd-instar larvae were frozen in liquid nitrogen and ground to a powder with a mortar and pestle; each larva yielded ~1 mg powder. The powder was re-suspended to a concentration of 50 mg/ml in ice-cold RIPA buffer (10 mM Tris-Cl pH = 8.0, 1 mM EDTA, 1% Triton X-100, 0.1% sodium deoxycholate, 0.1% SDS, 140 mM NaCl) plus 1x HALT protease inhibitor cocktail (Thermo Scientific). Samples were centrifuged for 15 min at 4°C at 16,110 x g. The supernatant, containing the soluble fraction, was removed and mixed with Laemmli sample buffer (1X). The pellet, containing the insoluble fraction, was washed 3X in 1 ml chilled RIPA buffer per 75 mg

original powder, and resuspended to 50 mg/ml by vortexing in RIPA buffer. The pellet suspension was mixed with Laemmli sample buffer (2X final concentration). Samples were boiled for 5 min. and spun for 30 s at 16,110 x g. 15-30 μl (equivalent to about 1 larva) was loaded onto either 10% or 4-20% SDS PAGE gels (Bio-Rad Laboratories), transferred to nitrocellulose (GE Healthcare) and incubated with 1° antibodies overnight at 4°C followed by 2° antibody incubation (Li-Cor) at 1:2000 for 1 h at RT. Blots were developed and imaged with the Odyssey Infrared Imaging System (Li-Cor Biosciences). The 1° antibodies used to detect GFP were Rabbit anti-GFP (Torrey Pines Biolabs, Secaucus, NJ, catalog number TP401) at a dilution of 1:1000 or Rabbit anti-GFP (Abcam, catalog number ab6556) at a dilution of 1:1000. Antibodies used for loading controls were Mouse anti-Actin (EMD Millipore, catalog number MAB1501R) at a dilution of 1:2000 and Goat Anti-GAPDH (Imgenex, catalog number #IMG3073) at a dilution of 1:2500). Actin was used as the loading control for the insoluble fraction while GAPDH was used as the loading control for the soluble fraction.

Results

A lesion in the basement membrane at the site of repair

To analyze basement membrane repair, we utilized an established larval epidermal pinch-wound assay first described by Galko et al [111]. The larval epidermis is an epithelial monolayer of extremely flat cells, roughly 40 μm in diameter and 3 μm thick, with highly polyploid nuclei. On the apical side these cells secrete a thick chitinous cuticle exoskeleton, and on the basal side they sit on a basement membrane, the source of which is not known. To generate epidermal wounds, larvae were pinched

with blunted forceps on the dorsal side for approximately 10 seconds to inflict cellular and basement membrane damage without breaking the outer cuticle, resulting in a sterile wound that is not visually occluded by hemolymph clotting (Fig. 3A, B). By 24h after wounding, the wounds had closed. Pinch wounding created a cuticle indentation mirroring the damage to the underlying epithelium, and this indentation remained visible by DIC optics even 24 h after wounding, providing a reliable landmark for the location of the wound during and after repair (Fig. 3B).

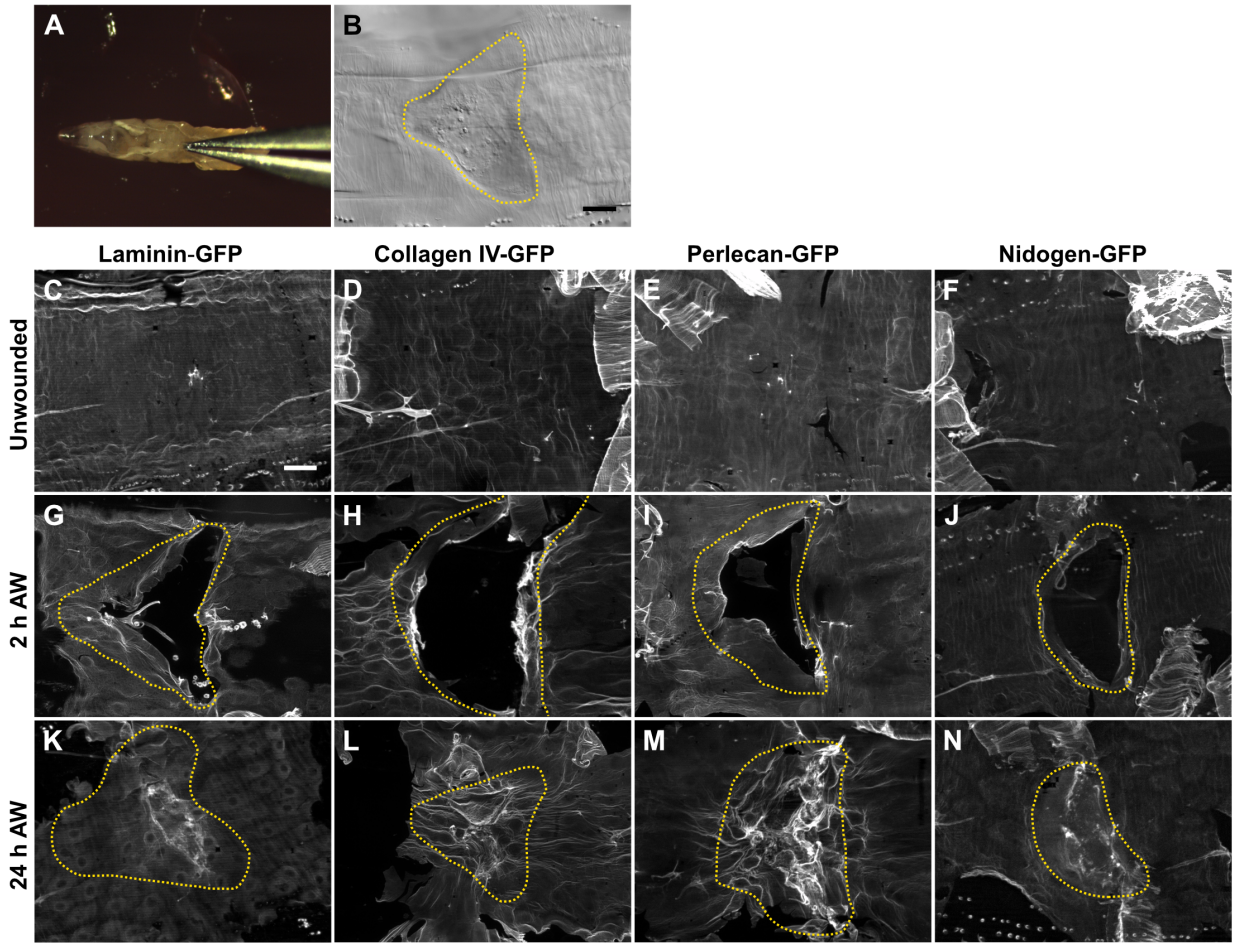

Figure 3: The basement membrane is damaged by pinch wounds and forms a scar upon repair.
A) To damage the basement membrane, blunt forceps were used to pinch larvae on the dorsal epidermis between the hair stripes of segments A3 and A4. **B)** Pinch wounds do not break the outer cuticle, but they do leave an indentation visible with DIC, outlined with yellow dotted line. **C-F)** Undamaged epidermal basement membrane visualized with GFP-fusion constructs of each of the core basement membrane proteins. Images are representative of the no-knockdown controls quantified in Fig. 6. **G-J)** Damaged epidermal basement membrane after pinch-wounding. **K-N)** Within 24 h, the basement membrane was repaired, leaving behind a visible scar in the region of the healed wound. Images are representative of the no-knockdown controls quantified in Fig. 8. Dotted yellow lines indicate original wound borders based on cuticle indentation. Scale bar, 50 μm.

To visualize basement membrane proteins, we used a functional GFP-fusion of each of the four main basement membrane proteins (Fig. 3C-F). Collagen IV and perlecan were imaged with *vkg-GFP* and *trol-GFP* protein-traps respectively, in which a GFP exon is inserted into the genomic region, resulting in the GFP fluorescent epitope spliced in-frame into the endogenous protein. These two GFP-fusion proteins are fully functional, as evidenced by their viability as homozygotes. Functional *LamininB1 (LanB1)-GFP* was provided as a transgene, a recombineered 44 kb genomic fragment encoding a C-terminal fusion of LanB1-GFP that fully rescued a *LanB1* mutant ([126] and our data not shown). *Nidogen (Ndg)-GFP* was also provided as a transgene, a recombineered 36 kb genomic fragment encoding a C-terminal fusion of Nidogen-GFP [126]. When imaged with each of these fusion proteins, the unwounded epidermal basement membrane appeared as a relatively smooth flat surface (Fig. 3C-F), although the epidermal fluorescence from Nidogen-GFP was considerably fainter than the other three fusion proteins. We refer to these four GFP fusion proteins collectively as BM-GFP.

After pinch-wounding, basement membrane and the overlying cells were visibly damaged at the site of the wound (Fig. 3G-J and Fig. 4), and the dimensions of damage were similar for both. Within 24 hours after injury, the basement membrane repaired to a continuous sheet in control animals. Strikingly, the basement membrane formed a lesion at the site of repair, evident with all four BM-GFP proteins (Fig. 3K-N). This lesion was characterized by regions of increased fluorescence, fibril-like in appearance, within the site of repair.

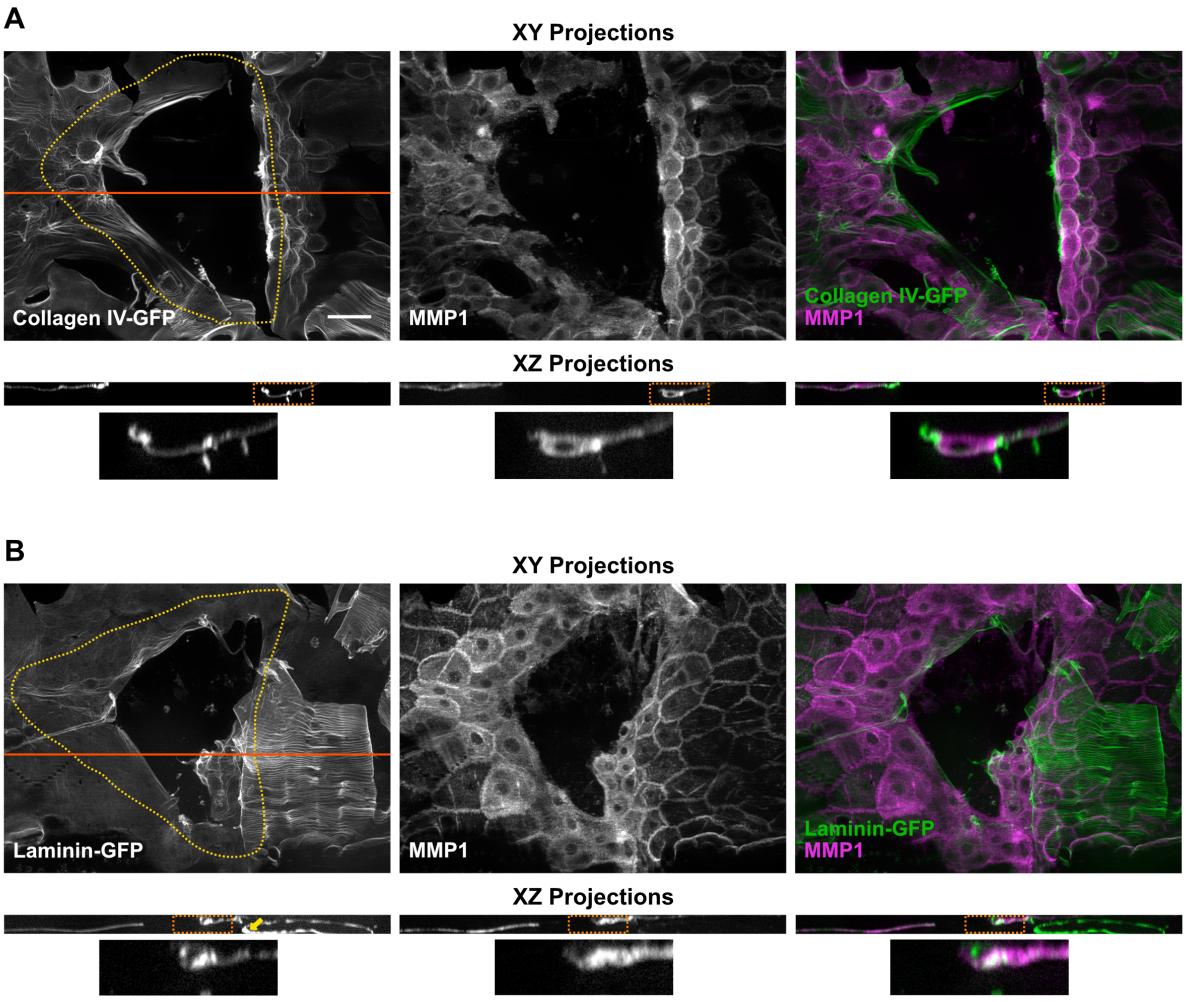

Figure 4: The damage in basement membrane mirrors associated cell damage. Basement membrane damage 2 h post wounding has similar dimensions to the overlying cell damage, as seen with collagen IV (A) or laminin (B). Yellow dotted lines indicate wound borders and orange solid lines indicate sections sampled for XZ projections. Orange dotted boxes indicate region of XZ projections that are magnified. Yellow arrow in Laminin-GFP XZ projection indicates muscle basement membrane. Scale bar, 50 μm.

These fibril-like structures were thicker than the unwounded basement membrane and were largely excluded from areas occupied by cell nuclei (Fig. 5). Furthermore, the thickening of basement membrane appeared to begin at the wound boundaries within 2 hours after pinch-wounding (Fig. 4). We refer to the matrix lesion that appears after repair as a basement membrane scar. As shown in Figs. 2 and 4, the basement membrane scar is typified by increased abundance of the basement membrane proteins collagen IV, laminin, perlecan, and nidogen in the area where the basement membrane was repaired, resulting in a thicker and more disorganized region of extracellular matrix.

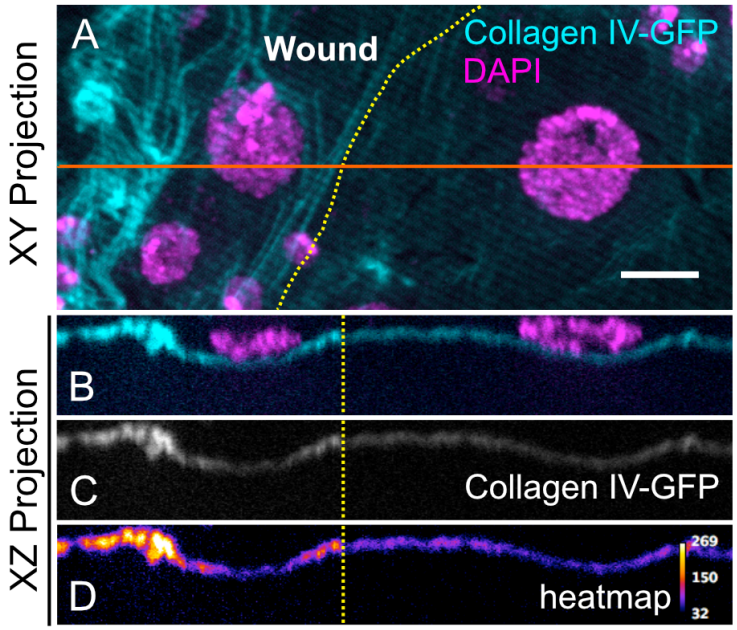

Figure 5: The basement membrane scar is thicker than unwounded basement membrane.
Yellow dotted lines indicate wound border. Orange solid line indicates location sampled for XZ projections. **A)** Basement membrane scar, evident on the left (wounded) side. **B-D)** Z-section shows increased thickness and fluorescence of collagen IV within the healed wound (N $\geq$ 3). Scale bar, 10μm.

The sources of epithelial basement membrane are the same during normal growth and wound repair

Since the repaired basement membrane within pinch wounds is morphologically distinct from the surrounding, undamaged basement membrane, the mechanism of repair may also be distinct from normal basement membrane assembly as the animal grows. One way repair might differ from assembly is in the source of each protein. During the 4 days after embryogenesis to the third larval instar, there is a dramatic ~40-fold expansion in epidermal area (8-fold in length and 5-fold in circumference [127]), requiring a similar expansion in basement membrane, but the source of these matrix proteins is not known. One possibility for either the growth source or the wound source is the epidermal cells. However, in *Drosophila*, there are many examples of basement membranes whose component proteins are derived from cellular sources that are not part of the tissue of a given basement membrane [116]. For example, as the *Drosophila* embryo develops, migrating hemocytes deposit matrix proteins to create *de novo* basement membrane throughout the tissues of the embryo, including the epidermis [128,129]. Intriguingly, after larval epidermal wounding, hemocytes are observed at the site of damage [130], so it seemed plausible that they may generate the matrix components required for basement membrane repair. Further, some vertebrate hemocytes secrete perlecan thought to promote wound repair [131]. A third candidate source is adipose tissue: other larval organs, including the wing disc and the ventral nerve cord, expand their basement membranes during growth by incorporating collagen IV secreted into the hemolymph from the fat body (*Drosophila* adipose tissue that regulates metabolism and immunity [99]). It seemed plausible that epidermal basement membrane might also incorporate collagen IV secreted from the fat body.

To determine the source of basement membrane in unwounded epidermis, we controlled the expression of each of the four BM-GFP fusion proteins in each of these candidate tissues, i.e., epidermis, hemocytes, and fat body, using an RNAi-based strategy. Each candidate tissue was engineered to specifically and constitutively express double-stranded RNA against GFP (*dsRNA*^{GFP}) in flies that contained a single allele of a BM-GFP. Importantly, expression of the wild-type matrix protein continued as normal throughout the animal's life so that the basement membrane itself was never disrupted, eliminating any compensatory mechanisms that might lead to expression from a different source tissue (Fig. 6A). The presence or absence of GFP in the epidermal basement membrane was used to assess the contribution of each candidate tissue (Fig. 6B). To control for the possibility of incomplete knockdown of GFP, we compared the basement membrane fluorescence after candidate tissue knockdowns to the fluorescence after ubiquitous knockdown with *Tub-Gal4* and to the autofluorescence within a tissue (Fig. 6C-F). Since the reliability of these experiments depended on the specificity of each driver used to express *dsRNA*^{GFP}, great care was taken to assess their specificity (Fig. 7), and we confirmed that *c564-Gal4* and *Hml-Gal4* were each specific to fat and hemocytes, respectively. Because the pan-epidermal drivers *A58-Gal4* and *e22C-Gal4* were not specific to epidermis but also expressed in the fat body of 3rd instar larvae (Fig. 7F, G), we knocked down GFP in the epidermis with *pnr-Gal4*, expressed in large patches along the dorsal side of the epidermis. Although the pattern of *pnr-Gal4* was not ubiquitous across the epidermis, we did not observe any pattern or

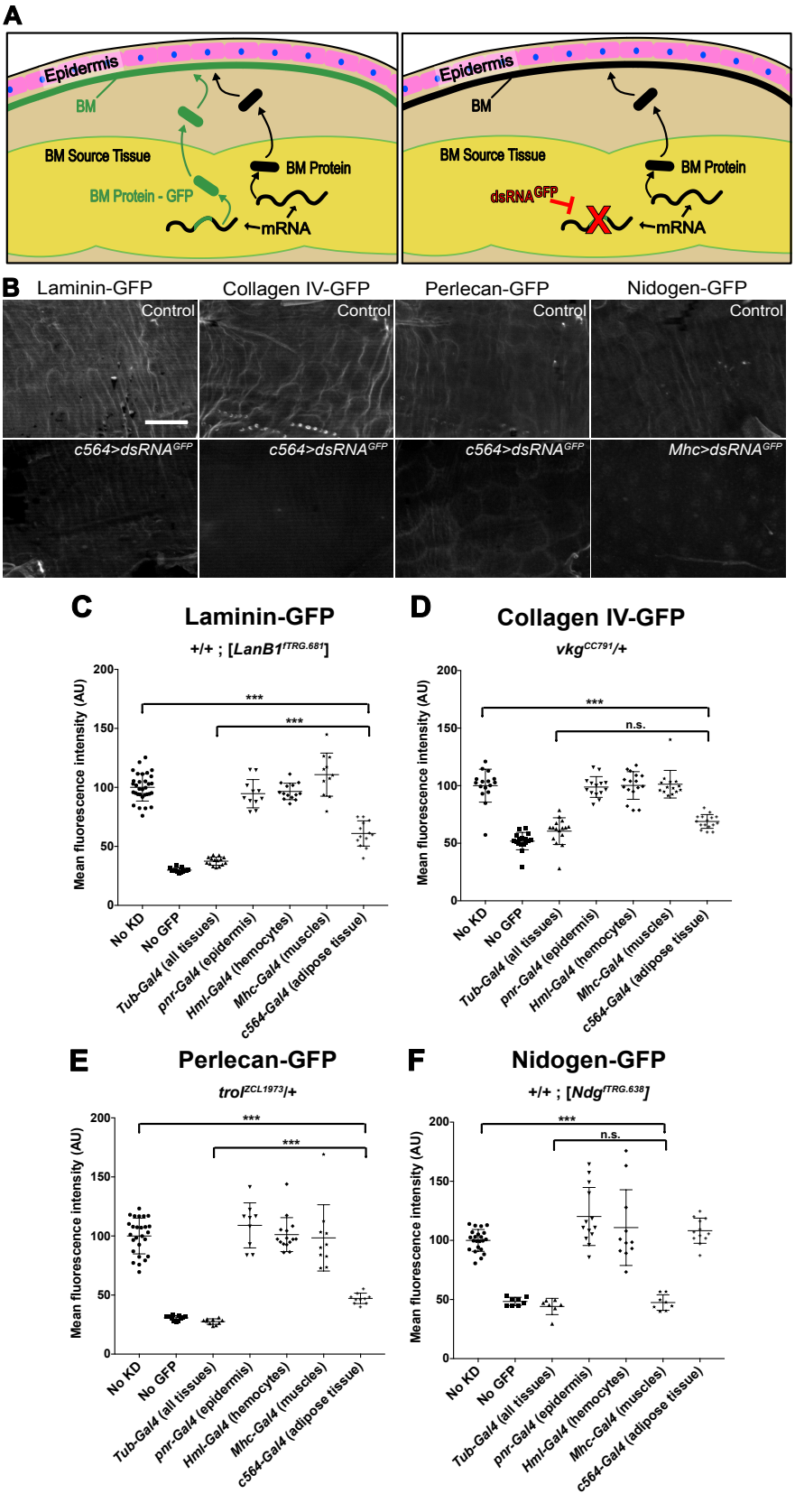
A
Epidermis
BM
BM Source Tissue
BM Protein
BM Protein - GFP
mRNA
dsRNA GFP
B
Laminin-GFP
Collagen IV-GFP
Perlecan-GFP
Nidogen-GFP
Control
c564>dsRNA GFP
Mhc>dsRNA GFP
C
Laminin-GFP
+/+ ; [LanB1 fTRG.681]
D
Collagen IV-GFP
vkg CC791/+
E
Perlecan-GFP
trol ZCL1973/+
F
Nidogen-GFP
+/+ ; [Ndg fTRG.638]
Mean fluorescence intensity (AU)
No KD
No GFP
Tub-Gal4 (all tissues)
pnr-Gal4 (epidermis)
Hml-Gal4 (hemocytes)
Mhc-Gal4 (muscles)
c564-Gal4 (adipose tissue)
***
n.s.

Figure 6: In unwounded epidermis, basement membrane proteins come from other tissues.
A) Experiment overview: tissue expressing a basement membrane protein allele fused to GFP (BM-GFP) and an allele not fused with GFP will secrete both forms for incorporation into the basement membrane, resulting in fluorescent basement membrane. When $dsRNA^{GFP}$ targets GFP in the source tissue, only the basement membrane protein lacking GFP will be secreted, resulting in non-fluorescent basement membrane. **B)** Example images without (top) and with (bottom) $dsRNA^{GFP}$ expression. Scale bar, 50 μm. **C-E)** Laminin-GFP, collagen IV-GFP, or perlecan-GFP is lost from the epidermal BM when $dsRNA^{GFP}$ is expressed in adipose tissue. **F)** Nidogen-GFP is lost from the epidermal BM when $dsRNA^{GFP}$ is expressed in the muscles. *** indicates $p \leq 0.001$.

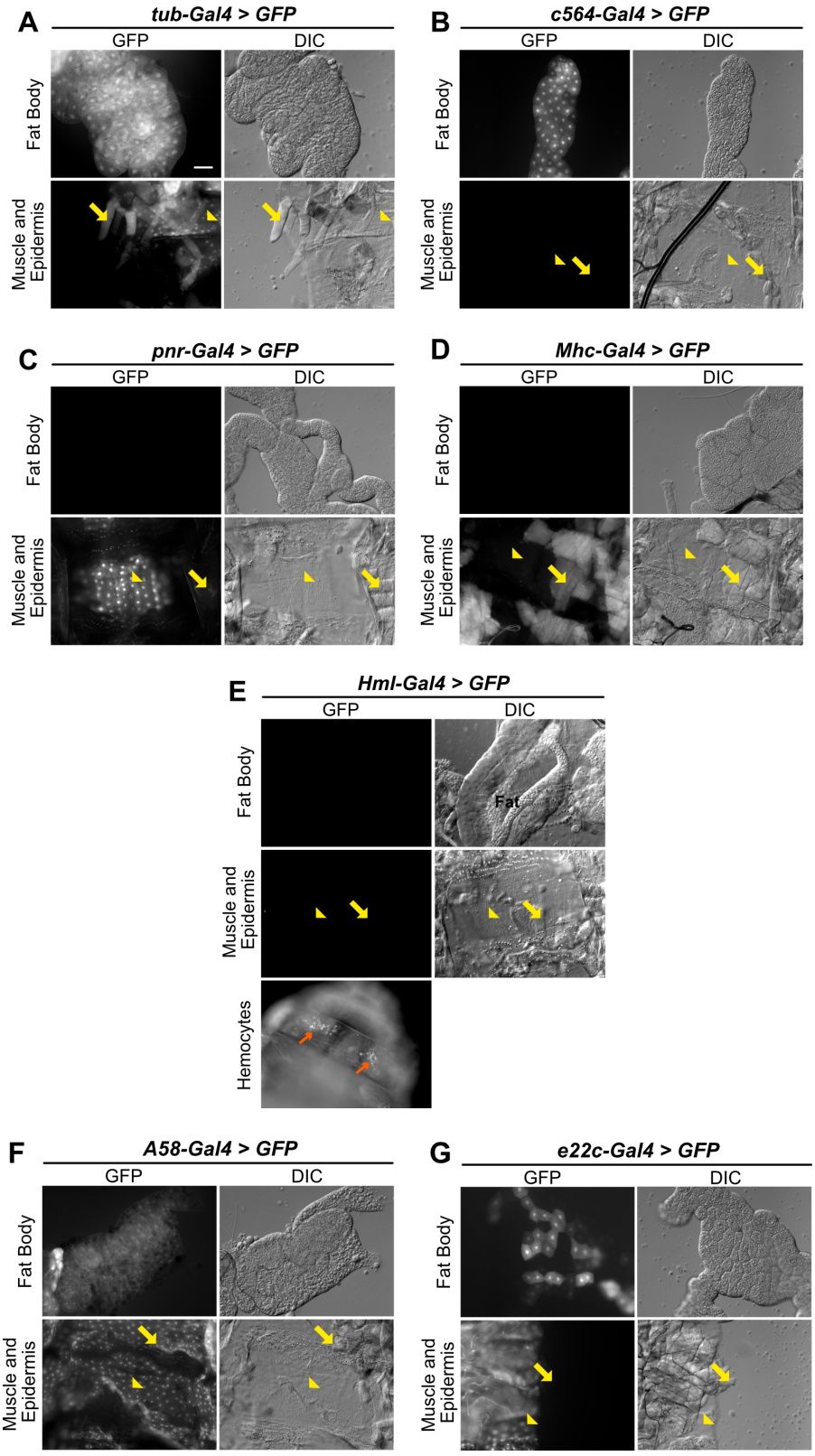
A
tub-Gal4 > GFP
GFP
DIC
Fat Body
Muscle and Epidermis
B
c564-Gal4 > GFP
GFP
DIC
Fat Body
Muscle and Epidermis
C
pnr-Gal4 > GFP
GFP
DIC
Fat Body
Muscle and Epidermis
D
Mhc-Gal4 > GFP
GFP
DIC
Fat Body
Muscle and Epidermis
E
Hml-Gal4 > GFP
GFP
DIC
Fat Body
Fat
Muscle and Epidermis
Hemocytes
F
A58-Gal4 > GFP
GFP
DIC
Fat Body
Muscle and Epidermis
G
e22c-Gal4 > GFP
GFP
DIC
Fat Body
Muscle and Epidermis

Figure 7: Characterizing *Gal4* expression patterns.
A-E) *Gal4* drivers used in this study. *Gal4* expression patterns were characterized in 3rd instar larvae by driving *UAS-GFP*. In addition to an open-ended evaluation of GFP expression throughout the animal, GFP expression was evaluated specifically in epidermis, fat body, muscle, and tracheae (not shown). Hemocyte expression was specifically evaluated in intact larvae only for *Hml-Gal4*. **F-G)** The epidermal *Gal4* drivers *A58* and *e22c* were not used in this study because they were not specific to epidermis, as each expressed also in the fat body. Yellow arrows indicate muscle. Yellow arrowheads indicate epidermis. Orange arrows indicate hemocytes. Fat body is labeled in *Hml-Gal4* panel. Scale bar, 100 μm. N $\geq$ 3 for each sample.

patchiness to the epidermal basement membrane fluorescence when each BM-GFP was knocked down with *pnr-Gal4*, nor did we measure any reduction in total fluorescence (Fig. 6).

In unwounded epidermal basement membrane, laminin, collagen IV, and perlecan were found to derive from the fat body. For collagen IV-GFP, expression of *dsRNA^{GFP}* in the fat body completely eliminated fluorescence from the epidermal basement membrane, with no significant difference between fat-body knockdown and ubiquitous knockdown (Fig. 6D). For laminin-GFP, expression of *dsRNA^{GFP}* in the fat body eliminated 62% of the fluorescence from the epidermal basement membrane compared to ubiquitous knockdown (Fig. 6C); and for perlecan-GFP, fat-body knock-down eliminated 73% of the fluorescence (Fig. 6E). Thus, although most of the laminin and perlecan in the epidermal basement membrane derive from the fat body, there appears to be a second source that makes a minor contribution. One possibility for this source is leftover laminin-GFP and perlecan-GFP from embryonic epidermal basement membrane deposited by hemocytes, or even from assembled basement membrane around other larval tissues (see Discussion).

To our surprise, nidogen in unwounded epidermal basement membrane did not originate from the fat body, hemocytes, or epidermis. We examined available expression data on nidogen and found that it is highly expressed in muscle progenitors [49]. After confirming the specificity of *Mhc-Gal4* for muscles (Fig. 7D), we tested muscle as a source of each basement membrane protein in the epidermis; we found that muscle contributes all of the nidogen to the epidermis (Fig. 6F), but does not contribute collagen IV, laminin, or perlecan.

We next asked if the same cellular source that supplied basement membrane proteins to growing epidermis also supplied basement membrane proteins for repair after epidermal wounding. To address this question, we focused on BM-GFP increased fluorescence within the wounded area compared to the background unwounded area: in control animals, the average fluorescence intensity of each of the four BM-GFPs was about two-fold brighter within the wound than outside the wound (Fig. 8). We reasoned that if the source for growth and repair were different, then when we knocked down GFP in the growth source, the repaired basement membrane should retain BM-GFP when the undamaged regions lost GFP, causing an increase in the ratio of fluorescence inside/outside the wound. Conversely, if the source for growth and repair were the same, then when we knocked down GFP in the growth source, significantly less BM-GFP would be incorporated into both the repairing basement membrane and the surrounding unwounded matrix, causing a reduction in fluorescence intensity inside the wound and a constant or decreased ratio inside/outside (see Fig. 8A for a schematic). For all four basement membrane proteins, we found that the ratio of fluorescence

intensity decreased when *dsRNA*^{GFP} knocked down the BM-GFP in the growth source tissue.

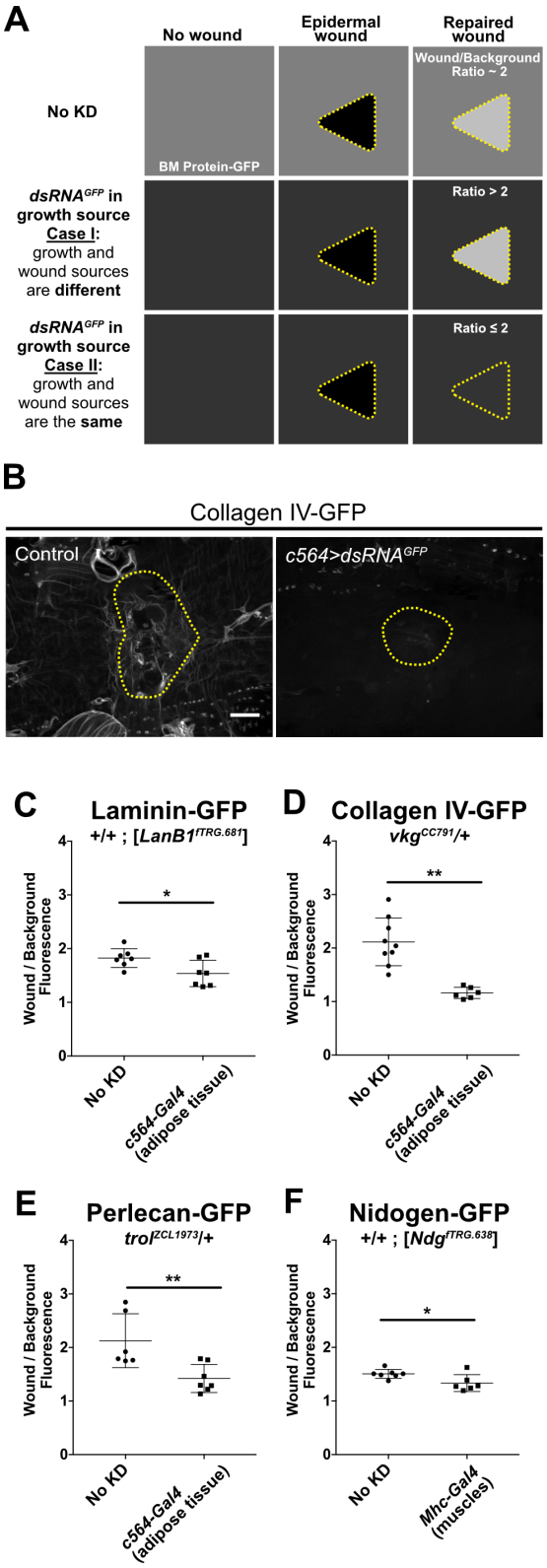

Figure 8: The sources of basement membrane for repairing damage are the same as for growth.
A) Schematic of possible outcomes to test for a wound-specific source of basement membrane. In control unwounded epidermis, the basement membrane is fluorescent (depicted as medium gray color, top left) from the incorporation of BM-GFP. After repair, the basement membrane in the wound area is about 2-fold brighter than background (top right). If the tissue sources for growth (unwounded) and repair of basement membrane are different, then the permanent knockdown of GFP in the growth source tissue will cause the intact basement membrane (background) to become dim, but the repaired area is expected to remain bright, increasing the wound/background ratio. If the tissue source for growth (unwounded) and repair is the same, the permanent knockdown of GFP in the source tissue is expected to affect basement membrane repair in a similar manner, maintaining or reducing the wound/background ratio. **B)** Example of repaired epidermal basement membrane in the absence of $dsRNA^{GFP}$ (left) or in the presence of $dsRNA^{GFP}$ expressed in the fat body (right). **C-F)** Ratio of average fluorescence inside the wound over outside the wound with or without $dsRNA^{GFP}$ expression in the growth source tissue for epidermal basement membrane. Components appear to come from the same source tissues for growth and repair of basement membrane. * indicates $p \leq 0.05$, ** indicates $p \leq 0.01$. Scale bar, 50 μm.

Thus, our results indicated that basement membrane proteins are secreted from a source tissue and can be incorporated into either expanding basement membrane or damaged basement membrane, with no significant alternative source during wound repair (Fig. 8).

Epidermal cells close wounds in the absence of a fully repaired basement membrane

Next, we sought to test the function of each of the four major basement membrane proteins in wound repair. Because knocking down or mutating laminin, collagen IV, or perlecan is lethal in *Drosophila* [87,132,133], we used the temperature sensitive *Gal4-Gal80^{ts}* system to express dsRNA against each basement membrane component ubiquitously throughout larvae (with *Tub-Gal4*), depleting the animals of

newly synthesized basement membrane protein after embryogenesis. Each larva was allowed to grow to 3rd instar, wounded, and allowed to recover for 24 h (see Experimental Procedures). Epidermal cells were able to close the wounds when each of the basement membrane proteins was depleted individually (Fig. 9).

In these basement membrane knockdown experiments, larvae knocked down for laminin or collagen IV were observed to be smaller than controls, and those lacking laminin, collagen IV, or perlecan died before adulthood. We expected that as a larva grew, the basement membrane proteins available in the hemolymph at the onset of knockdown would be assembled into extracellular matrices and thus be depleted from the hemolymph. We expected that these two pools could be identified biochemically as a soluble fraction (in the hemolymph) and an insoluble fraction (in the assembled basement membrane). To measure the extent of knockdown, we crossed in one copy of a BM-GFP into the knockdown background and performed anti-GFP western blots on soluble and insoluble larval fractions, as the GFP-tagged protein would be targeted by the same mechanism as the untagged protein. In control larvae, we had limited success in identifying intact basement membrane proteins in the soluble fraction (Fig. 10), although their degradation products could be readily detected, making it difficult to reproducibly quantify knockdown efficiency in the soluble fractions; but all basement

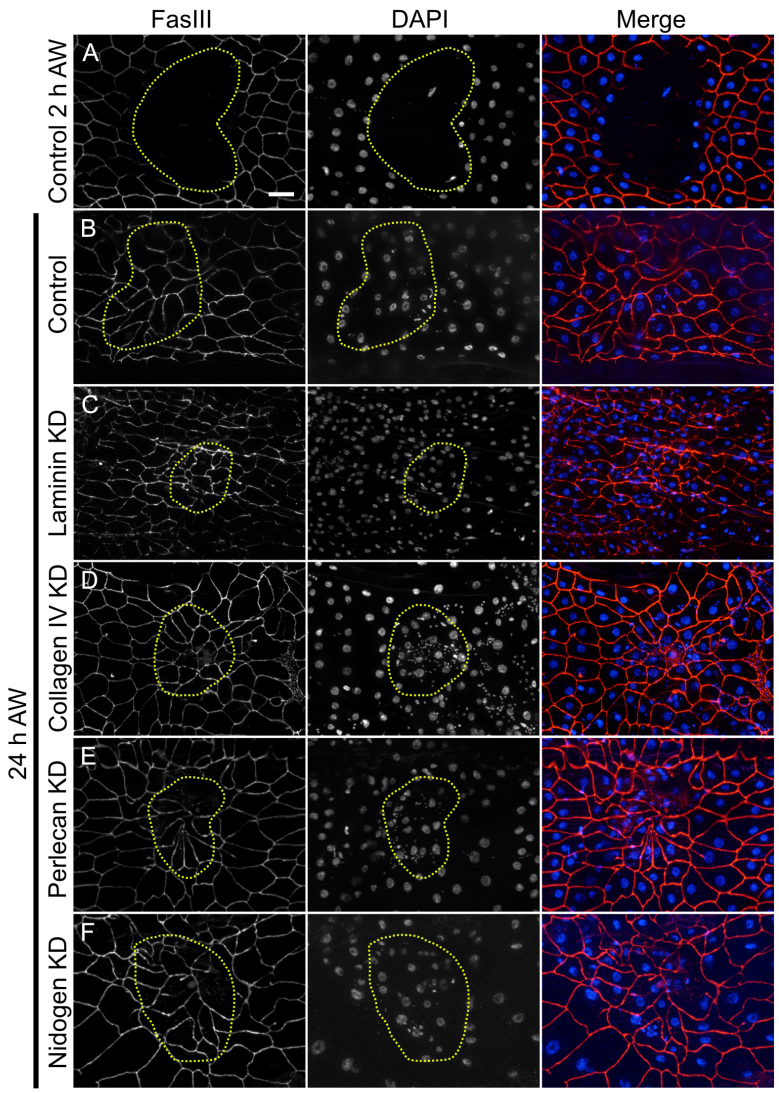

Figure 9: Cells do not require any of the core basement membrane proteins to close wounds.
A) 2 h after injury, wounds were open. **B-F)** 24 h after injury, cells had closed the wound in (**B**) controls, or (**C-F**) when laminin, collagen IV, perlecan, or nidogen was knocked down days before wounding. Note that multinucleate syncytial cells were present after repair in control as well as knockdown wounds as previously reported [111]. Panels A-F are representative of 7, 25, 16, 15, 18, and 14 wounds examined, respectively. Scale bar, 50 μm.

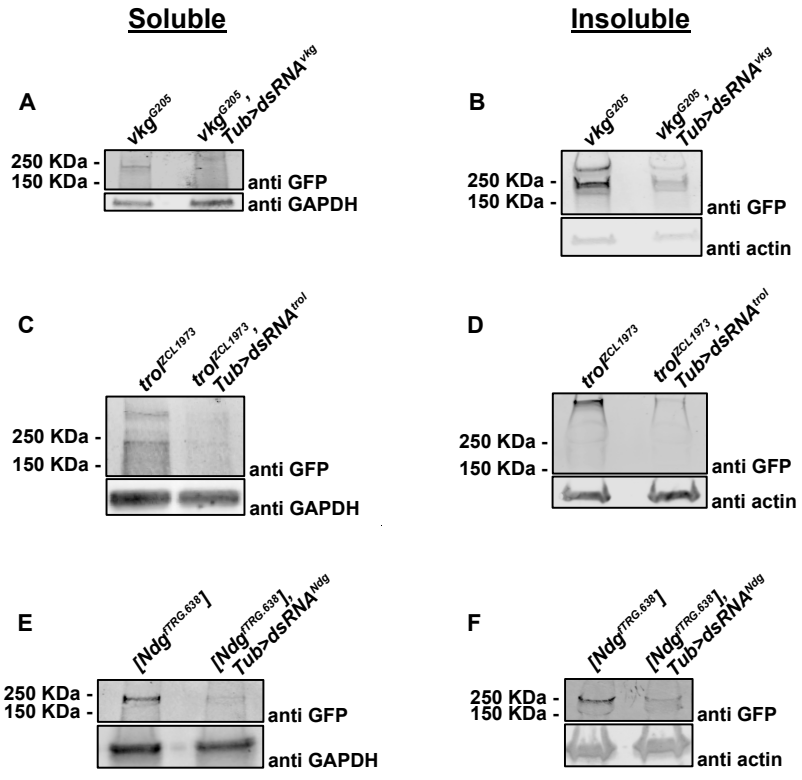

H

		% signal after knock down	
		insoluble	soluble
Laminin-GFP	sample 1	22%	7%
	sample 2	35%	(degraded)
	mean	**29%**	NA
Collagen IV-GFP	sample 1	29%	(degraded)
	sample 2	38%	4%
	mean	**33%**	NA
Perlecan-GFP	sample 1	9%	1%
	sample 2	5%	(degraded)
	mean	**7%**	NA
Nidogen-GFP	sample 1	22%	20%
	sample 2	26%	(degraded)
	mean	**24%**	NA

Figure 10: Collagen IV, Perlecan, Nidogen, and Laminin can be depleted by RNA interference.
A-B) Collagen IV (Vkg-GFP) is knocked down after expression of dsRNA against *vkg*. **C-D)** Perlecan (Trol-GFP) is knocked down after expression of dsRNA against *trol*. **E-F)** Nidogen (Ndg-GFP*)* is knocked down after expression of dsRNA against *Ndg*. Both nidogen blots were imaged together and thus are directly comparable. **G)** Laminin (LanB1-GFP) is knocked down after expression of dsRNA against *LanB1*. For insoluble LanB1-GFP, see Fig. 13C. Panel G and 13C were imaged at the same time and thus are directly comparable. **H)** Quantification of the extent of knockdown in all western blots.

membrane proteins could be reproducibly identified and quantified in the insoluble fraction of larval lysates. In insoluble fractions from whole animals, the average depletion efficiency was about 71% for LanB1, 67% for collagen IV α2 (Viking), 93% for perlecan, and 76% for nidogen, and it appears that the reduction of soluble proteins was even greater (Fig. 10 and Fig. 13C). An important validation of our strategy came from imaging the wounds in the knockdown animals: in every case the knocked-down BM-GFP protein was severely diminished within wound area 24 h after wounding, even though the cells had closed the wound (Fig. 11 B,H,N,T). Thus, the knockdown strategy was sufficient to impair basement membrane repair.

Most matrix proteins assemble independently of others during basement membrane repair

It was previously established that *de novo* basement membrane assembly occurs through a strict hierarchy: laminin creates a foundation that promotes collagen IV assembly, which in turn recruits perlecan [53,87,99]. We sought to determine if this hierarchy of assembly held true during wound repair by analyzing the scar made by each of the four BM-GFP proteins when each basement membrane protein was knocked down. We used the same temporally conditional, spatially ubiquitous strategy of knocking down basement membrane proteins as for examining wound closure, except that we imaged a BM-GFP rather than cells (Fig. 11). Scars in control animals were easily recognizable and consistent, characterized by regions of highly fluorescent BM-GFP staining interspersed with regions of low-intensity fluorescence. We refer to this juxtaposition of high/low fluorescence within the wound as fluorescence anisotropy.

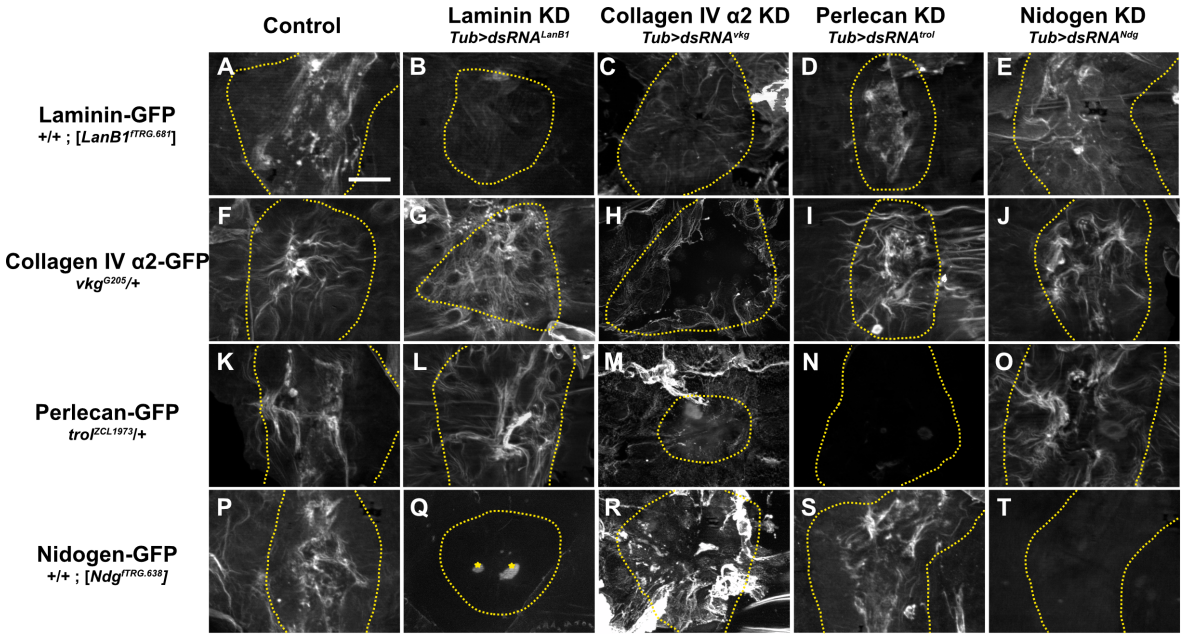
Control
Laminin KD
Tub>dsRNALanB1
Collagen IV α2 KD
Tub>dsRNAvkg
Perlecan KD
Tub>dsRNAtrol
Nidogen KD
Tub>dsRNANdg
Laminin-GFP
+/+ ; [LanB1fTRG.681]
Collagen IV α2-GFP
vkgG205/+
Perlecan-GFP
trolZCL1973/+
Nidogen-GFP
+/+ ; [NdgfTRG.638]
A
B
C
D
E
F
G
H
I
J
K
L
M
N
O
P
Q
R
S
T

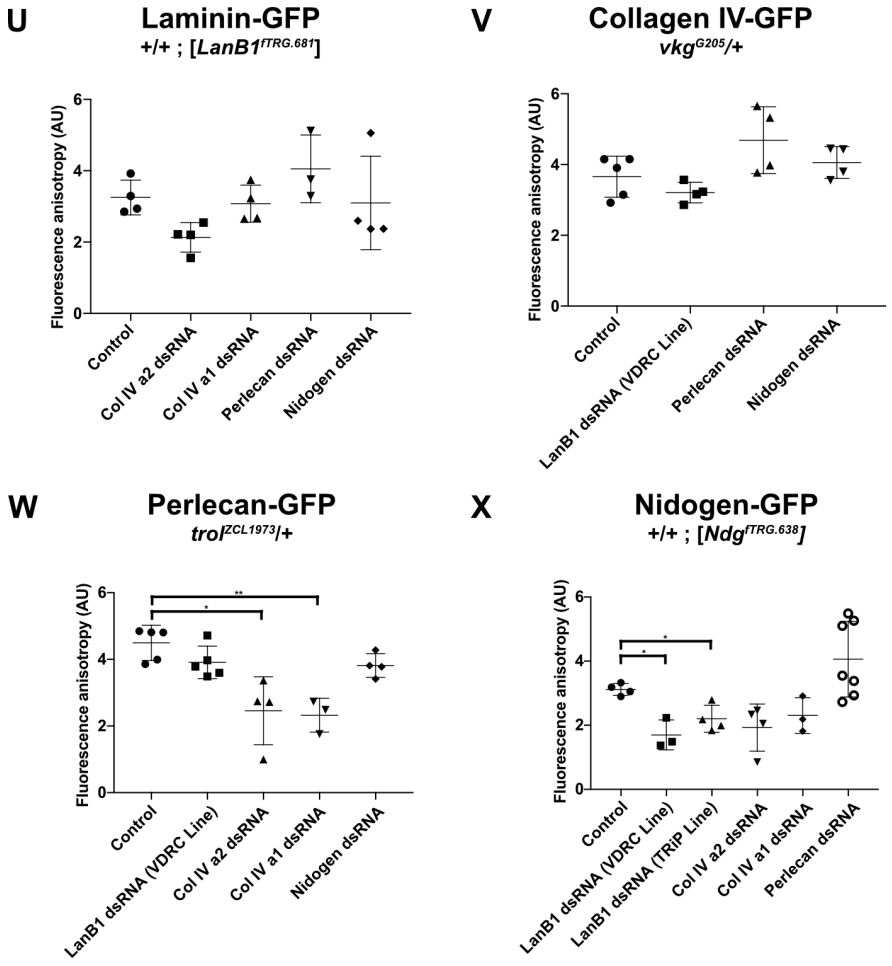
U
Laminin-GFP
+/+ ; [LanB1fTRG.681]
Fluorescence anisotropy (AU)
Control
Col IV a2 dsRNA
Col IV a1 dsRNA
Perlecan dsRNA
Nidogen dsRNA
V
Collagen IV-GFP
vkgG205/+
LanB1 dsRNA (VDRC Line)
W
Perlecan-GFP
trolZCL1973/+
X
Nidogen-GFP
+/+ ; [NdgfTRG.638]
LanB1 dsRNA (TRiP Line)

Figure 11: Hierarchy of basement membrane assembly during repair.
A-E) Laminin assembled into repaired basement membrane independent of any other basement membrane proteins. **F-J)** Collagen IV assembled into repaired basement membrane independent of any other basement membrane proteins. **K-O)** Although perlecan assembled into repaired basement membrane independent of any other basement membrane proteins, its assembly into the scar required collagen IV **(M)**. **P-T)** Nidogen required laminin **(Q)** but not collagen IV **(R)** or perlecan **(S)** to assemble into repaired basement membrane. In collagen knock-down wounds **(C,H,M,R)**, scars appear to extend outside the wound area, see text. In panel **Q**, the bright dots at the wound center (marked by yellow stars) are autofluorescent melanization, see Experimental Procedures. **U-X)** Quantification of fluorescence anisotropy in repaired basement membranes. * indicates $p \leq 0.05$, ** indicates $p \leq 0.01$. Unless otherwise indicated, no significant difference was observed. Scale bar, 50 μm.

To address the requirements for basement membrane assembly in a quantitative manner, we measured the fluorescence anisotropy within the wound boundaries of each sample by measuring the mean fluorescence of the brightest 5% of pixels within the unobstructed wound bed, normalized to the area of low fluorescence within each wound (see Experimental Procedures). Because we found some initial changes in the scars of collagen IV and laminin knockdowns, we tested second dsRNA lines to knock down collagen and laminin, to establish specificity. In agreement with embryo *de novo* assembly data, laminin deposition into the repaired basement membrane did not require any of the other basement membrane proteins (Fig. 11A-E, U). Although the intensity of the laminin scar decreased modestly in some samples when collagen IV α2 (*vkg)* was knocked down, this apparent change was not statistically significant ($p \geqq 0.05$) nor was it reproducible when we knocked down collagen IV α1 (*Col4a1*), the obligate partner of collagen IV α2 in the *Drosophila* collagen IV heterotrimer. Depletion of perlecan or nidogen had no effect on laminin anisotropy within the repaired wound (Fig. 11U).

Therefore, we concluded that laminin deposition into the basement membrane scar was independent from any other basement membrane proteins.

In contrast to what has been reported in embryos [87], collagen IV deposition into the repaired basement membrane was not perturbed by the depletion of other basement membrane proteins, including the depletion of laminin (Fig. 11F-J, V), a surprising result that we tested further (see next section). Next, we analyzed perlecan deposition into the repaired basement membrane and found that it was significantly altered by the depletion of collagen IV (Fig. 11K-O, W). Although the accumulation of perlecan in the repaired basement membrane did not require collagen IV like it does in the growing wing disc [99], when either collagen IVα2 or collagen IVα1 was depleted, perlecan deposition was more uniform within the repaired region of basement membrane (Fig. 11M and Fig. 12D), appearing significantly different from the anisotropy of perlecan in control wounds (Fig. 11W). Finally, for nidogen, measurements of fluorescence anisotropy within the wound showed a significant difference only in the case of laminin depletion (Fig. 11P-T, X). These results were reproduced with two different dsRNA constructs targeting the laminin gene. When laminin was knocked down, nidogen-GFP

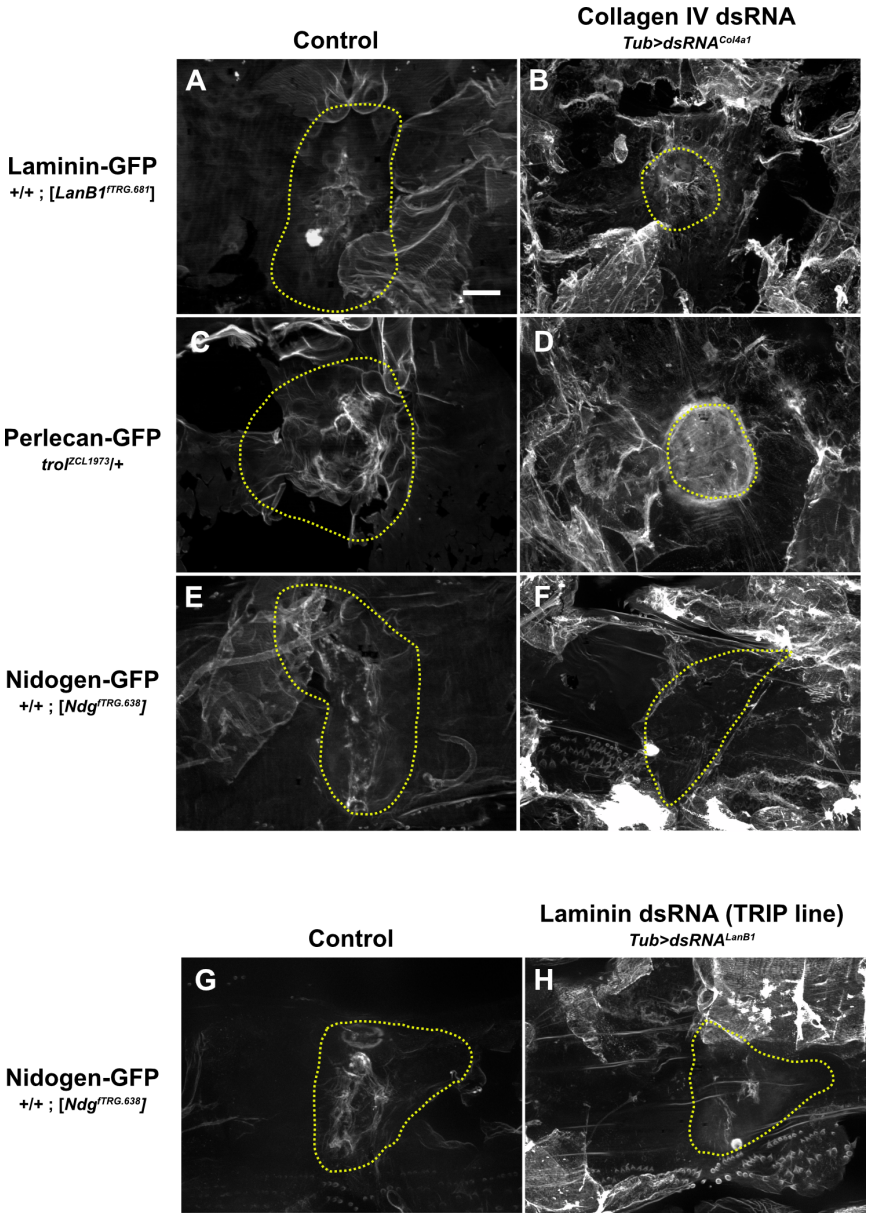

Figure 12: Secondary dsRNA lines.
A-F) Knocking down expression of *Col4a1* has a similar effect on the repair of other basement membrane proteins as knocking down *vkg*. In both collagen knockdown conditions, Laminin-GFP and Nidogen-GFP form scars in the repaired region whereas perlecan is deposited more uniformly within the repaired wound. See Fig. 11 for quantification. **G-H)** Nidogen deposition into the repaired basement membrane is decreased in the absence of laminin when using a different dsRNA line against the *LanB1* gene. See Fig. 11 for quantification. Yellow dotted line indicates wound borders. Scale bar, 50 μm. All wounds were imaged 24 h after wounding.

fluorescence decreased outside the wound area as well as in the scar, indicating that laminin is required for nidogen recruitment to the basement membrane during assembly and/or growth, as well as repair. Thus, in repairing basement membranes, laminin and collagen IV assemble independently of the other protein components, whereas nidogen depends on laminin and perlecan is organized by collagen IV.

Whenever either subunit of collagen IV was knocked down, the basement membrane was noticeably more fragile upon dissection, consistent with the role of collagen IV in determining the mechanical strength of basement membrane. In these knockdowns, the appearance of all the basement membrane proteins was visibly altered both inside and outside the wound, as though the entire basement membrane was scarred even outside the intended wound area, which we find a plausible outcome when collagen IV is not present for support. Because of this extensive change outside the wound, the scar within the wound appeared to spread across the wound bed rather than be focused in the center as in controls (see Figs. 11 and 12). This apparent increase in scarring is evident with all the basement membrane proteins in collagen IV knockdowns.

Collagen IV assembles into basement membrane scars by a different mechanism than de novo assembly

The finding that collagen IV did not require laminin to assemble in wounds suggested two possibilities: 1) collagen IV assembly into basement-membrane scars occurs via a distinct mechanism from that of *de novo* assembly, or 2) the laminin depletion was not efficient enough to observe a phenotype. We reasoned that if the *de novo* and repair mechanisms are the same, and collagen IV requires only a limited

amount of laminin to assemble, then a similar efficiency of knockdown would be enough to prevent collagen IV deposition into the basement membrane during *de novo* assembly in embryos. Using the same *LanB1-GFP* and *dsRNA* constructs as for larval wounds, we assessed the efficiency of laminin knockdown in embryos by measuring the fluorescence of Laminin-GFP in stage 16-17 embryos. Fluorescence levels in *LanB1* knockdown embryos were 32% that of controls (Fig. 13A-B). This knockdown efficiency was remarkably similar to what we measured in larvae via western blot, in which Laminin-GFP levels were 29% that of controls (Fig. 13C, Fig. 10). Next we assessed collagen IV assembly in these *LanB1* knockdown embryos, and found that collagen IV-GFP deposition into the basement membrane was disrupted (Fig. 13D) as previously described [53,87], but unlike what we observed for wound repair in larvae. These results indicate that basement membrane repair occurs via a distinct mechanism from that of *de novo* assembly.

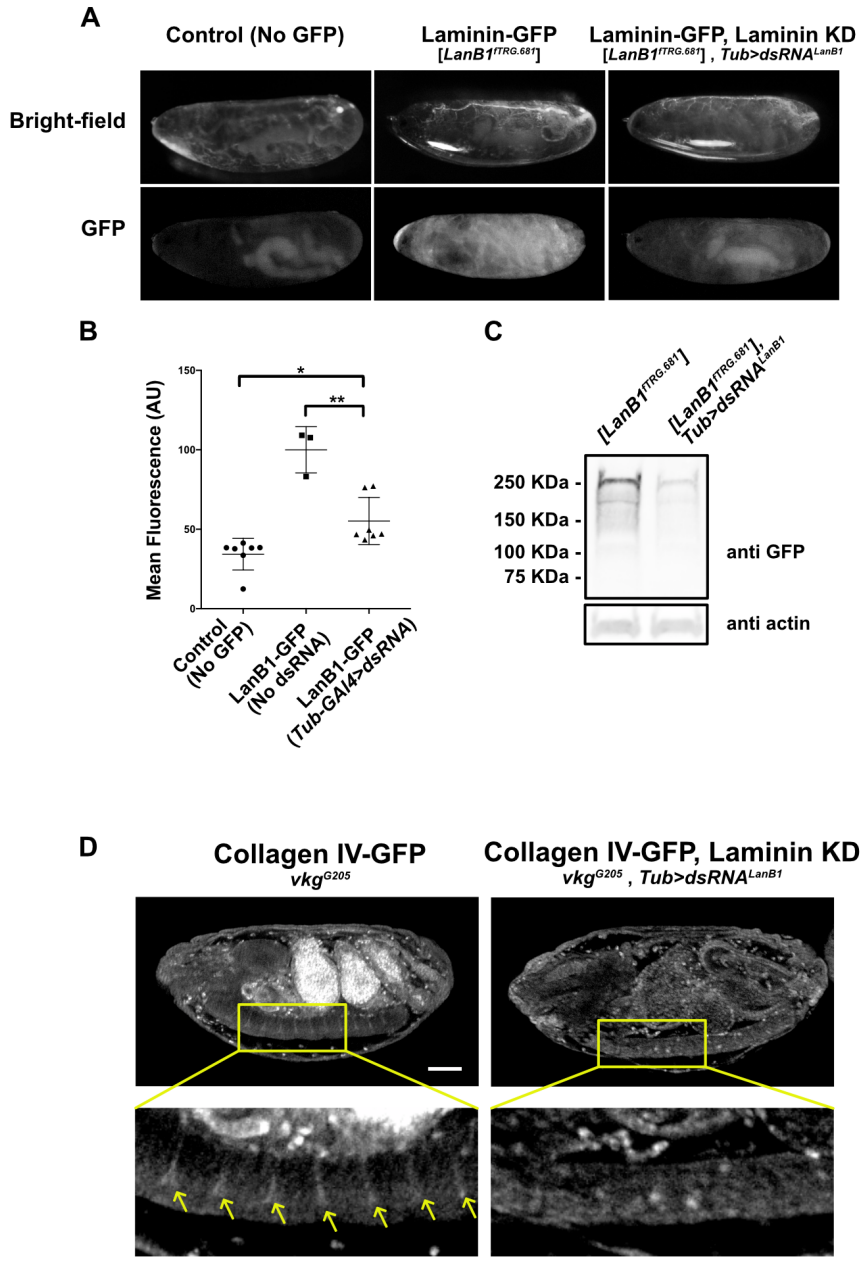

Figure 13: The requirement for laminin is different between basement membrane *de novo* assembly and repair.
A) Expression of dsRNA against *LanB1* knocked down LanB1-GFP levels in stage 16-17 embryos, as determined by GFP fluorescence. **B)** Quantification of GFP fluorescence in embryos showed dsRNA against *LanB1* reduced LanB1-GFP levels by 68%. **C)** For comparison, expression of the same dsRNA against *LanB1* in larvae depleted LanB1-GFP by 71% as measured by western blot (see also Fig. 10). **D)** Expression of dsRNA against *LanB1* was sufficient to disrupt collagen IV deposition into the basement membrane of ventral nerve cord channels in stage 16-17 embryos, as visible in controls (yellow arrows) (N ≥ 3). Scale bar, 50 μm.

Discussion

In this report, we systematically analyzed aspects of basement membrane repair in a genetically tractable system, *Drosophila* larval epidermis. Importantly, although damaged basement membrane can be repaired to a continuous sheet within 24 h after the infliction of a ~100 μm wound, this repaired sheet has a visibly altered structure that is non-uniform with respect to all four basement membrane proteins. Thus, basement membrane repairs through formation of a disorganized scar. Comparing basement membrane repair to normal growth, we find that basement membrane proteins originate from the same sources for repair and growth. However, there are some differences between repair and *de novo* assembly mechanisms. Similar to *de novo* assembly, perlecan depends on collagen IV for proper incorporation into the basement membrane scar. Yet unlike *de novo* assembly, collagen IV does not depend on laminin for its incorporation into the scar, even though similar knockdown of laminin did prevent collagen IV incorporation into new basement membranes in embryos. Though not required for collagen IV, laminin is required for the deposition of nidogen into the growing and repairing basement membrane. The dependency of nidogen on laminin *in vivo* has not been previously reported, although nidogen has been reported to bind to laminin *in vitro* [68,117,118].

Basement membrane repair leaves behind a scar-like lesion

This is the first study we are aware of that demonstrates a scar in the basement membrane following wound repair. The basement membrane scar is characterized by increased deposition of the core basement membrane components laminin, collagen IV,

perlecan, and nidogen into the repaired wound, often displaying a fibril-like appearance. The formation of a scar may explain why repaired basement membrane does not recover its full adhesive function for months following corneal wound repair [122]. It is not possible to test whether the basement membrane scar recedes over time in larvae because they undergo metamorphosis and replace the epidermis only a few hours after our experiments ended. It is possible that the presence of a continuing basement membrane scar in larvae 24 h after wounding may trigger changes in gene expression in cells that contact the scar. For example, levels of the matrix remodeling protease Mmp1 remain elevated long after re-epithelialization [134], and levels of the actin binding protein Profilin remain elevated across the original wound bed even 24 h after wounding [135].

Reepithelialization does not require a complete basement membrane

We examined the requirement for laminin, collagen IV, perlecan, and nidogen for the epidermis to close the wound, and interestingly none of these basement membrane proteins is required individually, indicating that none of these individual proteins is crucial as a provisional matrix for cells to migrate on during larval epidermal wound closure. A previous study showed that basement membrane is visible by electron microscopy (EM) on the basal surface of larval epidermal cells during the process of wound closure, as they migrate toward the wound, and similarly, we observe that the edge of the basement membrane appears coincident with the leading edge of the cells during wound closure. The lack of genetic requirement for wound closure, combined with the observations that matrix closes with the cells, suggests that the epidermal cells

assemble the basement membrane during migration and that they migrate on the clot or cuticle on the apical side of the epidermis [111].

Repaired epidermal basement membrane originates from non-epidermal sources

Although it would be easy to assume that the basement membrane components were secreted by the wound-responsive epidermal cells in a cell-autonomous manner, our data contradict that assumption. Previous studies have identified three *Drosophila* cell types that generate the protein components of basement membranes: blood cells responsible for embryonic basement membranes [128,129], fat-body cells responsible for some components of the larval imaginal disc basement membranes [99], and follicle epithelial cells responsible for reinforcing the basement membrane surrounding the growing oocyte [136,137]. We find that laminin, collagen IV, and perlecan all originate from the fat body, a distant adipose tissue. In contrast, epidermal nidogen originates from the muscles. Body wall muscles directly contact the epidermis but do not completely cover it, so that nidogen must diffuse from its cellular source like the other matrix proteins [138]. Thus, our analysis identified a fourth tissue source of basement membrane in *Drosophila*. These results indicate that, like for basement membrane growth, basement membrane repair is accomplished by utilizing soluble matrix proteins that reach damaged basement membranes simply by diffusing within the hemolymph, which bathes the basement membranes of the larval body. Interestingly, in corneal basement membrane wounds, nidogen and perlecan originate from non-epithelial stromal tissues [106], suggesting that the non-autonomy of basement membrane components is not limited to *Drosophila*.

Basement membrane proteins may be released into the hemolymph

There are many reasons to analyze basement membrane repair *in vivo*. Matrix and tissue architecture cannot easily be recapitulated in cell culture systems, and because repair is a cell non-autonomous process, it is important that all cell types of the organism are able to participate. By using *Drosophila* larvae, we have been able to capitalize on these strengths, using the flexible genetic approaches of *Drosophila* to identify source cells and requirements for assembly. However, this *in-vivo* approach has limitations as well. In order to generate a functional basement membrane before damage, we used a conditional RNAi-based knockdown strategy to deplete basement membrane components after assembly and before wounding. Because basement membrane components are secreted into hemolymph by distant tissues, we had hoped that inducing RNAi would deplete the soluble (hemolymph) fraction of protein while sparing the insoluble (assembled) fraction. A significant portion of each larval matrix protein is soluble, as indicated by fractionating control lysates followed by western blotting. However, western blots showed that the insoluble fractions were significantly reduced after knockdown, ranging from 67% loss (collagen IV) to 93% loss (perlecan). The reduction of protein from the assembled basement membrane no doubt represents "thinning" of basement membranes due to continued matrix expansion over two days of knockdown, and the reduction may be augmented by a concentration-dependent disassembly of insoluble basement membrane to restore the soluble portion. If soluble protein is released from deposited basement membranes, it would generate a pool of available protein in the hemolymph that cannot be experimentally eliminated, in addition to the inherent leakiness of RNAi that allows a small amount of continued protein

synthesis. Free exchange between polymerized basement membrane protein and soluble subunits seems especially reasonable for laminin, which is polymerized via many weak interactions [139]. It is possible that exchange of subunits between soluble and deposited basement membrane may explain the second minor source of laminin and/or perlecan in epidermal growth, and this pool may also contribute to basement membrane repair after wounding.

Loss of collagen IV alters perlecan organization in repaired basement membrane

The observation that the organization of perlecan within the repaired wound is altered in the absence of collagen IV is similar to previous studies showing that collagen IV is required for perlecan deposition during the growth of several larval basement membranes [99]. However, the phenotype we observed was subtly different: in the absence of collagen IV, perlecan was present within the repaired basement membrane but its appearance was altered. The heparan sulfate chains that characterize heparan sulfate proteoglycans like perlecan can interact with hundreds of different proteins [140]. It is possible that the absence of collagen IV from the repaired basement membrane liberates perlecan to bind non-specifically with other molecules, creating the fluorescent haze we observed around wounds repaired in the absence of collagen IV. Alternatively, perlecan may bind specifically to multiple basement membrane proteins *in vivo*.

The requirements for basement membrane assembly are altered during repair

It was surprising to find that collagen IV deposition is not sensitive to laminin levels in the repaired wound. This lack of dependency stands in contrast to data

showing laminin to be crucial for collagen IV deposition in the developing embryo [53,87]. The difference in wound repair may be that collagen IV is already present in the epidermal basement membrane prior to the depletion of laminin. Upon laminin depletion, collagen IV is maintained outside the wound borders after laminin knockdown. This assembled collagen IV matrix may provide scaffolding from which newly deposited collagen IV can self-assemble, extending into the repaired wound independently of laminin. In contrast, the deposition of nidogen into the basement membrane scar appeared to be entirely dependent on the presence of laminin. Though nidogen has been shown to bind laminin, collagen IV, and perlecan [3], our analysis indicates that laminin is the crucial component for nidogen recruitment into the basement membrane scar.

Chapter 3

Conclusions and future directions

Wound repair creates basement membrane scars via an unknown mechanism

The repair of basement membrane leaves behind a lesion that is referred to in this study as a basement membrane scar. The basement membrane scar is characterized by the presence of fibril-like deposits of basement membrane proteins that can be clearly identified when viewed from below the epidermis (XY plane of view). It is composed of all four of the core basement membrane proteins (laminin, collagen IV, perlecan, and nidogen) and appears to be thicker than the undamaged basement membrane when viewed as a cross-section (XZ plane of view). The components of the basement membrane scar in larval epidermis originate from the same cells that produce basement membrane during normal growth. Unlike *de novo* basement membrane assembly in embryos, only nidogen appears to require the presence of laminin for its incorporation into the basement membrane scar. Thus, mechanisms of basement membrane repair differ from *de novo* assembly.

Characterization of the basement membrane scar was simplified by the structure of *Drosophila* larva epidermis. Due to the difficulty of dissecting basement membranes from the associated tissue, cross sections are typically used for imaging basement membrane in other organisms. Though much can be learned from imaging the basement membrane in this way, a full understanding of morphology during repair required images from the XY plane of view as well. Such images were easily obtained

in this study because the basement membrane of *Drosophila* larva epidermis is not associated with an underlying dermal layer that would have otherwise required removal. Muscles in *Drosophila* larvae do anchor to the body wall, but they connect at distinct points and are relatively easy to remove without severely damaging the epidermal basement membrane. This advantage, plus the availability of fly stocks with GFP-fused basement membrane proteins, allowed for detailed observations of the basement membrane scar.

An unfortunate shortcoming of this study is that it is still not clean why the morphology of repaired basement membrane differs from undamaged regions. As a *Drosophila* larva grows, its basement membranes must also grow, requiring continuous remodeling and addition of components. Presumably, basement membrane repair is also a process of remodeling and addition, yet the resulting morphology is different from undamaged regions. When comparing how basement membrane is built during wound repair to that of normal growth, a number of possible mechanisms should be considered. Those mechanisms and how to determine if they play a role in scar formation are discussed below.

Matrix metalloproteinases (MMPs) and integrins may promote scar formation

Previous studies suggest that both MMPs and integrins play a role in building basement membranes. Integrins, among other receptors, promote laminin polymerization and recruitment to cell surfaces [141,142]. In addition to promoting the assembly of and anchoring to the basement membrane, integrins provide a mechanism for cells to detect the biophysical properties of a basement membrane via

mechanotrasduction. Mechanotrasduction relies on a group of mechanosensitive focal adhesion proteins, collectively called the “molecular clutch”, that connect extracellular matrix-bound integrins to the actin cytoskeleton and trigger biochemical signals that can alter cellular behavior [143]. While integrins recruit basement membrane proteins to the cell surface and provide biophysical information about an assembled basement membrane, the secretion of MMPs can degrade and remodel an already existing basement membrane. Such remodeling allows basement membranes to accommodate the growth and development of associated tissues [144]. Furthermore, the remodeling of basement membranes by MMPs alters their biophysical properties, which can in turn be detected by cells through integrin-based adhesions (discussed in Appendix). By degrading portions of existing basement membrane, MMPs may create openings into which new basement membrane proteins can be inserted. One example of this is in *Drosophila* larvae, where it has been shown that MMPs promote collagen IV incorporation into the epidermal basement membrane [134].

Following injury in *Drosophila* larvae epidermis, both integrin and MMP levels are increased around the wound borders [134,145]. Since integrins and MMPs promote basement membrane assembly, and the basement membrane scar appears to, in part, be characterized by an increase of basement membrane proteins, increased integrin and/or MMP levels may promote basement membrane scar formation. To test this hypothesis, the expression of integrins and/or MMPs should be suppressed during wound repair, and observations of the repaired basement membrane should be made 24 hours after injury. Both MMPs and integrins are necessary for reepithelialization, meaning a complete knockdown of either of these proteins would halt wound repair prior

to when a basement membrane scar is expected to form. However, less efficient dsRNA constructs against integrins still allow for wound closure 20-80% of the time [145], and reepithelialization may progress in some MMP knockdown samples if the efficiency of the knockdown can be decreased. For testing the role of integrins in scar formation, the *A58-Gal4* driver should be used to express less efficient dsRNA constructs, starting with VDRC stock number 29619, against integrin β_{PS} (*myospheroid*) in the epidermis of *Drosophila* larvae [145]. *Myospheroid* appears to be the only β integrin expressed in larvae epidermis [145,146], and therefore its depletion is expected to affect all integrin heterodimers. The *A58-Gal4* driver is expressed in the epidermis during early larval development [111], and has previously been used to knock down integrin expression in 3rd instar *Drosophila* larvae prior to wounding [145]. Since the goal is to not completely knock down integrin expression, some scarring would still be expected even if integrins are necessary for basement membrane scar formation. Therefore, a quantification method will be required to characterize changes in the amount of scar formation, and the same fluorescence anisotropy measurement used in Chapter 2 may be a good starting point. To test the role of MMPs in basement membrane scar formation, dsRNA constructs should also be expressed against Mmp1 and/or Mmp2, using the *A58-Gal4* driver. The *Gal4* driver is temperature sensitive, so if all dsRNA constructs against MMPs are too efficient, preventing reepithelialization, then it may be possible to decrease efficiency by maintaining animals at 18°C.

The above experiments would test if increased MMP and/or integrin levels are necessary for basement membrane scar formation. But, it is also possible that increased integrin and/or MMP levels are sufficient for scar formation. To test this

hypothesis, the *pnr-Gal4* driver should be used in conjunction with *Gal80^{ts}* to overexpress MMPs and/or integrins in dorsal patches on the epidermis of *Drosophila* larvae. By restricting expression to patches on the dorsal side of the epidermis, wild type regions will be present in each animal to compare possible changes in basement membrane morphology. The *pnr-Gal4* driver is expressed during embryogenesis [49] and the over-expression of MMPs is lethal [127], so controlling the timing of over-expression with *Gal80^{ts}* will be crucial to allow larvae to develop to 3rd instars prior to each experiment. Exactly what that timing should be will have to be determined empirically.

Fat body production of basement membrane proteins may respond to injury

The data from this study demonstrate that the epidermal basement membrane in *Drosophila* larvae does not originate from the epithelial cells it underlies. Though muscles are responsible for supplying nidogen to this basement membrane, the fat body appears to be the primary source for most epidermal basement membrane proteins during both normal growth and wound repair. Since *Drosophila* larvae grow continuously as they develop from 1st to 3rd instars [127], it may be expected that basement membrane proteins are constantly produced and secreted by the fat body during these stages. However, while expression of these basement membrane genes has been confirmed in the larval fat body [49], it is not clear if the levels of gene expression remain constant in all stages or if such levels of expression are sufficient to repair a damaged basement membrane. Furthermore, it has been established that the fat body detects and responds to damage in other tissues [147,148]. Therefore, it is at least

possible that the fat body can respond to injury by upregulating basement membrane production. The following experiments should be performed to test this hypothesis.

Expression of laminin, collagen IV, and perlecan should be measured in the fat body before pinch wounding and at multiple time points after wounding. The fat body is easily dissected out of 3rd instar larvae, making multiple techniques for measuring expression possible. Quantitative reverse transcription PCR (RT-qPCR) should be used to measure changes in transcription. For this experiment, fat bodies should be dissected out of 3rd instar larvae before pinch wounding, 2 hours after wounding, 6 hours after wounding, 12 hours after wounding, and 24 hours after wounding. These time points will likely be sufficient to detect any changes in transcription throughout the repair process. Control samples that have not been injured should be collected at each time point as well. If the fat body increases transcription of basement membrane genes in response to wounding, RT-qPCR should show an increase of mRNA transcripts, over time, in wounded samples relative to controls.

Unfortunately, mRNA levels do not always correlate with protein production, especially during short term cellular responses to stress [149]. Therefore, it would be prudent to also directly measure protein levels at each of the time points used for mRNA measurements. First, the fat body should be evaluated visually, through fluorescence microscopy, for local buildup of basement membrane proteins. Second, since basement membrane proteins may be exported too efficiently to observe a local buildup, protein levels should also be directly measured in the hemolymph. Bleeding larvae and measuring protein levels by western blot is technically feasible, but data from this study suggest that soluble basement membrane proteins may be sensitive to

degradation (Fig. 10), so this technical challenge would have to be overcome. Alternatively, it has been reported that the fluorescence from GFP-fusion constructs of basement membrane proteins in the hemolymph can be detected directly [64,99]. Measuring proteins levels by quantifying the fluorescence of hemolymph may take considerably less time than prepping samples for western blot, reducing the extent of protein degradation. Should it be found that the fat body does respond to wounding by increasing basement membrane protein production, efforts should be made to determine what signaling pathways trigger such a response.

Hemocytes may act as basement membrane transporters

Drosophila blood cells (hemocytes) play a major role in fighting infection, such as those that may occur as the result of an injury. During development, hemocytes are also responsible for contributing laminin, collagen IV, and perlecan to newly forming basement membranes throughout the embryo. Therefore, it was surprising to find that hemocytes do not appear to supply basement membrane components to the larval epidermis during normal growth or wound repair. It is still possible, however, that hemocytes play a different role. During our studies, hemocytes were occasionally observed at or around the site of the wound, and sometimes appeared to contain laminin (Fig. 14). One explanation for this observation could be that, rather than producing basement membrane proteins for epidermal repair, hemocytes serve to shuttle basement membrane proteins from the source tissue to the wounded area.

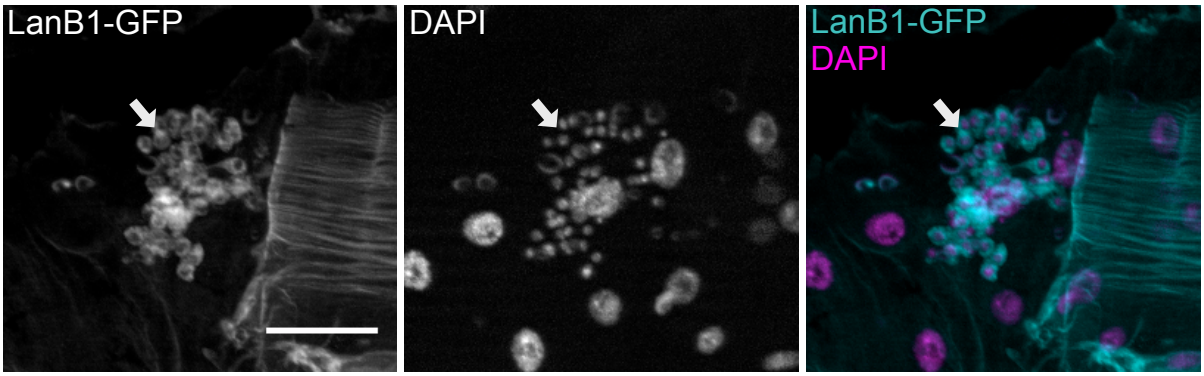

Figure 14: Hemocytes contain laminin in some 3rd instar larvae. In the course of imaging basement membrane scars, hemocytes (white arrows) were occasionally noted to stain positive for laminin-GFP. Whether or not hemocytes were GFP positive did not appear to correlate with proximity to the wound. Scale bar, 50 μm.

To test this hypothesis, hemocytes should first be more carefully inspected for the presence of basement membrane proteins before and during wound repair in *Drosophila* larvae. Though laminin was observed to localize with hemocytes in this study, it remains unclear if other basement membrane proteins are also present. However, hemocytes were never the primary focus of this study and hemolymph was not collected for observation. Consequently, any hemocytes imaged during this study were just the fraction that happened to remain adhered to the larval pelts by the time they were mounted on slides. The association of larval hemocytes with basement membrane proteins may be dependent on whether or not the animals have been injured, so hemolymph should be collected before, during, and after wound repair. Initial time points should include immediately before pinch-wounding, 2 hours after, 12 hours after, and 24 hours after wounding. Once collected, hemocytes should be stained and imaged, for each basement membrane protein, by fluorescence microscopy. Currently, there are no reliable antibodies for directly imaging *Drosophila* basement membrane, so larvae with GFP-fused basement membrane proteins will have to be

used unless better antibodies can be generated. If hemocytes are found to be in association with other basement membrane proteins, it will provide evidence that shuttling basement membrane proteins to distant tissues is at least one possible function. If no other basement membrane proteins are found in association with hemocytes, then additional experiments should focus on laminin.

Next, for any basement membrane proteins found to be associated with hemocytes, experiments should be done to confirm the origin of those proteins. The results of this study provide strong evidence that the fat body produces the vast majority of basement membrane that is associated with the epidermis. However, basement membrane proteins found on hemocytes may serve a yet unknown function that does not involve the epidermal basement membrane, meaning the fact that epidermal basement membrane originates from the fat body would not be predictive of hemocyte basement membrane origin. Therefore, it is still possible that such proteins could be produced by the hemocytes themselves. To determine the origin of such proteins, the same technique used in Chapter 2 to find the source of epidermal basement membrane should be applied to hemocytes. The hemocyte-specific *Hml-Gal4* driver and fat body specific *c564-Gal4* driver should be used in separate experiments with *UAS-dsRNA*^{GFP} to see if knocking down GFP expression in either tissue eliminates GFP-fused basement membrane proteins from *Drosophila* blood cells. *Tub-Gal4* should be used as a control experiment. If basement membrane proteins on hemocytes originate from those cells, it will suggest they have an unknown function that does not involve the epidermis because this study already established the fat body and muscles to be the source of epidermal basement membrane. If those proteins originate from the fat body,

it will leave open the possibility that hemocytes play a role in transporting those proteins to their target tissue.

Finally, hemocytes should be genetically ablated in larvae prior to wounding. Though prone to infection, *Drosophila* larvae are viable in the absence of hemocytes [150] and reepithelialization following epidermal injury does not appear to be perturbed [130]. The *Hml-Gal4* driver should be used to express *UAS-hid* in order to promote apoptosis. The *Hml-Gal4* driver is only expressed after the completion of embryogenesis [150], so the initial establishment of basement membrane in embryos is not expected to be perturbed. The epidermal basement membrane should be imaged 24 hours after pinch wounding hemocyte-depleted 3rd instar larvae to determine if repair is altered in comparison to wild type animals. Since laminin has been observed in larval hemocytes, it would be a good candidate to image first, but all of the core basement membrane components should be imaged as well. Failure of the basement membrane to repair in the absence of hemocytes may indicate a role for hemocytes in transporting basement membrane proteins to the site of injury. Alternatively, should the basement membrane still repair normally, interpreting such a result will depend upon the efficiency of hemocyte ablation. The *Hml-Gal4* driver has been shown to express in over 96% of plasmatocytes [150], which account for over 95% of all hemocytes [151]. Therefore, the vast majority of hemocytes are expected to be eliminated from larvae using the described method. However, only a careful counting of hemocytes will determine the true efficiency of hemocyte ablation.

Hemocytes may promote basement membrane cross-linking

Regardless of whether hemocytes transport basement membrane proteins to the epidermis, they may be responsible for stabilizing the basement membrane scar by secreting peroxidasin. Peroxidasin is responsible for catalyzing the sulfilimine bond that cross-links two collagen IV trimers at their NC1 domains [63]. Hemocytes appear to be the primary cell type to express peroxidasin in larvae [152] and they may secrete it at the site of basement membrane repair. Changes in basement membrane stiffness can have profound implications for tissue morphology (discussed in Appendix), and may also affect scar formation. Furthermore, it has been observed that basement membrane repair in the *Drosophila* gut requires peroxidasin [153]. If the basement membrane repairs when hemocytes are genetically ablated, as described in the previous section, it may do so with less collagen IV cross-linking. The following experiments would determine if hemocytes promote collagen IV cross-linking in the basement membrane scar.

First, the stiffness of the basement membrane scar should be characterized in wild type larvae. The increased fluorescent signal and thickness of the basement membrane scar, relative to unwounded regions, appears to indicate that an excess of basement membrane proteins is deposited at the repaired wound. Therefore, one might expect the basement membrane scar to be stiffer, relative to unwounded regions, due to the presence of more cross-linked collagen IV. However, until direct measurements of stiffness are taken, this is only an assumption. To test this hypothesis, atomic force microscopy could be used to directly measure the stiffness of basement membrane scars, relative to unwounded regions, in wild type *Drosophila* larvae 24 hours after

wounding. Even if the basement membrane scar is no stiffer than the surrounding basement membrane, these measurements will be of value in characterizing the physical properties of basement membrane scars prior to testing if hemocytes affect those properties.

Second, the genetic ablation of hemocytes (described in the previous section) would help determine if hemocytes are required for cross linking the basement membrane scar. If the basement membrane still repairs in the absence of hemocytes, then stiffness should be evaluated by atomic force microscopy. In this case, measurements of scar stiffness would have to be compared directly to scars in wild type animals, instead of just comparing scar stiffness relative to unwounded regions, because the mechanisms of cross-linking scars are likely to be the same as the mechanisms of cross-linking undamaged basement membrane. In this experiment, decreased stiffness may indicate that hemocytes do contribute to repaired basement membrane cross-linking. However, if the appearance of the scar is also altered, in terms of brightness and thickness, then decreased stiffness may simply be a result of less basement membrane proteins being delivered to the site of repair. The following experiments would help distinguish between these two possibilities.

Peroxidasin expression should be knocked down in hemocytes by driving dsRNA expression with *Hml-Gal4*. If removing peroxidasin from hemocytes phenocopies genetically ablating hemocytes, in the context of basement membrane scar formation, it will be strong evidence for hemocytes promoting scar formation by delivering peroxidasin to the site of repair. If the resulting phenotype differs from hemocyte ablation, in terms of scar thickness and brightness, then it will provide further evidence

that any basement membrane scar phenotypes observed upon ablating hemocytes are likely a result of basement membrane proteins not being delivered to the site of repair. For a positive control, dsRNA against peroxidasin should be expressed with *Tub-Gal4*. It is already known that peroxidasin is required for collagen IV cross-linking, so knocking down peroxidasin in all tissues will likely produce a phenotype. If knocking down peroxidasin expression with *Tub-Gal4* proves to be embryonic lethal, then *Tub-Gal80*^{ts} could be used as well to control when the dsRNA is expressed.

The basement membrane scar may be remodeled over time

Unfortunately, due to fact that larvae pupariated shortly after wound repair in this study, it is still not clear if the basement membrane scar eventually resolves. Adult *Drosophila* can live for months and therefore may be a good model for tracking the basement membrane scar over long periods of time. Though the adult *Drosophila* epidermis differs from that of the larva by being composed of diploid cells, these cells still form syncytia in order to close a wound [154]. Since reepithelialization occurs via similar mechanisms in larvae and adults, basement membrane scars may form in adults as well. A possible complication to using adults is that, so far, only puncture wounds have been used in this model and it is not clear if the composition of the adult cuticle would be amenable to pinch wounding. One of the reasons pinch wounds were used in my experiments is because puncture wounds created autofluorescent scabs that were difficult to differentiate from the basement membrane scar. However, now that the basement membrane scar has been well characterized, differentiating between autofluorescent scabs and basement membrane may be less challenging. Therefore,

experiments in adult *Drosophila* should be performed to determine if basement membrane scars are remodeled over time.

Initial experiments would seek to determine if basement membrane scars form in adult *Drosophila* post injury. Collagen IV-GFP would be a good first candidate for visualizing basement membrane scars in adults because, in larvae, it fluoresces bright enough for imaging without antibody staining. Assuming it also produces a strong signal in adults, not having to use fluorescent antibodies would speed up initial screens for basement membrane scarring. However, all the core basement membrane proteins should also be imaged to determine if they are part of the scar, as seen in *Drosophila* larvae. Puncture wounds in adult flies, approximately 4000 μm^2 in size, close within 2 days [154]. Therefore, initial images should be taken immediately before wounding, immediately after wounding, and 48 hours post wounding. Like larvae, adult flies would not be amenable to live imaging of repairing wounds, so multiple fixed samples would have to be imaged at each time point. If a basement membrane scar is observed in adults after wound closure, then samples should be imaged at later time points to determine whether or not they persist. Imaging samples at 1-week intervals post injury would be a good starting point because it would minimize the initial number of dissections required if basement membrane scars persist late into the adult fly's lifetime. If the scar is observed to resolve between two of those timepoints, then additional samples could be imaged at one day intervals within that timespan to further narrow down how long basement membrane scars persist.

If a basement membrane scar that resolves over time is observed, the next step would be to determine how it resolves. A possible mechanism for resolving the

basement membrane scar may be the secretion of MMPs. The primary role of MMPs is to degrade extracellular matrix, and they have been shown to degrade basement membranes [144]. During epidermal wound repair in *Drosophila* larvae, the level of MMPs is noticeably increased, which appears to be necessary for cell migration and the incorporation of new basement membrane. However, MMP levels remain elevated even after wound closure [134] and it is not clear if those increased MMP levels continue to have a specific function. During this study, the depletion of laminin from *Drosophila* larvae appeared to correlated with a decrease in basal MMP levels within the epidermis prior to wounding, suggesting that MMP levels are influenced by the amount of laminin present in the basement membrane. Therefore, if MMPs are continuing to be secreted after wound closure, it may be in response to excessive basement membrane components in the scar.

To determine if MMPs remodel the basement membrane scar, the tissue inhibitor of metalloproteinases (TIMP) could be overexpressed to inhibit MMP function following wound closure in adult *Drosophila*. There is only one TIMP in *Drosophila* that regulates both MMPs, and using the *A58-Gal4* driver to overexpress TIMP in the larvae epidermis has been shown to be effective in disrupting MMP function during wound repair [134]. However, since MMPs are necessary for wound closure, *A58-Gal4* will likely need to be used in conjunction with temperature sensitive $Gal80^{ts}$ to control the timing of TIMP overexpression. To inhibit MMP function as soon as possible following scar formation, TIMP overexpression will have to be induced as early as is possible without preventing wound closure, the exact timing of which will have to be determined empirically. If

MMPs are responsible for remodeling the basement membrane scar, then TIMP overexpression would be expected to slow down or completely halt scar remodeling.

Live imaging is required to study the dynamics of basement membrane repair

Within two hours of injury, the basement membrane appears to become thicker at the wound margins, suggesting that basement membrane scars begin to form before reepithelialization is complete. However, questions remain about the spatiotemporal dynamics of basement membrane repair. Does the scar really begin on the wound margins and move in as cells close the wound? Is the scar made entirely of newly incorporated proteins, or is the basement membrane pulled in from the edges of an open wound?

This study was hindered by the fact that samples had to be fixed and dissected prior to imaging, meaning new samples had to be prepared for every time point of interest. Gaining a complete understanding of the dynamics of basement membrane repair will ultimately require live imaging capabilities. Techniques have been developed to image live *Drosophila* larvae by immobilizing them in a PDMS chip that is vacuum sealed with a glass cover slip [155]. In this study, however, acquiring high resolution live images of repairing basement membrane proved to be too challenging with such a device because larvae were still able to wiggle just enough to move the epidermis out of focus. To overcome this challenge, it will be necessary to pair a PDMS device with the capability of anesthetizing larvae to prevent any movement. If such a technique can be developed, imaging basement membrane dynamics live will also require the creation of new *Drosophila* basement membrane constructs that fuse each component to

fluorescent proteins other than GFP. For example, fusing basement membrane proteins to a photoconvertible fluorophore would allow distinct regions of basement membrane to be highlighted and tracked over time. This would allow for a better understanding of the movements of basement membrane around the wound margins during repair. Additionally, having basement membrane constructs that fuse each component with RFP would allow for the ability to image multiple components at once. Paired with live imaging, it may then be possible to track the order of each component's incorporation into the basement membrane scar as it forms.

Creating the tools for live imaging in *Drosophila* larvae and optimizing the technique would likely be time consuming. Therefore, if basement membrane scarring is conserved in other model organisms, it would be advantageous to study the dynamics of scar formation, and possibly remodeling, in an organism in which high resolution, live imaging of basement membrane has already been accomplished. Therefore, *C. elegans* may be the ideal system for the live analysis of basement membrane scars. Protocols for live imaging basement membrane in sedated *C. elegans* have already been developed [156], and both puncture-wounding and laser-wounding procedures have also been published [157]. *C. elegans* reach adulthood in approximately 3 days and can live for a total of approximately 3 weeks [158]. Most importantly, they remain transparent as adults, allowing for easy visualization of internal tissues. Constructs of laminin, collagen IV, perlecan, and nidogen that are fused to fluorescent proteins, including photoconvertible fluorophores, are currently available (personal communication, David Sherwood). *C. elegans* laser-wounds that are 2-5 μm in size appear to close within 24 hours [157].

Assuming basement membrane scarring is conserved in *C.* elegans, the first step to understanding its spatiotemporal dynamics would be to simply image it over time. Laminin-GFP would be a good first candidate for live imaging the basement membrane because it has already been shown, in *C. elegans,* to produce a bright enough signal to acquire multiple images over time. Using the established protocols, *C. elegans* cannot be sedated for the entire time frame needed to complete wound repair [156]. However, they can be sedated multiple times, allowing for the acquisition of multiple images of the same wound over 24 hours. To decide how often to acquire images over the course of an experiment, it will first be necessary to determine how quickly Laminin-GFP photobleaches. Assuming at least 12 images can be taken without severe photobleaching, separate experiments could look at the first and last 12 hours of basement membrane repair, acquiring one image every hour. Of course, time between images could be adjusted if photobleaching becomes a problem. A cell marker, like tubulin, could be visualized in a different channel to keep track of reepithelialization as the basement membrane repairs. If the basement membrane scar is built from the outside in, one would expect the hole in the basement membrane to gradually get smaller over time. However, it is also possible that basement membrane repair depends upon the availability of cell surface receptors. In this scenario, a scar could either form from the outside in conjunction with reepithelialization, or appear in all areas of the wound site at once if there is a lag between reepithelialization and basement membrane repair. It should be noted that a previous student in the lab, Erica Shannon, observed speckles of basement membrane in the center of some repairing puncture wounds in *Drosophila* larvae. This observation provides evidence for basement

membrane repairing in all areas of the wound at once, but live imaging will offer a more detailed understanding of the process.

Though thicker and brighter areas of basement membrane within the scar suggest new proteins are incorporated during repair, existing basement membrane may also be repurposed to close a wound. During *C. elegans* development, the anchor cell invades its underlying basement membrane to connect the uterine and vulval tissues in hermaphrodites [159]. As a part of this process, it has been documented that, in the absence of basement membrane degrading MMPs, the cell can compensate by exerting enough force to push basement membrane aside as it invades [160]. If cells can push basement membrane aside, they may also be able to pull basement membrane with them as they close a wound. To test this hypothesis, photoconvertible fluorophores could be used to track the movement of basement membrane on the margins of a wound during repair. Laminin-Dendra has been used to document basement membrane sliding during anchor cell invasion, making it a good first candidates for imaging. Immediately after wounding, a section of basement membrane surrounding the wound border should be photoconverted and imaged. After imaging the wound site upon the completion of repair, the circumference of the photoconvertible section should be measured in each image. If the basement membrane is pulled inward as the wound closes, then the circumference of the photoconverted region would be expected to decrease following repair. Alternatively, if the basement membrane immediately surrounding the wound is spread thinner it is pulled inward, then the total area of photoconverted basement membrane may increase while the circumference remains relatively unchanged.

Concluding remarks

The simplicity of *Drosophila* epidermis and the genetic tools available in flies allowed for a detailed characterization of repaired basement membrane *in* vivo. The central discovery of this work is that basement membrane repair leaves behind a scar that is composed of every core component. More commonly studied mammalian models of wound repair are far more complex tissues that would have made imaging the basement challenging. Corneas, for example, are composed of a stratified epithelium and underlying stroma that are separated by a basement membrane [102]. Similarly, mammalian skin contains a stratified epidermal layer and underlying dermis that are separated by a basement membrane [161]. In both cases, extracellular matrix that is not part of the basement membrane, including fibrillar collagens, are present in the dermal and stromal layers [101,162]. Separating the basement membrane from either of these layers would have been tedious, if not impossible, preventing the acquisition of clear images from above or below the basement membrane. The epidermis of *Drosophila* larvae, on the other hand, is composed of a single layer of transparent epithelial cells that anchor to a basement membrane, which is not associated with an underlying dermal layer or additional extracellular matrix proteins. The distinct anchoring points for body wall muscles in *Drosophila* larvae can be easily removed while inflicting minimal damage to the basement membrane, making it possible to fillet open the epidermis and image the basement membrane from below.

It must be acknowledged, however, that the simplicity of *Drosophila* larvae epidermis also limits the extent to which this body of work can be generalized to

mammals. The more complex structure of mammalian corneas and skin means a more complex wound healing process. In skin, blood clotting forms a provisional matrix, composed of platelets, fibrin, fibronectin, and other proteins, that serves as a scaffolding for migrating keratinocytes as the wound closes. As fibroblasts migrate into the wound, fibrillar collagens are deposited (collagen III initially, which is later replaced by collagen I) that eventually account for up around 50% of resulting scar tissue. Additionally, fibroblasts transform into myofibroblasts and begin to contract, pulling the surrounding tissue together. As keratinocytes proliferate and migrate into the wound bed, they, along with dermal fibroblasts, produce new basement membrane [162]. Corneal wound healing proceeds via similar mechanisms, but it should be noted that the cornea is avascular and therefore the scab of the cornea contains no platelets. Additionally, the cornea appears to resist stimuli that would promote fibrosis in skin, possibly preventing changes in the tissue structure that could inhibit function [101].

Though puncture wounds in *Drosophila* do create a melanized clot that could be considered analogous to a scab [111], the pinch wounds used in this study did not break the outer cuticle and therefore did not elicit a clotting response. Therefore, no provisional matrix was present for epidermal cells to migrate through, and it is not entirely clear how reepithelialization takes place in this scenario. In the absence of a scab, cells may simply use the outer cuticle as a substrate for migration. Also distinct from mammals, the epidermal cells of *Drosophila* larvae do not undergo proliferation as part of wound closure. Instead, epidermal cells form syncytia, creating large multinucleate cells, that appear to promote wound closure. Finally, in the absence of a dermal layer or stroma, containing fibrillar extracellular matrix proteins, basement

membrane is the only extracellular matrix involved in *Drosophila* larva wound repair. All of these differences make wound repair in *Drosophila* larvae quite unique, and may affect the exact morphology of the basement membrane scar.

Despite the differences between *Drosophila* and mammalian wound healing, the observation that basement membrane repairs imperfectly is a novel finding. Going forward, model organisms with easily visualized basement membranes and simplified tissue structure, like *Drosophila* and *C. elegans*, will be crucial to determining the mechanisms by which basement membrane scars form, if and how they are remodeled, and the potential implications for associated cells. Though the mechanisms driving scar formation remain unknown, many of them likely overlap with mechanisms of *de novo* basement membrane assembly. Furthermore, while it is yet to be determined if other kinds of injuries create basement membrane scars, or if basement membrane scars exist in other organisms, many of those mechanisms responsible for *de novo* basement membrane assembly are widely conserved from *Drosophila* to mammals. Basement membrane abnormalities have been documented in the context of many human diseases, and are now suspected to help drive disease progression in some cases. For example, aberrant basement membrane formation in hepatic sinusoids is a recognized feature of progressive liver disease that directly impairs function [163], and glomerular basement membrane thickening is a common feature of diabetic nephropathy [164]. The mechanisms driving such diseases are complex and certainly cannot be modeled in *Drosophila* epidermis. However, the fundamental, conserved components of basement membrane and the proteins responsible for promoting its assembly likely do play a role each case. Therefore, it is entirely possible that elucidating the mechanisms of

basement membrane scar formation in a simplified model such as *Drosophila* may yet offer insights into complex human pathology.

Appendix

Basement membrane mechanics shape development

This appendix has been adapted from Ramos-Lewis, W. and Page-McCaw, A. Basement membrane mechanics shape development: Lessons from the fly. *Matrix Biology* 75-76*,* 72-81(2019). doi.org/10.1016/j.matbio.2018.04.004. It has been placed at the end of this dissertation to further put in perspective the work that is discussed in Chapter 2. The biomechanical properties of basement membrane are determined by its composition and by the way those components are organized. Because the basement membrane scar is characterized by a change in the organization of its components, future experiments may find that biomechanical properties of the scar differ from undamaged basement membrane.

Introduction

The basement membrane is a sheet-like extracellular matrix that underlies epithelial cells and endothelial cells and ensheathes muscles, fat and nerves [3]. Ranging from less than 100 nm to as much as 10 μm thick [10], basement membrane is assembled from core components conserved throughout the animal kingdom: laminin, collagen IV, nidogen, and perlecan [4]. Collagen IV is primarily responsible for bestowing stiffness upon the basement membrane, and the importance of this stiffness is supported by its presence in all metazoans, except some primitive sponges [62]. Notably, collagen IV is present in ctenophores, which is thought to be one of the earliest branching extant animal phyla [5]. In addition to providing structural support to epithelial

cells, basement membrane helps direct cellular differentiation and function by signaling via integrin and dystroglycan receptors and by binding to and modulating the diffusion of secreted growth factors [3]. In cultured cells, matrix stiffness affects cellular differentiation [165] and behavior [166]. *In vivo*, because basement membranes are assembled prior to the completion of embryogenesis [53,110,167], basement membranes must constantly be modified to accommodate changes within a given tissue as the organism grows and develops over time. Such changes can come in the form of increased deposition or degradation of basement membrane-associated proteins or adjusting the composition of proteins within the basement membrane. All of these possible alterations affect the mechanical stiffness of basement membrane [8]. Understanding the ways in which the mechanical properties of basement membrane affect the development of associated tissues *in vivo* requires a model organism that provides tools to easily manipulate basement membrane stiffness. One such model organism that has been used successfully for this topic is *Drosophila melanogaster*.

Drosophila is an excellent model for the study of basement membrane dynamics for several reasons: all of the major basement membrane components are conserved [168], the number of genes coding for each protein are significantly fewer than in mammals (see Table 2), and sophisticated tools have been developed for genetic studies in flies allowing temporal and spatial control of any gene in virtually any cell or tissue. Additionally, there are functional GFP-fusion proteins, expressed by endogenous regulatory sequences, for each of the four major basement membrane proteins in *Drosophila*, identified either as endogenous gene traps or generated as

genomic fragments in BAC transgenes. Finally, the contribution of basement membrane to development can be analyzed at many different stages.

Surprisingly, basement membrane is assembled from different sources at different times during *Drosophila* development (Fig. 15). Here is a brief summary of the dynamics of basement membrane deposition and degradation in *Drosophila* throughout its life cycle: (1) During oogenesis, each *Drosophila* egg develops from germ cells surrounded by basement membrane secreted from migratory hemocytes (Drosophila blood cells) and the distant fat body organ [169]. These develop into egg chambers surrounded by a basement membrane secreted from epithelial follicle

Table 2: Genes encoding basement membrane proteins in mice and flies. Data from Flybase, release FB2017_06 [49].

	Basement membrane protein family	Mouse genes	*Drosophila* genes
Structural proteins	**Laminin**	**11 genes**	**4 genes**
	α-chain	*Lama1* *Lama2* *Lama3* *Lama4* *Lama5*	*Laminin A (LanA)* *wing blister (wb)*
	β-chain	*Lamb1* *Lamb2* *Lamb3*	*LanB1*
	γ-chain	*Lamc1* *Lamc2* *Lamc3*	*Laminin B2 (LanB2)*
	Collagen IV	**6 genes**	**2 genes**
	Collagen IV α1	*Col4a1*	*Collagen IV alpha 1 (Col4A1)*
	Collagen IV α2	*Col4a2*	*Viking (vkg)*
	Collagen IV α3	*Col4a3*	(not present)
	Collagen IV α4	*Col4a4*	(not present)
	Collagen IV α5	*Col4a5*	(not present)
	Collagen IV α6	*Col4a6*	(not present)
	Perlecan	**1 gene** *Hspg2*	**1 gene** *terribly reduced optic lobes (trol)*
	Nidogen	**2 genes** *Nid1* *Nid2*	**1 gene** *Nidogen/entactin (Ndg)*
Extracellular BM Modifying Enzymes	**Matrix Metalloproteinase**	***24 genes*** *Mmp1a, Mmp1b, Mmp2, Mmp3, Mmp7, Mmp8, Mmp9, Mmp10, Mmp11, Mmp12, Mmp13, Mmp14, Mmp15, Mmp16, Mmp17, Mmp19, Mmp20, Mmp21, Mmp23, Mmp24, Mmp25, Mmp27, Mmp28, Mmp29*	**2 genes** *Matrix metalloproteinase 1 (Mmp1)* *Matrix metalloproteinase 2 (Mmp2)*
	Peroxidasin	***1 gene*** *Pxdn*	**1 gene** *Peroxidasin (Pxn)*
	Lysyl Oxidase	***5 genes*** *Lox* *Loxl1* *Loxl2* *Loxl3* *Loxl4*	**2 genes** *Lysyl oxidase-like 1 (Loxl1)* *Lysyl oxidase-like 2 (Loxl2)*

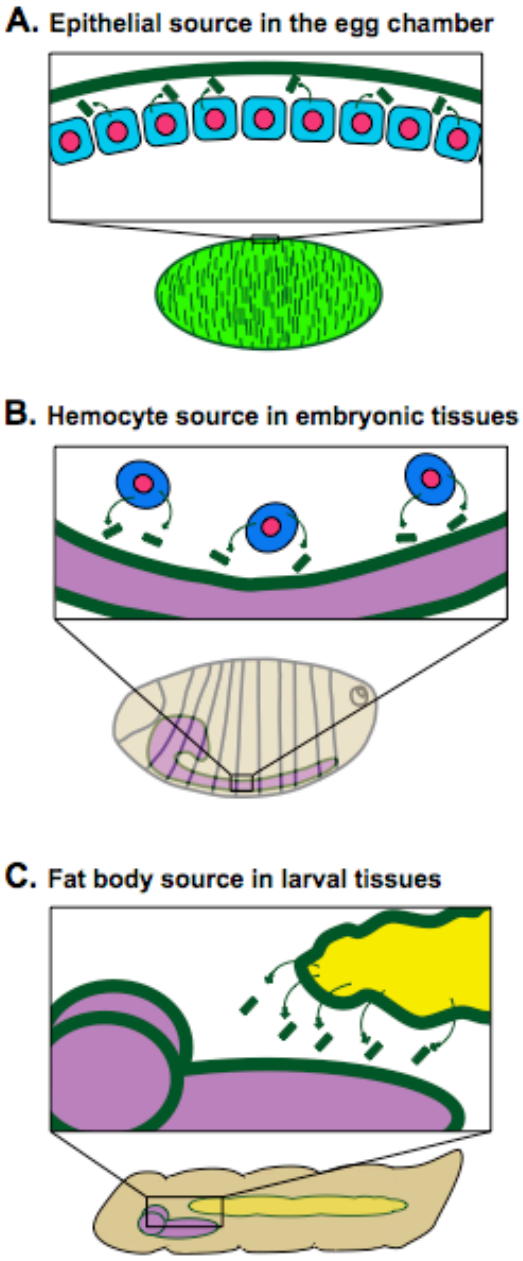

Figure 15. Cellular sources of basement membrane in *Drosophila*.
Basement membrane is synthesized and secreted from several different types of cells during Drosophila development. **A)** In developing egg chambers, follicle cells (blue) secrete their own basement membrane (green) during egg chamber elongation. **B)** During embryogenesis, hemocytes (blue) secrete basement membrane (green) onto developing organs, such as the ventral nerve cord (purple). **C)** In larvae, the fat body (yellow) secretes basement membrane proteins (green) into the open circulatory system, which are then deposited onto tissues throughout the body including the central nervous system (purple).

cells [136,169,170]. As the egg develops, additional basement membrane is deposited in parallel alignment by neighboring follicle cells, generating patterns in the basement membrane that allow egg shape elongation [137,171]. (2) During embryogenesis, hemocytes secrete basement membrane onto the developing organs in the late embryo, and this matrix deposition is necessary for completion of embryogenesis [128,129]. (3) Once the embryo hatches into a larva, basement membrane proteins are secreted into the hemolymph of the larval open circulatory system, primarily from the fat body, an adipose tissue that functions to regulate metabolism and immunity. These secreted proteins are then incorporated into the basement membranes of growing tissues and organs, such as the central nervous system and the wing disc, as the larva develops from 1st to 3rd instar [99]. (4) When the larva undergoes metamorphosis to take on its adult form, the larval tissues must be broken down as the adult tissues develop from the imaginal tissues. At this time, basement membranes are also broken down, both around the histolyzing larval tissues and around the imaginal discs that are undergoing rapid growth and eversion to create the structures of an adult fly [125,172]. These adult structures will themselves be associated with newly formed basement membrane, though little is known about how this new basement membrane is deposited. These developmental stages offer many opportunities for investigating the assembly and function of basement membranes in shaping and maintaining the organs they encase, as described below.

Egg chamber basement membrane: stiffness determines organ shape

Drosophila eggs develop within an egg chamber, consisting of 16 germline cells surrounded by a monolayer of epithelial (follicle) cells [173]. Each egg chamber forms within a smooth sheet-like basement membrane that envelops it [170]. As the egg chamber develops, its volume increases ~5000-fold, and its shape changes from a sphere with an aspect ratio of ~1, to an ellipsoid with an aspect ratio of ~2 [174]. As the egg chamber grows, the basement membrane must expand and remodel to accommodate such a dramatic transformation. However, in recent years it has become apparent that basement membrane remodeling does not merely take place to accommodate egg chamber elongation; rather basement membrane actually drives the process (summarized in Fig. 16A).

Live imaging reveals that the entire *Drosophila* egg chamber rotates inside its basement membrane covering, around the anterior-posterior axis (A-P axis), until stage 9 of egg development [171]. Rotation results from the follicle epithelial cells collectively crawling on the basement membrane, aligning contractile actin bundles across the tissue so that they are parallel to their migration path [171,175]. During rotation, elongated aggregates of extracellular matrix are deposited beneath the follicle cells, appearing as basement membrane fibrils parallel to the actin bundles [137]. Because egg chamber elongation is co-incident with both rotation and matrix deposition, several labs have used genetic manipulations to investigate the causality among these three phenomena – rotation, basement membrane, and elongation. The existence of a *fat2* hypomorphic condition with egg chambers that did not appear to rotate *ex vivo* but nevertheless elongated suggested that rotation and elongation were independent [176]. However, it

was recently determined that egg chambers of the same mutant condition do indeed rotate *in vivo*, albeit more slowly; this result was enabled by a new tool that identifies the path of a migrating cell by its secreted extracellular matrix [177]. Thus, elongation and

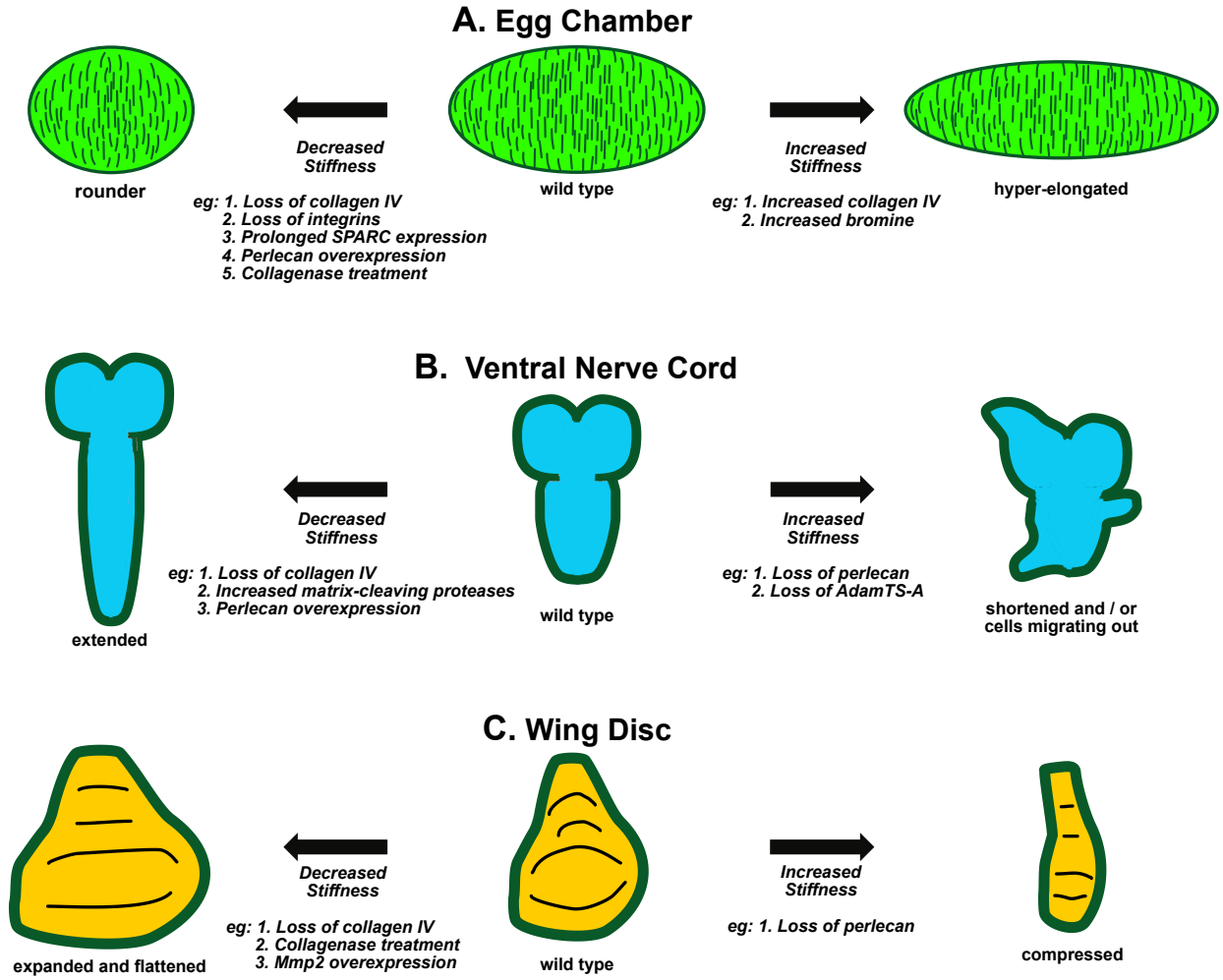

Figure 16. Basement membrane stiffness alters organ shape.
All *Drosophila* organs are surrounded by a continuous sheet of basement membrane. **A)** The basement membrane surrounding wild-type developing egg chambers does not have uniform stiffness, but rather is more stiff in the middle and less stiff toward the poles. Perturbations that decrease the stiffness lead to rounded egg chambers, whereas those that increase the stiffness leads to hyper-elongated egg chambers. See text for details.
B) The larval central nervous system is composed of two brain lobes (top) and an elongated ventral nerve cord. Perturbations that soften the basement membrane allow hyper-elongation of the ventral nerve cord, whereas those that generate stiffer basement membrane result in compaction of the ventral nerve cord and mobilize neural progenitor cells to migrate out of the central nervous system, as described in the text.
C) The larval wing disc is the precursor of adult wing and notum tissues, and it has a characteristic shape. Softer basement membrane allows the wing disc to expand and flatten, whereas stiffer basement membrane compresses it, as described in the text.

rotation remain inseparable, and any perturbation that halts rotation also inhibits elongation.

As the egg chamber rotates, aggregates of collagen IV and other matrix proteins are deposited from follicle cells into the basement membrane, forming aligned fibrils in the direction of cellular migration [170,171,178]. A recent study has shown that these fibrils are secreted from cells basal-laterally into the pericellular space between follicle epithelial cells before being deposited onto the underlying basement membrane [137]. When the integrin β_{PS} subunit *myospheroid (mys*) or the collagen IV α2 *viking (vkg*) were mutated, both egg chamber rotation and elongation were disrupted, providing the first evidence that the deposition of this basement membrane influences the elongation of the egg chambers [171], although it was not possible to distinguish whether basement membrane was acting directly by constraining shape or indirectly by promoting rotation. Basement membrane was shown to be the driving force behind egg chamber elongation in an experiment in which the expression of Secreted Protein Acidic and Rich in

Cysteine (SPARC) was prolonged into the timeframe when collagen IV fibrils are being deposited [179]. SPARC is thought to solubilize collagen IV, and therefore decrease how much is deposited into the basement membrane [99,180]. The continued expression of SPARC did not disrupt rotation of the follicle epithelium but did result in a substantial decrease in egg chamber elongation, firmly establishing the role of basement membrane in driving elongation independently of rotation [179].

Recently, two studies made a giant leap forward by analyzing the stiffness of this basement membrane at a quantitative level using atomic force microscopy (AFM) [114,115]. AFM measures the compressive modulus, or stiffness, of a material. Here, AFM was used to measure the stiffness of basement membrane when compressed radially from outside the egg chamber toward the center (along the apical-basal axis of the follicle cells). When measured this way, basement membrane stiffness varies along the long (anterior-posterior) axis of a stage 7-8 egg chamber, with stiffness greatest at the center and decreasing towards the poles. Importantly, the basement membrane itself is responsible for creating the tissue stiffness gradient along the anterior-posterior axis, as stiffness is reduced upon collagenase treatment but not upon actin depolymerization with latrunculin A. This anisotropy or difference in stiffness along the anterior-posterior axis is an important driver of elongation, as demonstrated in experiments that separate the anisotropy from absolute stiffness. When overall basement membrane stiffness was decreased by 20% but the anisotropy remained, egg chamber elongation was unchanged. Complementary experiments eliminated the anisotropy by evening out the stiffness along the axis, in one case depleting collagen IV specifically in the middle region of the follicle epithelium, resulting in a 30% decrease in egg chamber elongation.

Conversely, when collagen IV deposition was increased, and the anisotropic gradient increased by 20%, the egg chamber became hyper-elongated [114]. These results suggest that as the egg chamber increases in volume, the regions nearer the poles expand radially (along the apical/basal axis of the follicle cells) because of the decreased polar matrix stiffness, whereas the central region is constrained by stiffer matrix. Yet this stiffness anisotropy along the anterior-posterior axis does not appear to account for all the elongation, as egg chambers still elongate 70% of their normal length when stiffness is made constant.

A possible second mechanism is suggested by measurements of the stiffness of individual matrix fibrils deposited by the rotating follicle epithelium. As expected, these fibrils are stiffer than surrounding fibril-free regions [115]. The alignment of these long parallel fibrils would create another kind of stiffness anisotropy in the 2D plane of the basement membrane: resistance to stretching in one direction (circumferential expansion) but not the other (anterior-posterior elongation). This anisotropy would represent a difference in tensile stiffness in the planar dimensions of the basement membrane, which unfortunately cannot be measured by AFM as it measures compressive stiffness (i.e., resistance to pushing rather than pulling forces); and measures it along a different axis, from the outside in (apical/basal axis) rather than in the basement membrane plane [114,115]. A quantitative analysis of the X-Y stiffness anisotropy generated by the aligned fibers awaits the development of an assay to measure tensile stiffness in the basement membrane plane, one that would likely utilize a sheet of decellularized follicular basement membrane [115].

In addition to its direct role in constraining egg chamber shape, basement membrane also plays an indirect role in increasing egg chamber volume, which is necessary for elongation. Egg chambers develop inside a peristaltic muscle sheath, which rhythmically contracts and propels the egg chambers posteriorly toward the oviduct for laying. Surprisingly, muscle sheath contractions are also important for oocyte yolk uptake from the surrounding hemolymph fluid, and when this muscle function is compromised, the oocyte does not increase in volume as much as wild-type, and egg elongation is reduced [181]. Muscular dystrophy research has illustrated the importance of muscle basement membranes for muscle function, as they distribute actomyosin contractile forces across the muscle surface and thus protect against muscles shredding themselves under the force of contraction [182]. Similarly, egg chamber muscle sheath function requires basement membrane integrity. Thus, when laminin or integrins are depleted from muscle sheaths, muscle contractions are compromised. Without the muscle contractions, egg chambers are smaller in volume and less elongated [181].

Much of basement membrane's mechanical strength is derived from the significant cross-linking that takes place between collagen IV trimers [58,61]. Since egg chamber elongation is driven by basement membrane stiffness, elongation was used to probe the mechanism of collagen IV crosslinking, resulting in the identification of bromine as a new essential element. Bromine is a required cofactor for the enzyme peroxidasin in the reaction that generates sulfilimine bonds crosslinking collagen IV. This *in vitro* requirement suggested that bromine is an element essential in animals. To test the bromine requirement *in vivo*, flies were fed a bromine-free diet. Flies could not

survive without bromine, confirming that bromine is an essential element. Interestingly, before they died, female flies laid eggs that were rounder than those that consumed bromine-supplemented food. In addition to decreased aspect ratios, eggs depleted of bromine or with peroxidasin inhibited had significantly smaller volumes than control eggs [64]. These results indicate that bromine-dependent sulfilimine crosslinking is critical for basement membrane function, especially in the sheath muscles required for increases in oocyte volume. Interestingly, when food was supplemented with bromine above physiological levels, elongation was increased above control levels, and this bromine-induced hyper-elongation was dependent on peroxidasin, which catalyzes the collagen IV sulfilimine crosslink. These chemico-genetic experiments provide important *in vivo* confirmation of the *in vitro* mechanism of bromide-dependent collagen IV crosslinking; they also illustrate the role of basement membrane stiffness in muscle function and egg chamber elongation [64].

The above studies demonstrate how *Drosophila* egg chamber development is proving to be a powerful *in vivo* model for analyzing the role of basement membrane in shaping organs. It is becoming an exceptional model when the mechanical properties of basement membrane are at the center of these questions.

Central nervous system basement membrane: stiffness alters migration

As *Drosophila* larvae grow from first to third instars, the central nervous system grows along with it. The central nervous system is comprised of two brain lobes and an elongated ventral nerve cord, and it is encased by a basement membrane called the neural lamella, which is important for separating the developing nervous system from

the nearby epidermis during embryonic development [183]. This neural lamella is deposited by migrating hemocytes (Drosophila inflammatory cells), and interestingly, the laminin secreted by the hemocytes aids in their migration, as they seem to assemble autonomously a substrate for their migration [129,183]. The relationship between basement membrane composition, stiffness, and organ shape in the ventral nerve cord has been explored in several studies. Changes in matrix composition alter the shape of the ventral nerve cord: specifically, a shorter ventral nerve cord is observed upon the loss of perlecan [99]. This result indicates that matrix stiffness constrains nerve cord elongation, because several studies have determined that perlecan counters basement membrane stiffness. The role of perlecan in softening basement membrane is supported by direct AFM measurement of egg chamber basement membrane stiffness: when perlecan is overexpressed, the basement membrane becomes less stiff [114]. This role of perlecan is also supported by the observation that the same manipulation makes eggs rounder and by several other qualitative phenotypes in which perlecan opposes the action of collagen IV [99,112,113,179]. When perlecan levels are reduced by RNAi in the egg chamber basement membrane, electron microscopy shows that the resulting basement membrane is visibly damaged, and this damage is accompanied by reduction in stiffness measured by AFM [115]. We speculate that perlecan's role in opposing basement membrane stiffness may be essential for rapid basement membrane expansion without damage.

In contrast to the shorter ventral nerve cord caused by the loss of perlecan, the ventral nerve cord elongates upon the overexpression of perlecan, the loss of collagen IV, or the overexpression of several matrix-cleaving proteases, including the matrix

metalloproteinases Mmp2, the ADAM Kuzbanian, and AdamTS-A [99,113,184,185] (summarized in Fig. 16B). Like the perlecan results, these protease results suggest that a loss of matrix stiffness leads to a longer ventral nerve cord and that the basement membrane constrains the length of this organ. It is straightforward to assume that protease cleavage results in a softer matrix, but surprisingly, the inactivation of Mmp2 by expression of its inhibitor Timp or a dominant-negative construct also results in a longer ventral nerve cord, as does the dominant-negative AdamTS-A [113,184]. One possibility is that, in addition to cleaving matrix components directly, these proteases may also activate matrix turnover indirectly by binding to partners that affect this process.

Remarkably, loss-of-function of AdamTS-A or perlecan causes a dramatic cellular phenotype in the central nervous system. In perlecan mutants, neural progenitor cells appear to bulge out of the CNS [99,113] while the loss of AdamTS-A causes them to migrate out of the nervous system and invade other tissues [113]. This aberrant morphology seems to be triggered by increases in matrix stiffness, as the invasion phenotype caused by the loss of AdamTS-A is suppressed by the overexpression of perlecan or loss of function in collagen IV or β-integrin; and when AdamTS-A is reduced, aggregates of basement membrane proteins decorate the normally smooth neural lamella. This aberrant migration is consistent with studies of cultured cells showing that increasing ECM stiffness promotes cell migration [186].

Further evidence for basement membrane stiffness regulating the migration of cells out of the central nervous system comes from a study that used *Drosophila* eye development as a model for glial tumors. *Drosophila* retinal glial cells originate in the

optic stalk and migrate along it toward the eye disc. In a *Drosophila* glioma model, ectopic activation of PVR (homolog of PDGF- and VEGF-Receptors) leads to increased glial cell migration in 3rd instar larvae. This glial cell migration depends directly on basement membrane stiffness, and migration requires glial-cell specific Lysyl oxidase (Lox) activity, which crosslinks lysine residues in the ECM and thus increases ECM stiffness. Either chemical inhibition or genetic knock-down of Lox leads to a decrease in glial cell migration. The stiffness of the neural lamella was directly assessed via AFM, confirming that the stiffness of the neural lamella is decreased in the absence of Lox function [187]. Thus *in vivo* as in cultured cells, matrix stiffness can promote cell migration.

Wing disc basement membrane: distinguishing between the roles of cellular compression and ligand retention

Studies in the *Drosophila* wing disc have illustrated that basement membrane can have multiple mechanical functions, both altering tissue forces through cellular compression and acting as a physical barrier to ligand diffusion. The wing disc is one of the imaginal discs, specialized insect tissues that contain precursor cells that will develop into adult tissues and organs after metamorphosis. This seemingly simple structure has been studied as a model for tissue morphogenesis for decades [188]. More recently, the wing disc has been an excellent context for interrogating hypotheses about how basement membrane drives the shape of developing tissues, using genetic approaches. Basement membrane surrounds all imaginal discs and is important for determining the shape of the wing disc in the larval stage. For example, depletion of

collagen IV by RNAi or collagenase treatment causes the wing disc to expand; conversely depletion of perlecan compresses the wing disc [99] (summarized in Fig. 16C). These observations were used to test the hypothesis that basement-membrane based mechanical signaling alters cellular proliferation, which would lead to changes in the eventual shape of the later adult wing [189]. The depletion of perlecan does appear to increase the compressive forces of the basement membrane around the wing disc, as the apical area of cells in the wing disc decreases dramatically. Contrary to predictions, however, this increase in compression does not affect the size or shape of the later adult wing [112]. The converse experiment, releasing basement membrane constriction in the wing disc, was performed by overexpressing the matrix metalloproteinase Mmp2, which leads to an expanded wing disc made of cells with larger apical area. The mechanical signaling hypothesis predicts that the loss of compression would stimulate cells to proliferate, resulting in a larger adult wing. However, the opposite was observed: adult wings were about 30% smaller. These results suggest that although the basement membrane does influence the final organ size, it is not a mechanically-based signal. Instead, further experiments found that the basement membrane shapes the adult wing by acting as a physical barrier to diffusion of the signaling ligand Dpp, a member of the TGFβ family that is known to bind collagen IV *in vivo* [21]. Dpp is generated by cells within the wing disc and is retained within the disc environment by the surrounding basement membrane. When this matrix was removed by the expression of *Mmp2*, Dpp diffused away from the wing disc and was taken up in other distant tissues, with the result that wing disc Dpp signaling was reduced. Thus the reduction in final wing size was attributed to loss of the Dpp signaling ligand without

basement membrane to retain it in the wing [112]. In this role, basement membrane acts as a signaling insulator, trapping diffusible signaling molecules in the vicinity of their cellular sources.

This study illustrates the detailed investigation of mechanical-based models of basement membrane function possible in *Drosophila*. Although it appears that basement membrane stiffness has a profound influence on the associated tissues, great care must be taken to unravel the ways in which basement membrane composition affects morphology, as both mechanical forces and ligand based signaling can be altered by basement membranes.

Concluding remarks

The studies discussed in this review illustrate how *Drosophila* offers an *in vivo* model to manipulate basement membrane mechanics and to discern the contributions of basement membrane mechanics to development. The contributions of these studies include a greater understanding of the mechanism by which basement membrane shapes organs, influences cellular migration, and facilitates cell signaling. One important conclusion from these collected *Drosophila* basement membrane studies is that basement membrane stiffness is not uniform. Even within one organ system, the egg chamber, stiffness reproducibly varies by 300% across a region that is only 13 cells and 100 μm wide [114]. This observation leads to intriguing questions about how the stiffness is determined and to what extent cells can alter it. Clearly altering the ratios of collagen IV and perlecan can affect dramatic changes in stiffness. In addition to changing basement membrane composition, another mechanism that could alter

stiffness is changing basement membrane crosslinking. Indeed, the extent of sulfilimine crosslinking of collagen IV molecules varies between tissues in a stereotyped manner, with mammalian placental basement membrane about 50% more crosslinked than glomerular basement membrane, and sulfilimine crosslinking is essential for organ shape and viability [64]. Importantly, *Drosophila* glial cells migrating over neural lamella use Lox-based matrix crosslinking to alter the stiffness of that basement membrane about two-fold. Expression of *lox* is under control of an integrin-based signaling system, indicating that the cell senses matrix stiffness and then increases it [187]. Thus, in this tumor model, cells regulate matrix stiffness in a dynamic manner, a finding that suggests cells may dynamically alter stiffness under normal physiological or developmental conditions as well. Indeed, an analysis of basement membrane stiffness in mosaic egg chambers where some follicle cells have been genetically manipulated to secrete less collagen IV suggests that basement membrane stiffness is rapidly altered by follicle cells [115]. It will be interesting to discover how relative and absolute levels of basement membrane stiffness are set during development and to discover how those set-points are changed in response to developmental and environmental cues.

Finally, while this review has focused on the contributions of *Drosophila* to our understanding of basement membrane mechanics, it is important to acknowledge that *C. elegans*, the other major invertebrate model organism, is also revolutionizing our understanding of basement membrane biology. Notable work in *C. elegans* has illuminated the intricacies of basement membrane invasion [159], identified new structures in basement membrane architecture [190], and has added to our knowledge of the basement membrane's role in nervous system development [191]. As the genetic tools in

both *Drosophila* and *C. elegans* continue to evolve, there is no doubt that both model systems will continue play an essential role in the field.

References

1. Özbek, S., Balasubramanian, P. G., Chiquet-Ehrismann, R., Tucker, R. P. & Adams, J. C. The Evolution of Extracellular Matrix. *Molecular Biology of the Cell* **21,** 4300–4305 (2010).

2. Hynes, R. O. & Naba, A. Overview of the Matrisome--An Inventory of Extracellular Matrix Constituents and Functions. *Cold Spring Harbor Perspectives in Biology* **4,** 1–16 (2012).

3. Yurchenco, P. D. Basement Membranes: Cell Scaffoldings and Signaling Platforms. *Cold Spring Harbor Perspectives in Biology* **3,** 1–27 (2011).

4. Hynes, R. O. The evolution of metazoan extracellular matrix. *The Journal of Cell Biology* **196,** 671–679 (2012).

5. Fidler, A. L. *et al.* Collagen IV and basement membrane at the evolutionary dawn of metazoan tissues. *Elife* **6,** 1–24 (2017).

6. Pozzi, A., Yurchenco, P. D. & Iozzo, R. V. The nature and biology of basement membranes. *Matrix Biology* **57-58,** 1–11 (2017).

7. Jayadev, R. & Sherwood, D. R. Basement membranes. *Current Biology* **27,** R207–R211 (2017).

8. Miller, R. T. Mechanical properties of basement membrane in health and disease. *Matrix Biology* **57-58,** 366–373 (2017).

9. Funk, S. D., Lin, M.-H. & Miner, J. H. Alport syndrome and Pierson syndrome: Diseases of the glomerular basement membrane. *Matrix Biology* **71-72,** 250–261 (2018).

10. Halfter, W. *et al.* Protein composition and biomechanical properties of in vivo-derived basement membranes. *Cell Adhesion & Migration* **7,** 64–71 (2014).

11. Languino, L. R. *et al.* Endothelial cells use alpha 2 beta 1 integrin as a laminin receptor. *The Journal of Cell Biology* **109,** 2455–2462 (1989).

12. Hall, D. E. The alpha 1/beta 1 and alpha 6/beta 1 integrin heterodimers mediate cell attachment to distinct sites on laminin. *The Journal of Cell Biology* **110,** 2175–2184 (1990).

13. Ignatius, M. J. & Reichardt, L. Identification of a neuronal laminin receptor: an Mr 200K/120K integrin heterodimer that binds laminin in a divalent cation-dependent manner. *Neuron* **1,** 713–725 (1988).

14. Ervasti, J. M. & Campbell, K. A role for the dystrophin-glycoprotein complex as a transmembrane linker between laminin and actin. *The Journal of Cell Biology* **122,** 809–823 (1993).

15. Yamada, H., Shimizu, T., Tanaka, T., Campbell, K. P. & Matsumura, K. Dystroglycan is a binding protein of laminin and merosin in peripheral nerve. *FEBS Letters* **352,** 49–53 (1994).

16. Li, S. *et al.* Integrin and dystroglycan compensate each other to mediate laminin-dependent basement membrane assembly and epiblast polarization. *Matrix Biology* **57-58,** 272–284 (2017).

17. Roberts, D. D. *et al.* Laminin binds specifically to sulfated glycolipids. *Proc. Natl. Acad. Sci. U.S.A.* **82,** 1306–1310 (1985).

18. Lee, J. L. & Streuli, C. H. Integrins and epithelial cell polarity. *Journal of Cell Science* **127,** 3217–3225 (2014).

19. Goulas, S., Conder, R. & Knoblich, J. A. The Par Complex and Integrins Direct Asymmetric Cell Division in Adult Intestinal Stem Cells. *Cell Stem Cell* **11,** 529–540 (2012).

20. Constantin, B. Dystrophin complex functions as a scaffold for signalling proteins. *BBA - Biomembranes* **1838,** 635–642 (2014).

21. Wang, X., Harris, R. E., Bayston, L. J. & Ashe, H. L. Type IV collagens regulate BMP signalling in Drosophila. *Nature* **455,** 72–77 (2008).

22. Bunt, S. *et al.* Hemocyte-Secreted Type IV Collagen Enhances BMP Signaling to Guide Renal Tubule Morphogenesis in Drosophila. *Developmental Cell* **19,** 296–306 (2010).

23. Dolez, M., Nicolas, J. F. & Hirsinger, E. Laminins, via heparan sulfate proteoglycans, participate in zebrafish myotome morphogenesis by modulating the pattern of Bmp responsiveness. *Development* **138,** 1015–1015 (2011).

24. Hollway, G. & Currie, P. Vertebrate myotome development. *Birth Defects Research (Part C)* **75,** 172–179 (2005).

25. Yurchenco, P. D., McKee, K. K., Reinhard, J. R. & Rüegg, M. A. Laminin-deficient muscular dystrophy: Molecular pathogenesis and structural repair strategies. *Matrix Biology* **71-72,** 174–187 (2018).

26. Xu, H., Wu, X.-R., Wewer, U. M. & Engvall, E. Murine muscular dystrophy caused by a mutation in the laminin α2 (Lama2) gene. *Nat. Genet.* **8,** 297–302 (1994).

27. Groffen, A. J. *et al.* Agrin is a major heparan sulfate proteoglycan in the human glomerular basement membrane. *The Journal of Histochemistry and Cytochemistry* **46,** 19–27 (1998).

28. Bassat, E. *et al.* The extracellular matrix protein agrin promotes heart regeneration in mice. *Nature* 1–17 (2017). doi:10.1038/nature22978

29. Broadie, K., Baumgartner, S. & Prokop, A. Extracellular matrix and its receptors in drosophila neural development. *Devel Neurobio* **71,** 1102–1130 (2011).

30. Timpl, R. *et al.* Laminin--a glycoprotein from basement membranes. *The Journal of Biological Chemistry* **254,** 9933–9937 (1979).

31. Cooper, A. R., Kurkiken, M., Taylor, A. & Hogan, B. L. M. Studies on the Biosynthesis of Laminin by Murine Parietal Endoderm Cells. *European Journal of Biochemistry* **119,** 189–197 (1981).

32. Howe, C. C. & Dietzschold, B. Structural analysis of three subunits of laminin from teratocarcinoma-derived parietal endoderm cells. *Developmental Biology* **98,** 385–391 (1983).

33. Ott, U., Odermatt, E., Engel, J., Furthmayr, H. & Timpl, R. Protease Resistance and Conformation of Laminin. *European Journal of Biochemistry* **123,** 63–72 (1982).

34. Yurchenco, P. D., Tsilibary, E. C., Charonis, A. S. & Furthmayr, H. Laminin polymerization in vitro. Evidence for a two-step assembly with domain specificity. *The Journal of Biological Chemistry* **260,** 7636–7644 (1985).

35. Yurchenco, P. D. Laminin forms an independent network in basement membranes [published erratum appears in J Cell Biol 1992 Jun;118(2):493]. *The Journal of Cell Biology* **117,** 1119–1133 (1992).

36. Aumailley, M. *et al.* A simplified laminin nomenclature. *Matrix Biology* **24,** 326–332 (2005).

37. Paulsson, M. *et al.* Evidence for coiled-coil alpha-helical regions in the long arm of laminin. *The EMBO Journal* **4,** 309–316 (1985).

38. Engel, J., Odermatt, E. & Engel, A. Shapes, domain organizations and flexibility of laminin and fibronectin, two multifunctional proteins of the extracellular matrix. *J. Mol. Biol.* **150,** 97–120 (1981).

39. Schittny, J. C. & Yurchenco, P. D. Terminal short arm domains of basement membrane laminin are critical for its self-assembly. *The Journal of Cell Biology* **110,** 825–832 (1990).

40. Kramer, R. H. *et al.* Laminin-binding integrin α7β1: functional characterization and expression in normal and malignant melanocytes. *Cell Regulation* **2,** 805–817 (1991).

41. Lee, E. C., Lotz, M. M., (null), G. S. & Mercurio, A. M. The integrin alpha 6 beta 4 is a laminin receptor. *The Journal of Cell Biology* **117,** 671–678 (1992).

42. Gee, S. H. *et al.* Laminin-binding protein 120 from brain is closely related to the dystrophin-associated glycoprotein, dystroglycan, and binds with high affinity to the major heparin binding domain of laminin. *The Journal of Biological Chemistry* **268,** 14972–14980 (1993).

43. Colognato-Pyke, H. *et al.* Mapping of Network-forming, Heparin-binding, and α1β1 Integrin-recognition Sites within the α-Chain Short Arm of Laminin-1. *The Journal of Biological Chemistry* **270,** 9398–9406 (1995).

44. Colognato, H., MacCarrick, M., O'Rear, J. J. & Yurchenco, P. D. The Laminin α2-Chain Short Arm Mediates Cell Adhesion through Both the α1β1 and α2β1 Integrins. *The Journal of Biological Chemistry* **272,** 29330–29336 (1997).

45. Beck, K., Dixon, T. W., Engel, J. & Parry, D. Ionic interactions in the coiled-coil domain of laminin determine the specificity of chain assembly. *J. Mol. Biol.* **231,** 311–323 (1993).

46. Gullberg, M. K., Garrison, K., MacKrell, A. J., Fessler, L. I. & Fessler, J. H. Laminin A chain: expression during Drosophila development and genomic sequence. *The EMBO Journal* **11,** 4519–4527 (1992).

47. Garrison, K., MacKrell, A. J. & Fessler, J. H. Drosophila laminin A chain sequence, interspecies comparison, and domain structure of a major carboxyl portion. *The Journal of Biological Chemistry* **266,** 22899–22904 (1991).

48. Martin, D. *et al.* wing blister, A New DrosophilaLaminin α Chain Required for Cell Adhesion and Migration during Embryonic and Imaginal Development. *The Journal of Cell Biology* **145,** 191–201 (1999).

49. Gramates, L. S. *et al.* FlyBase at 25: looking to the future. *Nucleic Acids Research* **45,** D663–D671 (2017).

50. Wiradjaja, F., DiTommaso, T. & Smyth, I. Basement membranes in development and disease. *Birth Defects Research (Part C)* **90,** 8–31 (2010).

51. Timpl, R., Wiedemann, H., Van Delden, V., Furthmayr, H. & Kuhn, K. A Network Model for the Organization of Type IV Collagen Molecules in Basement Membranes. *European Journal of Biochemistry* **120,** 203–211 (1981).

52. Brown, K. L., Cummings, C. F., Vanacore, R. M. & Hudson, B. G. Building collagen IV smart scaffolds on the outside of cells. *Protein Science* **26,** 2151–2161 (2017).

53. Pöschl, E. *et al.* Collagen IV is essential for basement membrane stability but dispensable for initiation of its assembly during early development. *Development* **131,** 1619–1628 (2004).

54. Pöschl, E., Pollner, R. & Kühn, K. The genes for the alpha 1(IV) and alpha 2(IV) chains of human basement membrane collagen type IV are arranged head-to-head and separated by a bidirectional promoter of unique structure. *The EMBO Journal* **7,** 2687–2695 (1988).

55. Burbelo, P. D., Martin, G. R. & Yamada, Y. Alpha 1(IV) and alpha 2(IV) collagen genes are regulated by a bidirectional promoter and a shared enhancer. *Proc. Natl. Acad. Sci. U.S.A.* **85,** 9679–9682 (1988).

56. Yasothornsrikul, S., Davis, W. J., Cramer, G., Kimbrell, D. A. & Dearolf, C. R. viking: identification and characterization of a second type IV collagen in Drosophila. *Gene* **198,** 17–25 (1997).

57. Natzle, J. E., Monson, J. M. & McCarthy, B. J. Cytogenetic location and expression of collagen-like genes in Drosophila. *Nature* **296,** 368–371 (1982).

58. Bhave, G., Colon, S. & Ferrell, N. The sulfilimine cross-link of collagen IV contributes to kidney tubular basement membrane stiffness. *American Journal of Physiology-Renal Physiology* **313,** F596–F602 (2017).

59. Añazco, C. *et al.* Lysyl Oxidase-like-2 Cross-links Collagen IV of Glomerular Basement Membrane. *The Journal of Biological Chemistry* **291,** 25999–26012 (2016).

60. Kuhn, K. *et al.* Macromolecular structure of basement membrane collagens. *FEBS Letters* **125,** 123–128 (1981).

61. Vanacore, R. *et al.* A sulfilimine bond identified in collagen IV. *Science* **325,** 1230–1234 (2009).

62. Fidler, A. L. *et al.* A unique covalent bond in basement membrane is a primordial innovation for tissue evolution. *Proc. Natl. Acad. Sci. U.S.A.* **111,** 331–336 (2014).

63. Bhave, G. *et al.* Peroxidasin forms sulfilimine chemical bonds using hypohalous acids in tissue genesis. *Nature Chemical Biology* **8,** 784–790 (2012).

64. McCall, A. S. *et al.* Bromine Is an Essential Trace Element for Assembly of Collagen IV Scaffolds in Tissue Development and Architecture. *Cell* **157,** 1380–1392 (2014).

65. Yurchenco, P. D. & Ruben, G. D. Basement membrane structure in situ: evidence for lateral associations in the type IV collagen network. *The Journal of Cell Biology* **105,** 2559–2568 (1987).

66. Yurchenco, P. D. & Furthmayr, H. Self-assembly of basement membrane collagen. *Biochemistry* **23,** 1839–1850 (1984).

67. Dziadek, M., Paulsson, M. & Timpl, R. Identification and interaction repertoire of large forms of the basement membrane protein nidogen. *The EMBO Journal* **4,** 2513–2518 (1985).

68. Fox, J. W. *et al.* Recombinant nidogen consists of three globular domains and mediates binding of laminin to collagen type IV. *The EMBO Journal* **10,** 3137–3146 (1991).

69. Reinhardt, D. *et al.* Mapping of nidogen binding sites for collagen type IV, heparan sulfate proteoglycan, and zinc. *The Journal of Biological Chemistry* **268,** 10881–10887 (1993).

70. Kohfeldt, E., Sasaki, T., Göhring, W. & Timpl, R. Nidogen-2: a new basement membrane protein with diverse binding properties. *J. Mol. Biol.* **282,** 99–109 (1998).

71. Ho, M. S. P., Böse, K., Mokkapati, S., Nischt, R. & Smyth, N. Nidogens—Extracellular matrix linker molecules. *Microsc. Res. Tech.* **71,** 387–395 (2008).

72. Miosge, N., Sasaki, T. & Timpl, R. Evidence of nidogen-2 compensation for nidogen-1 deficiency in transgenic mice. *Matrix Biology* **21,** 611–621 (2002).

73. Murdoch, A. D., Dodge, G. R., Cohen, I., Tuan, R. S. & Iozzo, R. V. Primary structure of the human heparan sulfate proteoglycan from basement membrane (HSPG2/perlecan). A chimeric molecule with multiple domains homologous to the low density lipoprotein receptor, laminin, neural cell adhesion molecules, and epidermal growth factor. *The Journal of Biological Chemistry* **267,** 8544–8557 (1992).

74. Paulsson, M., Yurchenco, P. D., Ruben, G. C., Engel, J. & Timpl, R. Structure of low density heparan sulfate proteoglycan isolated from a mouse tumor basement membrane. *J. Mol. Biol.* **197,** 297–313 (1987).

75. Gubbiotti, M. A., Neill, T. & Iozzo, R. V. A current view of perlecan in physiology and pathology: A mosaic of functions. *Matrix Biology* **57-58,** 285–298 (2017).

76. Zoeller, J. J., Whitelock, J. M. & Iozzo, R. V. Perlecan regulates developmental angiogenesis by modulating the VEGF-VEGFR2 axis. *Matrix Biology* **28,** 284–291 (2009).

77. Smith, S. M. L. *et al.* Heparan and chondroitin sulfate on growth plate perlecan mediate binding and delivery of FGF-2 to FGF receptors. *Matrix Biology* **26,** 175–184 (2007).

78. Rider, C. C. Heparin/heparan sulphate binding in the TGF-β cytokine superfamily. *Biochemical Society Transactions* **34,** 458–460 (2006).

79. Xu, Y.-X. *et al.* The glycosylation-dependent interaction of perlecan core protein with LDL: implications for atherosclerosis. *J. Lipid Res.* **56,** 266–276 (2015).

80. Mongiat, M. *et al.* The Protein Core of the Proteoglycan Perlecan Binds Specifically to Fibroblast Growth Factor-7. *The Journal of Biological Chemistry* **275,** 7095–7100 (2000).

81. Mongiat, M. *et al.* Fibroblast Growth Factor-binding Protein Is a Novel Partner for Perlecan Protein Core. *The Journal of Biological Chemistry* **276,** 10263–10271 (2001).

82. Göhring, W., Sasaki, T., Heldin, C. H. & Timpl, R. Mapping of the binding of platelet-derived growth factor to distinct domains of the basement membrane proteins BM-40 and perlecan and distinction from the BM-40 collagen-binding epitope. *European Journal of Biochemistry* **255,** 60–66 (1998).

83. Hopf, M., Göhring, W., Mann, K. & Timpl, R. Mapping of binding sites for nidogens, fibulin-2, fibronectin and heparin to different IG modules of perlecan 1 1Edited by M. F. Moody. *J. Mol. Biol.* **311,** 529–541 (2001).

84. Hopf, M., Göhring, W., Kohfeldt, E., Yamada, Y. & Timpl, R. Recombinant domain IV of perlecan binds to nidogens, laminin–nidogen complex, fibronectin, fibulin-2 and heparin. *European Journal of Biochemistry* **259,** 917–926 (1999).

85. Mongiat, M., Sweeney, S. M., San Antonio, J. D., Fu, J. & Iozzo, R. V. Endorepellin, a Novel Inhibitor of Angiogenesis Derived from the C Terminus of Perlecan. *The Journal of Biological Chemistry* **278,** 4238–4249 (2003).

86. Smyth, N. *et al.* Absence of basement membranes after targeting the LAMC1 gene results in embryonic lethality due to failure of endoderm differentiation. *The Journal of Cell Biology* **144,** 151–160 (1999).

87. Urbano, J. M. *et al.* Drosophila laminins act as key regulators of basement membrane assembly and morphogenesis. *Development* **136,** 4165–4176 (2009).

88. Henry, M. D. & Campbell, K. P. A Role for Dystroglycan in Basement Membrane Assembly. *Cell* **95,** 859–870 (1998).

89. Colognato, H., Winkelmann, D. A. & Yurchenco, P. D. Laminin polymerization induces a receptor–cytoskeleton network. *The Journal of Cell Biology* **145,** 619–631 (1999).

90. Lohikangas, L., Gullberg, D. & Johansson, S. Assembly of Laminin Polymers Is Dependent on β1-Integrins. *Exp. Cell Res.* **265,** 135–144 (2001).

91. Gerl, M., Mann, K., Aumailley, M. & Timpl, R. Localization of a major nidogen-binding site to domain III of laminin B2 chain. *European Journal of Biochemistry* **202,** 167–174 (1991).

92. Mayer, U. *et al.* A single EGF-like motif of laminin is responsible for high affinity nidogen binding. *The EMBO Journal* **12,** 1879–1885 (1993).

93. Pöschl, E. *et al.* Two non-contiguous regions contribute to nidogen binding to a single EGF-like motif of the laminin gamma 1 chain. *The EMBO Journal* **13,** 3741–3747 (1994).

94. Kang, S. H. & Kramer, J. M. Nidogen is nonessential and not required for normal type IV collagen localization in Caenorhabditis elegans. *Molecular Biology of the Cell* **11,** 3911–3923 (2000).

95. Dai, J. *et al.* Dissection of Nidogen function in Drosophila reveals tissue-specific mechanisms of basement membrane assembly. *PLoS Genet* **14,** 1–31 (2018).

96. Bader, B. L. *et al.* Compound Genetic Ablation of Nidogen 1 and 2 Causes Basement Membrane Defects and Perinatal Lethality in Mice. *Molecular and Cellular Biology* **25,** 6846–6856 (2005).

97. Bix, G. *et al.* Endorepellin causes endothelial cell disassembly of actin cytoskeleton and focal adhesions through α2β1 integrin. *The Journal of Cell Biology* **166,** 97–109 (2004).

98. Talts, J. F., Andac, Z., Göhring, W., Brancaccio, A. & Timpl, R. Binding of the G domains of laminin α1 and α2 chains and perlecan to heparin, sulfatides, α-dystroglycan and several extracellular matrix proteins. *The EMBO Journal* **18,** 863–870 (1999).

99. Pastor-Pareja, J. C. & Xu, T. Shaping Cells and Organs in Drosophila by Opposing Roles of Fat Body-Secreted Collagen IV and Perlecan. *Developmental Cell* **21,** 245–256 (2011).

100. Behrens, D. T. *et al.* The Epidermal Basement Membrane Is a Composite of Separate Laminin- or Collagen IV-containing Networks Connected by Aggregated Perlecan, but Not by Nidogens. *The Journal of Biological Chemistry* **287,** 18700–18709 (2012).

101. Fini, M. E. & Stramer, B. M. How the Cornea Heals: Cornea-specific Repair Mechanisms Affecting Surgical Outcomes. *Cornea* **24,** S2–S11 (2005).

102. Torricelli, A. A. M., Singh, V., Santhiago, M. R. & Wilson, S. E. The Corneal Epithelial Basement Membrane: Structure, Function, and Disease. *Investigative Ophthalmology & Visual Science* **54,** 6390–6400 (2013).

103. Marino, G. K., Santhiago, M. R., Santhanam, A., Torricelli, A. A. M. & Wilson, S. E. Regeneration of Defective Epithelial Basement Membrane and Restoration of Corneal Transparency After Photorefractive Keratectomy. *J Refract Surg* **33,** 337–346 (2017).

104. Fisher, G. & Rittié, L. Restoration of the basement membrane after wounding: a hallmark of young human skin altered with aging. 1–11 (2018). doi:10.1007/s12079-017-0417-3

105. Marinkovich, M. P., Keene, D. R., Rimberg, C. S. & Burgeson, R. E. Cellular origin of the dermal-epidermal basement membrane. *Developmental Dynamics* **197,** 255–267 (1993).

106. Torricelli, A. A. M. *et al.* Epithelial basement membrane proteins perlecan and nidogen-2 are up-regulated in stromal cells after epithelial injury in human corneas. *Experimental Eye Research* **134,** 33–38 (2015).

107. Stanley, J. R., Alvarez, O. M., Bere, E. W., Eaglstein, W. & Katz, S. I. Detection of basement membrane zone antigens during epidermal wound healing in pigs. *J Investig Dermatol* **77,** 240–243 (1981).

108. Clark, R. A. F. *et al.* Fibronectin and Fibrin Provide a Provisional Matrix for Epidermal Cell Migration During Wound Reepithelialization. *J Investig Dermatol* **79,** 264–269 (1982).

109. Miner, J. H., Cunningham, J. & Sanes, J. R. Roles for laminin in embryogenesis: exencephaly, syndactyly, and placentopathy in mice lacking the laminin alpha5 chain. *The Journal of Cell Biology* **143,** 1713–1723 (1998).

110. Costell, M. *et al.* Perlecan Maintains the Integrity of Cartilage and Some Basement Membranes. *The Journal of Cell Biology* **147,** 1109–1122 (1999).

111. Galko, M. J. & Krasnow, M. A. Cellular and Genetic Analysis of Wound Healing in Drosophila Larvae. *Plos Biol* **2,** 1114–1126 (2004).

112. Ma, M., Cao, X., Dai, J. & Pastor-Pareja, J. C. Basement Membrane Manipulation in Drosophila Wing Discs Affects Dpp Retention but Not Growth Mechanoregulation. *Developmental Cell* **42,** 97–106.e4 (2017).

113. Skeath, J. B. *et al.* The extracellular metalloprotease AdamTS-A anchors neural lineages in place within and preserves the architecture of the central nervous system. *Development* **144,** 3102–3113 (2017).

114. Crest, J., Diz-Muñoz, A., Chen, D.-Y., Fletcher, D. A. & Bilder, D. Organ sculpting by patterned extracellular matrix stiffness. *Elife* **6,** 1–16 (2017).

115. Chlasta, J. *et al.* Variations in basement membrane mechanics are linked to epithelial morphogenesis. *Development* **144,** 4350–4362 (2017).

116. Ramos-Lewis, W. & Page-McCaw, A. Basement membrane mechanics shape development: Lesson from the fly. *Matrix Biology* (2018). doi:10.1016/j.matbio.2018.04.004

117. Ries, A., Göhring, W., Fox, J. W., Rupert, T. & Sasaki, T. Recombinant domains of mouse nidogen-1 and their binding to basement membrane proteins and monoclonal antibodies. *European Journal of Biochemistry* 1–10 (2001).

118. Takagi, J., Yang, Y., Liu, J.-H., Wang, J.-H. & Springer, T. A. Complex between nidogen and laminin fragments reveals a paradigmatic β-propeller interface. *Nature* **424,** 969–974 (2003).

119. Amano, S. Possible Involvement of Basement Membrane Damage in Skin Photoaging. *Journal of Investigative Dermatology* **14,** 2–7 (2009).

120. Miner, J. H. The glomerular basement membrane. *Exp. Cell Res.* **318,** 973–978 (2012).

121. Fujikawa, L. S., Foster, C. S., Gipson, I. K. & Colvin, R. B. Basement membrane components in healing rabbit corneal epithelial wounds: immunofluorescence and ultrastructural studies. *The Journal of Cell Biology* **98,** 128–138 (1984).

122. Khodadoust, A. A., Silverstein, A. M., Kenyon, K. R. & Dowling, J. E. Adhesion of regenerating corneal epithelium. *American Journal of Ophthalmology* **65,** 339–348 (1968).

123. Buszczak, M. *et al.* The Carnegie Protein Trap Library: A Versatile Tool for Drosophila Developmental Studies. *Genetics* **175,** 1505–1531 (2006).

124. Kelso, R. J. *et al.* Flytrap, a database documenting a GFP protein-trap insertion screen in Drosophila melanogaster. *Nucleic Acids Research* **32,** D418–D420 (2004).

125. Page-McCaw, A., Serano, J., Santé, J. M. & Rubin, G. M. Drosophila Matrix Metalloproteinases Are Required for Tissue Remodeling, but Not Embryonic Development. *Developmental Cell* **4,** 95–106 (2003).

126. Sarov, M. *et al.* A genome-wide resource for the analysis of protein localisation in Drosophila. *Elife* **5,** e12068 (2016).

127. Glasheen, B. M., Robbins, R. M., Piette, C., Beitel, G. J. & Page-McCaw, A. A matrix metalloproteinase mediates airway remodeling in Drosophila. *Developmental Biology* **344,** 772–783 (2010).

128. Fessler, J. H. & Fessler, L. I. Drosophila extracellular matrix. *Annu. Rev. Cell Dev Biol.* **5,** 309–339 (1989).

129. Matsubayashi, Y. *et al.* A Moving Source of Matrix Components Is Essential for De Novo Basement Membrane Formation. *Current Biology* **27,** 3526–3534 (2017).

130. Babcock, D. T. *et al.* Circulating blood cells function as a surveillance system for damaged tissue in Drosophila larvae. *Proc. Natl. Acad. Sci. U.S.A.* **105,** 10017–10022 (2008).

131. Jung, M. *et al.* Mast cells produce novel shorter forms of perlecan that contain functional endorepellin: a role in angiogenesis and wound healing. *Journal of Biological Chemistry* **288,** 3289–3304 (2013).

132. Kelemen-Valkony, I. *et al.* Drosophila basement membrane collagen col4a1 mutations cause severe myopathy. *Matrix Biology* **31,** 29–37 (2012).

133. Voigt, A., Pflanz, R., Schäfer, U. & Jäckle, H. Perlecan participates in proliferation activation of quiescent Drosophila neuroblasts. *Developmental Dynamics* **224,** 403–412 (2002).

134. Stevens, L. J. & Page-McCaw, A. A secreted MMP is required for reepithelialization during wound healing. *Molecular Biology of the Cell* **23,** 1068–1079 (2012).

135. Brock, A. R. *et al.* Transcriptional regulation of Profilin during wound closure in Drosophila larvae. *Journal of Cell Science* **125,** 5667–5676 (2013).

136. Denef, N., Chen, Y., Weeks, S. D., Barcelo, G. & Schüpbach, T. Crag Regulates Epithelial Architecture and Polarized Deposition of Basement Membrane Proteins in Drosophila. *Developmental Cell* **14,** 354–364 (2008).

137. Isabella, A. J. & Horne-Badovinac, S. Rab10-Mediated Secretion Synergizes with Tissue Movement to Build a Polarized Basement Membrane Architecture for Organ Morphogenesis. *Developmental Cell* **38,** 47–60 (2016).

138. Galindo, R. L., Allport, J. A. & Olson, E. N. A Drosophila model of the rhabdomyosarcoma initiator PAX7-FKHR. *Proc. Natl. Acad. Sci. U.S.A.* **103,** 13439–13444 (2006).

139. Hussain, S. A., Carafoli, F. & Hohenester, E. Determinants of laminin polymerization revealed by the structure of the α5 chain amino-terminal region. *EMBO reports* **12,** 276–282 (2011).

140. Rabenstein, D. L. Heparin and heparan sulfate: structure and function. *Nat. Prod. Rep.* **19,** 312–331 (2002).

141. Fleischmajer, R. *et al.* Initiation of skin basement membrane formation at the epidermo-dermal interface involves assembly of laminins through binding to cell membrane receptors. *Journal of Cell Science* **111 (Pt 14),** 1929–1940 (1998).

142. Colognato, H. & Yurchenco, P. D. Form and function: The laminin family of heterotrimers. *Developmental Dynamics* **218,** 213–234 (2000).

143. Sun, Z., Guo, S. S. & Fassler, R. Integrin-mediated mechanotransduction. *The Journal of Cell Biology* **215,** 445–456 (2016).

144. Page-McCaw, A., Ewald, A. J. & Werb, Z. Matrix metalloproteinases and the regulation of tissue remodelling. *Nat Rev Mol Cell Biol* **8,** 221–233 (2007).

145. Park, S. H. *et al.* Requirement for and polarized localization of integrin proteins during Drosophila wound closure. *Molecular Biology of the Cell* **29,** (2018).

146. Yee, G. H. & Hynes, R. O. A novel, tissue-specific integrin subunit, beta nu, expressed in the midgut of Drosophila melanogaster. *Development* **118,** 845–858 (1993).

147. Kashio, S., Obata, F. & Miura, M. How tissue damage MET metabolism: Regulation of the systemic damage response. *Fly* **11,** 27–36 (2017).

148. Shaukat, Z., Liu, D. & Gregory, S. Sterile Inflammation in Drosophila. *Mediators of Inflammation* **2015,** 1–7 (2015).

149. Liu, Y., Beyer, A. & Aebersold, R. On the Dependency of Cellular Protein Levels on mRNA Abundance. *Cell* **165,** 535–550 (2016).

150. Charroux, B. & Royet, J. Elimination of plasmatocytes by targeted apoptosis reveals their role in multiple aspects of the Drosophila immune response. *Proc. Natl. Acad. Sci. U.S.A.* **106,** 9797–9802 (2009).

151. Goto, A., Kadowaki, T. & Kitagawa, Y. Drosophila hemolectin gene is expressed in embryonic and larval hemocytes and its knock down causes bleeding defects. *Developmental Biology* **264,** 582–591 (2003).

152. Nelson, R. E. *et al.* Peroxidasin: a novel enzyme-matrix protein of Drosophila development. *The EMBO Journal* **13,** 3438–3447 (1994).

153. Howard, A. M. *et al.* DSS-induced damage to basement membranes is repaired by matrix replacement and crosslinking. *Journal of Cell Science* **132,** 1–13 (2019).

154. Losick, V. P., Fox, D. T. & Spradling, A. C. Polyploidization and Cell Fusion Contribute to Wound Healing in the Adult Drosophila Epithelium. *Current Biology* **23,** 2224–2232 (2013).

155. Ghannad-Rezaie, M., Wang, X., Mishra, B., Collins, C. & Chronis, N. Microfluidic Chips for In Vivo Imaging of Cellular Responses to Neural Injury in Drosophila Larvae. *PLoS ONE* **7,** e29869–8 (2012).

156. Kelley, L. C. *et al.* Live-cell confocal microscopy and quantitative 4D image analysis of anchor-cell invasion through the basement membrane in Caenorhabditis elegans. *Nature Protocols* **12,** 2081–2096 (2017).

157. Pujol, N. *et al.* Distinct Innate Immune Responses to Infection and Wounding in the C. elegans Epidermis. *Current Biology* **18,** 481–489 (2008).

158. Chisholm, A. D. Epidermal Wound Healing in the Nematode Caenorhabditis elegans. *Advances in Wound Care* **4,** 264–271 (2014).

159. Hagedorn, E. J. & Sherwood, D. R. Cell invasion through basement membrane: the anchor cell breaches the barrier. *Current Opinion in Cell Biology* **23,** 589–596 (2011).

160. Kelley, L. C. *et al.* Adaptive F-Actin Polymerization and Localized ATP Production Drive Basement Membrane Invasion in the Absence of MMPs. *Developmental Cell* **48,** 313–328.e8 (2019).

161. Longmate, W. M. & DiPersio, C. M. Integrin Regulation of Epidermal Functions in Wounds. *Advances in Wound Care* **3,** 229–246 (2014).

162. Rousselle, P., Montmasson, M. & Garnier, C. Extracellular matrix contribution to skin wound re-epithelialization. *Matrix Biology* 1–15 (2018). doi:10.1016/j.matbio.2018.01.002

163. Mak, K. M. & Mei, R. Basement membrane type IV collagen and laminin: an overview of their biology and value as fibrosis biomarkers of liver disease. *Anat. Rec.* **300,** 1371–1390 (2017).

164. Marshall, C. B. Rethinking glomerular basement membrane thickening in diabetic nephropathy: adaptive or pathogenic? *American Journal of Physiology-Renal Physiology* **311,** F831–F843 (2016).

165. Engler, A. J., Sen, S., Sweeney, H. L. & Discher, D. E. Matrix Elasticity Directs Stem Cell Lineage Specification. *Cell* **126,** 677–689 (2006).

166. Wells, R. G. The role of matrix stiffness in regulating cell behavior. *Hepatology* **47,** 1394–1400 (2008).

167. Borchiellini, C., Coulon, J. & Le Parco, Y. The function of type IV collagen during Drosophila muscle development. *Mechanisms of Development* **58,** 179–191 (1996).

168. Hynes, R. O. & Zhao, Q. The Evolution of Cell Adhesion. *The Journal of Cell Biology* **150,** F89–F95 (2000).

169. Van De Bor, V. *et al.* Companion Blood Cells Control Ovarian Stem Cell Niche Microenvironment and Homeostasis. *Cell Reports* **13,** 546–560 (2015).

170. Gutzeit, H. O., Eberhardt, W. & Gratwohl, E. Laminin and basement membrane-associated microfilaments in wild-type and mutant Drosophila ovarian follicles. *Journal of Cell Science* **100,** 781–788 (1991).

171. Haigo, S. L. & Bilder, D. Global tissue revolutions in a morphogenetic movement controlling elongation. *Science* **331,** 1071–1074 (2011).

172. Srivastava, A., Pastor-Pareja, J. C., Igaki, T., Pagliarini, R. & Xu, T. Basement membrane remodeling is essential for Drosophila disc eversion and tumor invasion. *Proc. Natl. Acad. Sci. U.S.A.* **104,** 2721–2726 (2007).

173. Duhart, J. C., Parsons, T. T. & Raftery, L. A. The repertoire of epithelial morphogenesis on display: Progressive elaboration of Drosophila egg structure. *Mechanisms of Development* **148,** 18–39 (2017).

174. Bilder, D. & Haigo, S. L. Expanding the Morphogenetic Repertoire: Perspectives from the Drosophila Egg. *Developmental Cell* **22,** 12–23 (2012).

175. Cetera, M. *et al.* Epithelial rotation promotes the global alignment of contractile actin bundles during Drosophila egg chamber elongation. *Nature Communications* **5,** 1–12 (2014).

176. Aurich, F. & Dahmann, C. A Mutation in *fat2* Uncouples Tissue Elongation from Global Tissue Rotation. *Cell Reports* **14,** 2503–2510 (2016).

177. Chen, D.-Y., Crest, J. & Bilder, D. A Cell Migration Tracking Tool Supports Coupling of Tissue Rotation to Elongation. *Cell Reports* **21,** 559–569 (2017).

178. Schneider, M. *et al.* Perlecan and Dystroglycan act at the basal side of the Drosophila follicular epithelium to maintain epithelial organization. *Development* **133,** 3805–3815 (2006).

179. Isabella, A. J. & Horne-Badovinac, S. Dynamic regulation of basement membrane protein levels promotes egg chamber elongation in Drosophila. *Developmental Biology* **406,** 212–221 (2015).

180. Shahab, J. *et al.* Loss of SPARC dysregulates basal lamina assembly to disrupt larval fat body homeostasis in Drosophila melanogaster. *Developmental Dynamics* **244,** 540–552 (2015).

181. Andersen, D. & Horne-Badovinac, S. Influence of ovarian muscle contraction and oocyte growth on egg chamber elongation in Drosophila. *Development* **143,** 1375–1387 (2016).

182. Durbeej, M. in *Current Topics in Membranes* **76,** 31–60 (Elsevier, 2015).

183. Sánchez-Sánchez, B. J. *et al.* Drosophila Embryonic Hemocytes Produce Laminins to Strengthen Migratory Response. *Cell Reports* **21,** 1461–1470 (2017).

184. Meyer, S., Schmidt, I. & Klämbt, C. Glia ECM interactions are required to shape the Drosophila nervous system. *Mechanisms of Development* **133,** 105–116 (2014).

185. Borchiellini, C., Coulon, J. & Le Parco, Y. The function of type IV collagen during embryogenesis. *Roux's Arch Dev Biol* **205,** 468–475 (1996).

186. Pathak, A. & Kumar, S. Independent regulation of tumor cell migration by matrix stiffness and confinement. *Proc. Natl. Acad. Sci. U.S.A.* **109,** 10334–10339 (2012).

187. Kim, S. N. *et al.* ECM stiffness regulates glial migration in Drosophila and mammalian glioma models. *Development* **141,** 3233–3242 (2014).

188. Beira, J. V. & Paro, R. The legacy of Drosophila imaginal discs. *Chromosoma* 1–20 (2016). doi:10.1007/s00412-016-0595-4

189. Eder, D., Aegerter, C. & Basler, K. Forces controlling organ growth and size. *Mechanisms of Development* **144,** 53–61 (2017).

190. Morrissey, M. A. *et al.* B-LINK: A Hemicentin, Plakin, and Integrin-Dependent Adhesion System that Links Tissues by Connecting Adjacent Basement Membranes. *Developmental Cell* **31,** 319–331 (2014).

191. Qin, J., Liang, J. & Ding, M. Perlecan Antagonizes Collagen IV and ADAMTS9/GON-1 in Restricting the Growth of Presynaptic Boutons. *Journal of Neuroscience* **34,** 10311–10324 (2014).